

AD-A131 650

IN SITU CHARACTERIZATION OF SOILS FOR PREDICTION OF  
STRESS STRAIN RELATIO... (U) CALIFORNIA UNIV DAVIS DEPT  
OF CIVIL ENGINEERING K ARULANANDAN ET AL. 10 NOV 82

1/2

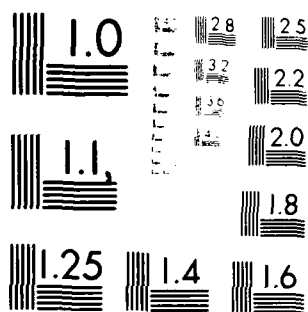
UNCLASSIFIED

AFOSR-TR-83-0680 AFOSR-81-0216

F/G 8/13

NL

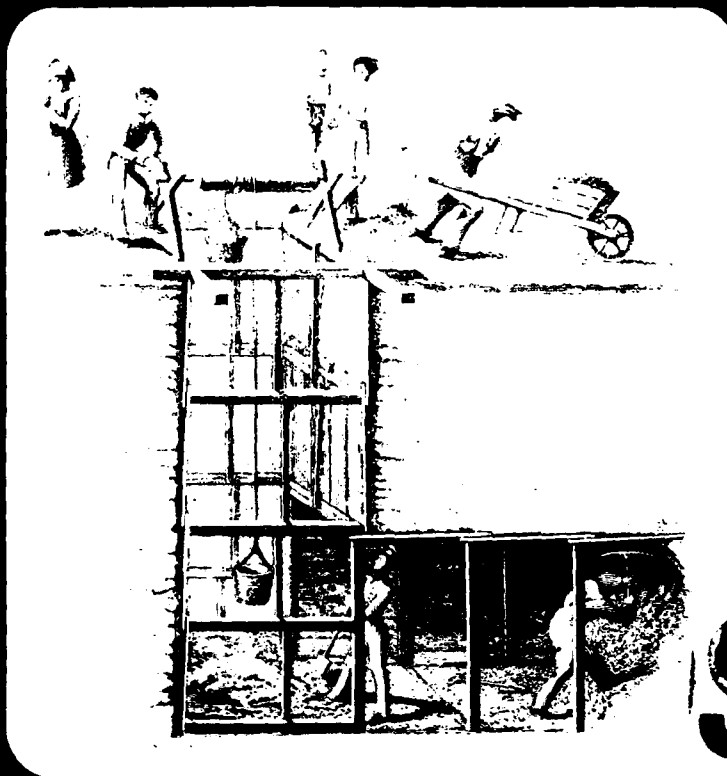




MICROCOPY RESOLUTION TEST CHART  
NATIONAL BUREAU OF STANDARDS-1963-A

ADA 131655

IN SITU CHARACTERIZATION OF SOILS FOR PREDICTION  
OF STRESS STRAIN RELATIONSHIP OF SOFT CLAY



DTIC  
AUG 22 1983

DTIC FILE COPY

Department of Civil Engineering

University of California, Davis

"Qualified requestors may obtain additional copies  
from the Defense Technical Information Service."

UNCLASSIFIED

SECURITY CLASSIFICATION OF THIS PAGE (When Data Entered)

REPORT DOCUMENTATION PAGE		READ INSTRUCTIONS BEFORE COMPLETING FORM
1. REPORT NUMBER <b>AFOSR-TR- 83-0680</b>	2. GOVT ACCESSION NO. <b>AD-A131650</b>	3. RECIPIENT'S CATALOG NUMBER
4. TITLE (and Subtitle)  <b>INSITU CHARACTERIZATION OF SOILS FOR PREDICTION OF STRESS STRAIN RELATIONSHIP OF SOFT CLAY</b>		5. TYPE OF REPORT & PERIOD COVERED <b>Annual August 1981-August 1982 (inc. dates)</b>
7. AUTHOR(s) <b>K. Arulanandan L. R. Herrmann A. Anandarajah Y. F. Dafalias</b>		6. PERFORMING ORG. REPORT NUMBER
9. PERFORMING ORGANIZATION NAME AND ADDRESS <b>Department of Civil Engineering University of California Davis, California 95616</b>		8. CONTRACT OR GRANT NUMBER(s) <b>AFOSR-81-0216</b>
11. CONTROLLING OFFICE NAME AND ADDRESS <b>AIR FORCE OFFICE OF SCIENTIFIC RESEARCH/NA BOLLING AFB, DC 20332</b>		10. PROGRAM ELEMENT PROJECT, TASK AREA & WORK UNIT NUMBERS <b>61102F 2307/C1</b>
14. MONITORING AGENCY NAME & ADDRESS (if different from Controlling Office)		12. REPORT DATE <b>10th of November 1982</b>
		13. NUMBER OF PAGES <b>125</b>
		15. SECURITY CLASS. (of this report) <b>Unclassified</b>
		15a. DECLASSIFICATION/DOWNGRADING SCHEDULE
16. DISTRIBUTION STATEMENT (of this Report)  <b>Approved for Public Release; Distribution Unlimited.</b>		
17. DISTRIBUTION STATEMENT (of the abstract entered in Block 20, if different from Report)		
18. SUPPLEMENTARY NOTES		
19. KEY WORDS (Continue on reverse side if necessary and identify by block number)  <b>Non-destructive Method, Electrical Method, Bounding Surface Model, Insitu Prediction of Mechanical Properties, Insitu Stress Strain Behavior</b>		
20. ABSTRACT (Continue on reverse side if necessary and identify by block number)  <b>An electrical method of characterizing fine grained soils is described. A non-destructive method of determining the stress-strain behavior of fine grained soils is developed based on this fundamental characterization of soils. A bounding surface plasticity model is used for the prediction of stress-strain behavior. Correlations are established relating the bounding surface model parameters to the appropriate electrical parameters. In situ prediction of stress-strain behavior of fine grained soils can be made by determining the electrical properties using an in situ measuring technique in a non-destructive</b>		

DD FORM 1 JAN 73 1473 EDITION OF 1 NOV 65 IS OBSOLETE

UNCLASSIFIED

SECURITY CLASSIFICATION OF THIS PAGE (When Data Entered)

**UNCLASSIFIED**

SECURITY CLASSIFICATION OF THIS PAGE (When Data Entered)

20. manner and obtaining the required bounding surface model parameters from the correlations established. The feasibility of applying this methodology for predicting the stress-strain behavior is demonstrated based on a limited number of laboratory experiments performed on normally consolidated fine grained soils.



Accession For	
NTIS GRA&I	<input checked="checked" type="checkbox"/>
DTIC TAB	<input type="checkbox"/>
Unannounced	<input type="checkbox"/>
Justification	
By	
Distribution/	
Availability Codes	
Avail and/or	
Special	
A	

**UNCLASSIFIED**

SECURITY CLASSIFICATION OF THIS PAGE (When Data Entered)

**IN SITU CHARACTERIZATION OF SOILS FOR PREDICTION  
OF STRESS STRAIN RELATIONSHIP OF SOFT CLAY**

By

K. Arulanandan<sup>1</sup>  
A. Anandarajah<sup>2</sup>  
Y.F. Dafalias<sup>3</sup>  
L.R. Herrmann<sup>4</sup>

REPORT TO THE AIR FORCE OFFICE OF SCIENTIFIC RESEARCH  
GRANT NO. AFOSR-82-0216, 1982

AIR FORCE OFFICE OF SCIENTIFIC RESEARCH (AFOSR)  
NOTICE OF TRANSMITTAL TO DTIC  
This technical report has been reviewed and is  
approved for public release IAW AFR 100-12.  
Distribution is unlimited.  
MATTHEW J. KERPER  
Chief, Technical Information Division

- <sup>1</sup> Professor of Civil Engineering, University of California, Davis
- <sup>2</sup> Assistant Professor of Civil Engineering, South Dakota School of Mines
- <sup>3</sup> Associate Professor of Civil Engineering, University of California, Davis
- <sup>4</sup> Professor of Civil Engineering, University of California, Davis

Conditions of Reproduction, reproduction, translation, publication, use and  
disposal in whole or in part by or for the United States Government is permitted.

## **IN SITU CHARACTERIZATION OF SOILS FOR PREDICTION OF STRESS STRAIN RELATIONSHIP OF SOFT CLAY**

### **1. Introduction.**

The difficulty of characterizing particulate systems in their composite form has resulted in the use of destructive tests to index the grain and aggregate properties of soils in situ and to the arbitrary division of soils into groups based on size and to the classification of soils based on grain size distribution and index tests such as Atterberg Limits. Due to the arbitrary nature of the current methods of classifying soils, any correlations established between the conventional indices used to classify soils and mechanical behavior need to be periodically changed to account for any deviations. This problem can be overcome if the method of classifying soils can index the compositional and aggregate properties of soils in their composite form. This can only be achieved by non-destructive means. One possible way of achieving the objectives of

- 1) classifying soils in their composite form
- 2) predicting the mechanical properties and engineering behavior of soils

is by the use of electrical methods.

The objectives of this report are:

- 1) characterization of soil by electrical methods
- 2) quantification of the compositional and aggregate properties of soils in terms of electrical parameters
- 3) quantification of the inter and intra cluster void ratios
- 4) establishment of correlations between electrical parameters and compression index  $\lambda$ , swell index  $K$ , and the slope of the critical state line,  $M$
- 5) methodology to predict stress strain relationship of clays in situ.

### **2. Characterization of Soils By Electrical Methods.**

When an alternating electric field is applied to a clay-water-electrolyte system, a response is produced which can be measured in terms of a resistance,  $R$ , and a

capacitance, C. The measured value of the capacitance can be converted into a quantity known as the dielectric constant. This value is defined as  $C/C_0$ , in which  $C_0$  is the capacitance of a condenser with only a vacuum between the electrodes. The dielectric constant is actually a measure of the ability of the clay to store electrical potential energy under the influence of an electric field. From a knowledge of the dimensions of the sample the dielectric constant and conductivity can be calculated from the following relationships.

$$\epsilon' \epsilon_a = \frac{Cd}{A} \quad (1)$$

$$\sigma = \frac{d}{RA} \quad (2)$$

in which  $d$  = length of a specimen;  $A$  = cross-sectional area; and  $\epsilon_a$  = the dielectric constant of vacuum ( $8.85 \times 10^{-14}$  F/cm).

The dielectric constant of a dry silicate material is 4.5, and that of water is about 79. A mixture of soil and water should, therefore, have a dielectric constant weighted between 4.5 and 79. However, when the dielectric constant of a clay-water-electrolyte system is measured with an alternating current in the radio-frequency range, it is found to be in excess of the sum of the weighted dielectric constant of the components. This measured value,  $\epsilon'$ , referred to as the "apparent dielectric constant" reflects the heterogeneous nature of the path of the current and the electrical properties of the pore fluid and the clay mineral as shown by Arulanandan and Smith (1973).

When the conductivity,  $\sigma$ , and apparent dielectric constant,  $\epsilon'$ , of a cohesive system are measured as a function of frequency, in the radio frequency range, it is found that  $\epsilon'$  and  $\sigma$  vary (see Fig. 2). This variation of  $\sigma$  and  $\epsilon'$  is referred to as electrical dispersion. However, for a granular system it has been observed that  $\sigma$  and  $\epsilon'$  are independent of frequency (see Fig. 1). It is thus possible to classify all particulate systems into two groups. All cohesive systems characterized by electrical dispersion behavior and all granular systems by nondispersive electrical behavior.

This method of classification is both quantitative and fundamental in nature as opposed to the present qualitative arbitrary methods of classifying soils based on size only.

The factors that influence the magnitude of dielectric dispersion  $\Delta\epsilon_0$  (see Fig. 1) were investigated in detail by Arulanandan et al. (1975). It was shown that  $\Delta\epsilon_0$  depend predominately on the type and amount of clay mineral and the fabric having a second order effect. Thus the composition of cohesive soils can be characterized nondestructively and quantified in terms of the parameters  $\Delta\epsilon_0$ . The significance of this parameter to the classification of soils Arulanandan et al. (1975), to the prediction of cation exchange capacity Fernando et al. (1975), swell potential Basu and Arulanandan (1973), lime reactivity Castle and Arulanandan (1979), erosion potential Heinzen and Arulanandan (1977) and compression index Scharlin (1974) has been demonstrated.

### 3. Electrical Models to Predict Electrical Dispersive Behavior

Arulanandan and Mitra (1970), Arulanandan and Smith (1973) have shown it is possible to describe the electrical dispersive behavior of cohesive systems by the use of a three element electrical network model.

The current through the sample is considered to have three paths (Fig. 3): (1) through the inter cluster solution and clusters, (2) through clusters in contact with each other, and (3) through the inter cluster solution. The corresponding three element model representation of the impedances of individual components is shown in Figure 4.

Referring to Figure 4,  $k_r$  = conductivity of the solution,  $\epsilon_r$  = dielectric constant of the cluster,  $\epsilon_s$  = dielectric constant of the solution,  $a$  = area of cluster-solution path,  $b$  = area of the particle contact path and  $c$  = area of the solution path. In the case of soils saturated in water,  $\epsilon_s$  is approximately 79 and  $k_s$  is approximately equal to the conductivity of the pore fluid.

The apparent dielectric constant,  $\epsilon'$ , and the apparent conductivity  $\sigma$ , for the model can be evaluated by elementary network analysis. The equations relating  $\epsilon'$  and

$\sigma$  to the frequency depend on the compositional and geometric parameters of the system, as follows:

$$\epsilon'_{th} = \frac{a}{d(1-d)s} \left[ \frac{\epsilon_r k_s^2}{1-d} + \frac{\epsilon_s k_r^2}{d} + \omega^2 \epsilon_v^2 \left( \frac{\epsilon_r \epsilon_s^2}{1-d} + \frac{\epsilon_r^2 \epsilon_s}{d} \right) \right] + b\epsilon_r + c\epsilon_s \quad (3)$$

$$\sigma_{th} = \frac{a}{d(1-d)s} \left[ \frac{k_r k_s^2}{1-d} + \frac{k_r^2 k_s}{d} + \omega^2 \epsilon_v^2 \left( \frac{\epsilon_s^2 k_r}{1-d} + \frac{\epsilon_r^2 k_s}{d} \right) \right] + bk_r + ck_s \quad (4)$$

where

$$s = \left( \frac{k_s}{1-d} + \frac{k_r}{d} \right)^2 + \omega^2 \alpha^2 \left( \frac{\epsilon_s}{1-d} + \frac{\epsilon_r}{d} \right)^2 \quad (3a)$$

where

$\alpha$  = the capacitance of a unit capacitor in vacuum ( $8.85 \times 10^{-4}$  f/cm)

and

$\omega$  = angular frequency.

A digital computer optimization program utilizing the simplex method was employed to analyze the dielectric constant and conductivity dispersion curves. The optimization program determines the values of the geometrical (a, b, c, d) and compositional ( $\epsilon_r$ ,  $k_r$ ,  $k_s$ ,  $\epsilon_s$ ) parameters of the model shown in Figure 4 such that the frequency dispersion curves of the apparent dielectric constant and conductivity calculated from the theoretical Equations 3, 4 fit the experimental results within acceptable error limits.  $\epsilon_s$ , the dielectric constant of water, was kept constant at 79 during all computer runs. The conductivity of the pore fluid,  $k_s$ , is easily determined, and for the initial choice of the parameters,  $k_r$  was made equal to  $k_s$ . The initial value of "b" is estimated to be in the order of 0.01 as "b", the area of contact, is very nearly equal to zero. The value of "a" is dependent on c since  $a + b + c = 1$ . A typical example of the comparison of experimental and theoretical dispersion curves is shown in Figure 5. There are, in fact, six random parameters c, d,  $\epsilon_r$ ,  $k_r$ ,  $\epsilon_s$  and  $k_s$  involved in the curve fitting procedure by optimization technique. At first sight, it might seem that the choice of six seemingly random parameters would be enough to fit almost any set of curves and that the physical meaning of the result is doubtful. It is important to realize, however, that only the three independent geometrical parameters are genuine unknowns (b, c, d) and as  $b \approx 0$ , there are only two independent

unknown parameters, "c" and "d". The respective conductivities,  $k_r$  and  $k_s$ , of the cluster and the interstitial solution and the dielectric constant of the solid particles must have values that are reasonable from the point of view of physical science. One would expect the conductivity of the interstitial solution to be of the same order as the conductivity of the pore fluid extract; the conductivity of the solid should be of the same order as the isoconductivity value (Arulanandan et al., 1973); the dielectric constant of the clusters should be between 4.5 (the dielectric constant of dry silicate mineral) and 79 (the dielectric constant of pure water), depending on the water content. Although these limitations were not written into the computer program, the numerous results obtained in earlier investigations show that the requirements were indeed met. However, a large number of computer runs are necessary to select the best set of parameters that fit the experimental curves and are reasonable from a physical science point of view.

Arulanandan (1980) proposed an approximate expression to quantify the intra cluster void ratio  $e_1$ , utilizing the dielectric constant of the cluster,  $\epsilon_r$ , determined by the above procedure. Assuming a simple mixing rule, i.e., that dielectric constant of the solution plus the dielectric constant of the solids in a mixture is equal to the dielectric constant of the mixture,  $\epsilon_r$ , then

$$\epsilon_r = n_1 \epsilon_s + (1 - n_1) \epsilon_{\text{particle}} \quad (5)$$

where  $n_1$  is the intra cluster porosity. Assuming  $\epsilon_s = 79$ ,  $\epsilon_{\text{particle}} \approx 4.5$  (dielectric constant of dry silicate mineral), Equation 5 becomes

$$\epsilon_r = 74.5 n_1 + 4.5 \quad (5a)$$

Thus by determining  $\epsilon_r$  of a clay water electrolyte system by use of the three-element model proposed above the value of  $n_1$  can be quantified, and thus, the intra cluster void ratio

$$e_1 = \frac{n_1}{1 + n_1} \quad (6)$$

Thus the three-element electrical model can be used to quantify the inter and intra cluster void ratios.

The quantification of the inter and intra cluster void ratios by the above approach is time-consuming, as several computer runs are needed to be made to obtain the model parameters, combined with a certain amount of judgement needed to choose the right parameters. This is due to the fact that Equations 3 and 4 are highly non-linear. In order to make the optimization technique more efficient and to choose the suitable model parameters, it was thought to be necessary to impose an additional constraint in the optimization. This would be achieved utilizing the measured water content of the soil as is explained below. The intra cluster void ratio,  $e_i$ , is expressed in terms of the dielectric constant of the clusters,  $\epsilon_c$ , as given by Equations 5, 6. The inter cluster void ratio,  $e_p$ , is expressed in terms of model parameters by relating the physical dimensions of the soil sample and the electrical dimensions associated with the three current paths and using the assumptions made by Olsen (1961). The total void ratio can then be expressed in terms of the three-element model parameters. The additional constraint incorporated in the optimization procedure is as follows: Measured water content = water content calculated from the three-element model parameters.

This constraint overcomes one more difficulty that could be encountered as follows: It was found that the dielectric constant and conductivity curves were lowered as the water content of the soil is decreased if the conductivity of the pore fluid remains the same. However, if the conductivity of the soil with lower water content is higher, it is possible to obtain identical set of curves at both higher and lower water contents. Since the conductivity of the pore fluid is allowed to vary in the optimization, one would obtain same set of parameter for the above cases although the water contents are different.

### 3a. Inter Cluster Void Ratio as a Function of Three-Element Model Parameters

Olsen (1961) has used a three-element electrical model, similar to the one described in the preceding sections, in his study of hydraulic flow through saturated clays. The total current through the soil sample was considered to consist of three components as shown in Figure 6. The derivation of the expressions for dielectric constant,  $\epsilon'$ , and the conductivity,  $\sigma$ , are given in Appendix I. Referring to Figure 6,  $A_{1e}$  = area of the solid-solution current path,  $A_{2e}$  = area of the contact area current path,  $A_{3e}$  = area of the solution current path,  $L_e$  = length of the current paths through each one of the elements. The assumptions made are:

- 1) The volume of the soil sample ( $A \times L$ ) is equal to the volume of the solid-solution path ( $A_{1e} \times L_e$ ).
- 2) The volume of the solution path of solid-solution element ( $A_{1e} \times L_{2e}$ ) is equal to the volume of the solution path of the solution element ( $a_{3e} \times L_e$ ).

Utilizing these assumptions and defining that  $a = 1/t^2$ ,  $b = A_{2e}/A_{1e}t^2$ ,  $c = A_{3e}/A_{1e}t^2$ ,  $d = L_{1e}/L_e$ ,  $1-d = L_{2e}/L_e$ , and  $t = L_e/L$ , the expressions for dielectric constant and conductivity became same as the ones derived by Arulanandan et al. (1973). However, as the consequence of imposing the assumptions made by Olsen, it was found that  $c = (1-d)a$ , whereas in the previous model  $a + b + c = 1$ . The model parameters are interpreted as follows:

- 1)  $\frac{c}{a} = (1-d) = \frac{A_{3e}}{A_{1e}} = \frac{\text{Area of the solution path}}{\text{Area of the solid-solution path}}$
- 2)  $\frac{b}{a} = \frac{A_{2e}}{A_{1e}} = \frac{\text{Area of the contact area path}}{\text{Area of the solid-solution path}}$
- 3)  $t = \frac{L_e}{L} = \frac{\text{Electrical length}}{\text{Actual length of sample}} = \text{tortuosity}$
- 4)  $\epsilon_r$  is the dielectric constant of the clusters

It should be noted that the tortuosity, defined as  $t = L_e/L$ , is an average value. This is due to the assumption that the length of solid-solution current path is equal to the length of solution current path. But one would expect the solution current path to be much more tortuous than the solid current path.

The inter cluster void ratio,  $e_p$ , can now be expressed in terms of the three-element electrical model parameters using Olsen's cluster model, shown in Figure 7. With the notations used in Figure 7 and assuming that all the clusters are identical,

$$n_I = \frac{V_I/N}{V_C/N} = \frac{V_I}{V_C} = \frac{V_I}{V_s} \frac{1}{\frac{V_I + V_s}{V_s}} = \frac{e_I}{1 + e_I} \quad (8)$$

$$e_I = \frac{n_I}{1 - n_I}$$

$$n_p = \frac{V_p}{V_p + V_C} = \frac{V_p}{V_s} \frac{1}{\frac{V_p}{V_s} + \frac{V_I}{V_s} + \frac{V_s}{V_s}} = \frac{e_p}{1 + e_p + e_I}$$

$$e_p = \frac{n_p}{1 - n_p} (1 + e_I) \quad (9)$$

Referring to Figure 6

$$n_p = \frac{A_{je} L_{2e}}{A_{je} L_e} = \frac{L_{2e}}{L_e} = 1 - d \quad (10)$$

Combining Equations 9 and 10

$$e_p = \frac{1}{d} (1 - d) (1 + e_I) \quad (11)$$

From Equations 5a and 6

$$e_I = \frac{\epsilon_r - 4.5}{\epsilon_s - \epsilon_r} \quad (12)$$

and

$$e = e_p + e_I \quad (13)$$

The water content of the soil can be calculated knowing the specific gravity of the soil,  $G_s$ , as follows:

$$\text{water content} = e/G_s \quad (14)$$

The validity of the model, when Olsen's assumptions are incorporated, was examined by optimizing some experimental electrical dispersion data obtained from Smith, S. (1971). It was found that there are more than one feasible solutions as given in Table 1. However, it was noted that one of these feasible solutions predicts a water content that is close to the experimentally determined water content as given in Table 2.

This observation was confirmed by optimizing several other experimental dispersion data as presented in Tables 3 and 4. This shows that the model can predict the water content of the soil.

#### 4. Experimental Procedure

A detailed experimental study was conducted in order to investigate the variation of electrical parameters such as  $F_v$ ,  $F_H$ ,  $A$  and the electrical dispersion behavior of soils as a function of water content. For this purpose, it was necessary to develop a cell so that the above properties can be measured as the soil is being consolidated.

Two identical square cells of 5" x 1 3/8" x 1 3/8" (Figure 8), fabricated out of plexiglass of 1/2" thickness, were used to measure the electrical properties of the soils.

One would be used for the determination of the electrical properties in the vertical direction using two porous brass plates as electrodes placed at top and bottom of the sample. The second cell would be used for the determination of the electrical properties in the horizontal direction using two brass plates as electrodes embedded into the plexiglass walls on either end of the sample. The electrodes in the cells would be connected to the impedance analyzer by a 6-inch long coaxial transmission cable.

Since the impedances of the transmission line and the cell would become very significant in the radio frequency range, they need to be determined accurately and accounted for in the determination of the dielectric constant and the conductivity of the sample. This is achieved by representing the system by an appropriate equivalent electrical network. The calibration procedures to determine the impedance characteristics of the transmission line and the cell, using water which has a dielectric constant of 79, is given in Appendix 2. Water does not exhibit dispersion behavior, and its conductivity can be determined independently. These known electrical properties of water are utilized for the calibration of the cells.

A Hewlett-Packard impedance analyzer (Figure 9), which is designed for the precise impedance measurements in the frequency range of 1 MHz - 1000 MHz, was used for the measurements in the radio frequency range. A low frequency Impedance Comparator (Figure 10) was used for the determination of the formation factor at a frequency of 1 KHz.

The soils used were:

1. Marysville red soil
2. Yolo loam
3. Na-Illite
4. Snow Cal (95%) + Bentonite (5%)
5. Snow Cal (60%) + Illite (40%)

The electrical dispersion curves at different water contents are presented in Figures 11-30. It could be observed from these figures that the variation of the magnitude of dielectric dispersion with water content,  $\Delta\epsilon_0$ , is negligible. Conductivity changes considerably, but the change in dielectric constant is not very significant.

The optimized model parameters using the experimental dispersion results corresponding to different water contents are presented in Tables 9-12. The anisotropy of the soil is mainly reflected in the model parameter "a" which represents the tortuosity of the current path. The variations of the ratios of the intra and inter void ratios,  $e_1/e_p$ , are almost independent of the direction of measurement. This

observation further confirms the validity of using the assumptions made by Olsen (1961), since the void ratios are scalar quantities, and consequently the ratio,  $e_l/e_p$ , should be independent of the direction of measurement. The relationship between  $e_l/e_p$  and the total void ratio,  $e$ , for different soils is shown in Figure 32.

There are distinct linear relationships between  $e_l/e_p$  Anandarajha (1982) and  $e$  intersecting the  $e$ -axis at a void ratio of about 0.47. The ratio  $e_l/e_p$  can only be zero when  $e_l = 0$ . At this consolidation state, it would appear that the total void ratio corresponds to a void ratio associated with the maximum packing of primary particles. This value of  $e = 0.47$  is very nearly equal to the void ratio associated with the maximum packing of spheres ( $e = 0.43$ ). This observation provides further justification of the procedures used to quantify the inter and intra cluster void ratios.

The average formation factor,  $\bar{F}$ , was plotted against the total porosity,  $n$ , (Tables 5-8) as shown in Figure 33. These results indicate that there exists a unique relationship between  $\bar{F}$  and  $n$  for a given soil. This unique relationship shows that the approximate relationship for sands,  $\bar{F} = n^{-\bar{f}}$ , developed using Bruggemen's integration technique (Dafalias et al., 1979) holds also for clays. The results also show that the shape factors,  $\bar{f}$ , are dependent on the type of soils. It could further be observed from the results presented in Tables 5-8 that the anisotropy index,  $A$ , increases with decreasing void ratio and reaches a constant value at low stress levels.

##### 5. Electrical Properties in Relation to Mechanical Properties.

It has been shown that the principal factors influencing the dielectric dispersion of fine grained soils in the radio frequency range ( $10^6 - 10^8$  HZ) are the compositional properties of the different phases and the heterogeneous nature of the system. The engineering properties of fine grained soils are also controlled by these factors. This mutual dependency is used as a basis to correlate the electrical properties to mechanical properties.

The purpose of this research is to establish possible correlations between those parameters which are needed for the prediction of stress-strain behavior of fine grained soils and the appropriate electrical parameters. It will then be possible to determine the stress-strain behavior of fine grained soils by estimating these mechanical properties from the above correlation and using them in a suitable constitutive model. This approach facilitates the determination of the stress-strain behavior of soils by non-destructive in situ measurements since the electrical properties can be determined in situ without disturbing the structure of the soil.

Any constitutive model for the prediction of stress-strain behavior of fine grained soils would require the knowledge of the slope of the consolidation line,  $\lambda$ , the slope of the swelling line,  $\kappa$ , the slope of the critical state line,  $M$ , the initial void ratio,  $e_0$ , and the overconsolidation ratio (along with other model parameters appropriate for the model under consideration). These parameters are defined in Figure 34. The water content of the fine grained soils can be determined by conventional procedures and the initial void ratio,  $e_0$ , could be evaluated. The correlations between the electrical properties and the mechanical properties  $\lambda$ ,  $\kappa$  and  $M$  for normally consolidated soils would be established in the following sections.

#### 5a. Compression Index, $\lambda$

Bolt (1956) has been able to predict the compression characteristics of clays using Gouy-Chapman diffuse double layer theory and Van't Hoff's theories of parallel platy particles. Compression characteristics of Na-Montmorillonite and Na-illite were found to be close to the predicted one. However, the theory was found to be useful only in the case of clays exhibiting very strong colloidal properties such as montmorillonite. Deviations from Bolt's findings have been reported by Mitchell (1960) and Olsen and Mitronovas (1962) and are ascribed mainly to particle orientation. Quigley and Thompson (1966) have observed fabric changes in natural Leda clay during consolidation using x-ray diffraction methods. It has further been shown by Rosenquist

(1959) that the compressibility of clay is dependent on the type as well as the valence and concentration of ions adsorbed on the surface of the clay particle. From this discussion it is evident that the compression index will depend on the type and amount of clay mineral and the electrical interaction between clay particles and the resulting structure of the soils.

The factors that influence the magnitude of dielectric constant,  $\Delta\epsilon_o$ , were investigated in detail by Arulanandan et al. (1973). It was shown that  $\Delta\epsilon_o$  predominantly depends on the type and amount of clay mineral and the structure of soils. The water content and the pore fluid composition have negligible effect on the magnitude of dielectric dispersion. The experimental results presented in Figures 11-30 further confirm this finding. Therefore one would expect a correlation between the slope of isotropic consolidation line,  $\lambda$  and the magnitude of dielectric dispersion,  $\Delta\epsilon_o$ , because of their mutual dependency. Sharlin, J.R. (1972) has shown that such relationship indeed exists in the case of fine grained soils as shown in Figure 35. The relationship between  $\lambda$ , obtained from the isotropic consolidation tests for the soils reported in this research (Figure 36) and  $\Delta\epsilon_o$  of the respective soils shows a close agreement with the earlier finding of Sharlin, J.F. (1971). This confirms the general validity of the relationship between the slope of isotropic line,  $\lambda$  and the magnitude of dielectric dispersion,  $\Delta\epsilon_o$ .

#### 5b. Swell Index, $\kappa$

Lambe (1960) discussed the physico-chemical forces acting on a clay particle. The fluid pressure between two clay particles is higher than the pore pressure of the free water due to the relatively higher cation concentration between the particles. The pressure difference between two points, one within two clay particles and the other in the free water, is considered to be numerically equal to the electrical repulsive forces acting between two platy clay particles. If these repulsive forces are very strong in a given type of soil, one would expect this soil to swell considerably on the

removal of the external loads so that the equilibrium forces acting on a particle would be maintained. The voids between two clay particles would be larger, if these repulsive forces are strong, compared to the inter particle voids in soils with weaker repulsive forces.

Thus, with the cluster concept (Michael et al., 1954 and Quirk, 1959) one could argue that the soil which has higher proportions of intra cluster void ratio with respect to the inter cluster void ratio at a particular total void ratio, would swell more on removal of load compared to the soil with lower proportions. The ratio of intra and inter cluster void ratios,  $e_i/e_p$  can not be quantified considering two parallel particles since the clay particles aggregate and exist in a random arrangement. The electrical method of quantifying  $e_i/e_p$  accounts for the structure of the soils, since no assumptions are made regarding the arrangement of clay particles in quantifying the inter and intra cluster void ratios using the electrical methods.

On the basis of the preceding discussion, the swell index,  $\kappa$ , was correlated with  $e_i/e_p$  at a common total void ratio of  $e = 1.0$ , i.e.  $(e_i/e_p)_e = 1.0$ . The values of  $e_i/e_p$  at  $e = 1.0$  for different soils were obtained from Figure 32 and the values of  $\kappa$  were obtained from Figure 36. A linear relationship between  $e_i/e_p$  at  $e = 1.0$  and  $\kappa$  is evident on a log-log space as shown in Figure 37 Anandarajha (1982).

### 5c. Slope of the Critical State Line, M

When a soil element is sheared under drained or undrained conditions, experimental results indicate that the soil element fails when the stress path reaches the critical state line independent of the initial stress state of the soil element (Schofield et al., 1968) as illustrated in Figure 34. At failure, the void ratio and the effective mean normal pressure lie on a unique line, referred to as a critical state line, on the  $e$ - $p$  space as shown in Figure 34. This concept, widely known as critical state concept (Roscoe et al., 1968) is the basis of the Cam-clay theory developed by the Cambridge group. From this discussion, it is evident that the slope of the critical state line, on the  $p$ - $q$  space, represents the ultimate shear strength of the soils.

Lambe (1960) has discussed the factors controlling the shear strength of soils. The major component of ultimate shear resistance of fine grained soil is considered to be friction. Figure 37 illustrates different ways in which dilatancy and frictional behavior could be mobilized. One could therefore say that "M" is a function of particle size, shape, surface texture and the structure of soils resulting from the electrical attractive and repulsive forces between clay particles.

The shape factor,  $\bar{f}$ , defined in the expression,  $\bar{F} = n^{-\bar{f}}$ , (Dafalias et al., 1979) is a function of the shape of the particles and cementation in the case of sands. However, in clays, the shape factor would reflect the physico-chemical interaction between particles which depends on shape, composition and arrangement of particles.

The factors influencing the formation factor can also be examined from the theoretical equations for conductivity obtained from the three-element electrical model. From Equations 3a and 4,

$$\sigma_{\omega=0} = \frac{ak_r k_s}{k_s(1 - n_p) + k_r n_p} + bk_r + ck_s \quad (15)$$

$$\frac{k_s}{\sigma_{\omega=0}} = \frac{(1 - n_p) + \left(\frac{k_r}{k_s}\right) n_p}{bn_p + b\left(\frac{k_r}{k_s}\right)^2 n_p + an_p(1 - n_p) + an_p^2\left(\frac{k_r}{k_s}\right) + a\left(\frac{k_r}{k_s}\right)} \quad (15a)$$

where  $a = 1/t^2$ ,  $n_p = 1 - d =$  inter cluster porosity,  $bt^2 =$  cluster contact area/area of the solution-cluster path.

It is approximately true that  $F \approx k_s/\sigma_{\omega=0}$ . Therefore,

$$F = \frac{k_s}{\sigma_{\omega=0}} = \text{function} \left( n_p, t, \frac{k_r}{k_s}, b \right) \quad (16)$$

The ratio of the conductivity of the cluster to the conductivity of solution  $k_r/k_s$ , reflects the intra cluster void ratio and fabric of the soil and,  $t$ , the tortuosity reflects the particle shape, size and the fabric of the soil.

Therefore, it could be argued that the shape factor,  $f$ , which relates the formation factor to the total porosity is a function of the shape, size and texture of the clay particles, and the fabric of the soils. The anisotropy index,  $A$ , was found to be another parameter controlling the strength in the case of sands. Soils which exhibit higher anisotropy would have lower strength when measurements are made in the direction of the major principal axis.

Based on these considerations, it is considered that an electrical index,  $A^2/\bar{I}$ , may be related to "M", since the factors influencing these two parameters are the same.

In order to be able to predict the stress path in the  $p$ - $q$  space and the stress-strain behavior in the  $q$ - $\epsilon$  space, it is necessary to obtain "M" so that when values of  $\lambda$ ,  $\kappa$ , and  $M$  are used in a chosen constitutive model, the predicted and the observed stress-strain relationships would be reasonably close. Two constitutive models, namely the basic Cam-clay model developed by the Cambridge group and a bounding surface plasticity model developed by Dafalias et al. (1980) were chosen for this purpose.

The procedures recommended by Schofield et al. (1968) were followed in obtaining the "M" values. According to Cam-clay theory, the relationship between  $\lambda \log_e p$  and  $q/p$  should be linear, where the stress variables correspond to undrained conditions. An example of the experimental relationship between  $\lambda \log_e p$  and  $q/p$  for the soil type Snow Cal (60%) + Illite (40%) is shown in Figure 39. The slope of this straight line is  $M(\lambda - \kappa)$ . Thus, knowing  $\lambda$  and  $\kappa$ , the slope of critical state line,  $M$ , can be determined.

A calibration procedure (Herrmann et al., 1981) was followed in obtaining "M" values using bounding surface plasticity model. The details of these theories would be found in the latter part of this report.

The relationship between the electrical index,  $A^2/\bar{I}$ , (Table 13) and the slope of the critical state line,  $M$ , obtained from Cam-clay theory and the bounding surface plasticity theory are shown in Figures 40 and 41, respectively. The reasonably good

non-linear relationship between  $M$  and  $A^2/\bar{f}$  indicates that the factors controlling " $M$ ", which is a mechanical property, and  $A^2/\bar{f}$ , which is an electrical property, are related to each other.

## **6. In Situ Prediction of Stress-Strain Behavior of Cohesive Soils**

Application of the theory of plasticity has gained wide popularity over the past few years for the analytical prediction of stress-strain relationship of soils. The most notable and earliest of the constitutive models developed using the theory of plasticity is the Cam-clay theory developed by the Cambridge group (Schofield et al., 1968). The Cam-clay model can represent the strain hardening behavior depending on the state of the soil with respect to the critical state line. The verification of the Cam-clay model under simple shear and triaxial stress states has been carried out satisfactorily on soils that are "wet" of critical state (Roscoe et al., 1968). However, this model has not been demonstrated to be representative of the strain softening behavior of the soils. Yield surface, along with the normality rule, gives rise to prediction of unrealistic behaviors off isotropic loading. This is due to the fact that the yield surface derived as the result of assumptions made in Cam-clay theory does not intersect the  $p$ -axis at right angle.

Roscoe et al. (1968) modified the theory by introducing an ellipse for the yield surface and using normality condition. The size of this elliptic yield surface is completely defined by the initial isotropic consolidation pressure,  $p_0$ , and the slope of the critical state line,  $M$ . The value of  $R$ , which is defined as the ratio of the mean normal pressure,  $p_0$ , at which the yield surface intersects the  $p$ -axis and the mean normal pressure,  $p_1$ , at which the yield surface intersects the critical state line (refer to Figure 42), is assumed to be 2.0, a constant value. It is, however, desirable to be able to use different values of  $R$  in the theory in order to be able to predict the stress-strain behavior of a broad range of soil types.

Numerous theories have since been developed to describe the stress-strain behavior of soils under a general loading condition. Bounding surface plasticity model (Dafalias et al., 1980), cap model (Di Maggio et al., 1971), endochronic theory (Valanis et al., 1971), and model developed by Prevost (1978) are some of them.

The bounding surface plasticity model has been developed to describe a generalized stress-strain behavior of fine grained soils under a variety of conditions such as normally consolidated and over consolidated, strain hardening and strain softening, monotonic and cyclic, compression and extension, loading paths in the tension zone (i.e., the effective mean normal stress is tension), etc. The verification of this theory under some of the above conditions has been carried out satisfactorily. The value of  $R$  can be varied as required to predict a given experimental stress-strain relationship, unlike in the case of critical state theory developed by Roscoe et al. (1968). When  $R = 2$ , these two theories predict identical stress-strain behavior in the case of normally consolidated soils.

For the purpose of this research, the feasibility of using the basic Cam-clay theory (Schofield et al., 1968) and a bounding surface plasticity theory developed by Dafalias et al. (1980) for the prediction of the stress-strain behavior of normally consolidated fine grained soils, will be discussed in the following sections.

#### 6a. Basic Cam-Clay Theory

The Cam-clay theory was developed utilizing the critical state concept, as discussed earlier. The stress and strain variables in the triaxial space are defined as follows:

$$\sigma_1' = \sigma_1 - u \quad (17a)$$

$$\sigma_3' = \sigma_3 - u \quad (17b)$$

$$q = \sigma_1' - \sigma_3' \quad (17c)$$

$$p = (\sigma_1' + 2\sigma_3')/3 \quad (17d)$$

$$\dot{\epsilon} = 2/3 (\dot{\epsilon}_1 - \dot{\epsilon}) \quad (17e)$$

$$\frac{\dot{v}}{v} = \dot{\epsilon}_1 + 2\dot{\epsilon}_3 \quad (17f)$$

$$\dot{\epsilon} = \dot{\epsilon}^e + \dot{\epsilon}^p \quad (17g)$$

$$\frac{\dot{v}}{v} = \left(\frac{\dot{v}}{v}\right)^e + \left(\frac{\dot{v}}{v}\right)^p \quad (17h)$$

where

$\sigma_1$	=	total vertical stress
$\sigma_3$	=	total lateral stress
$u$	=	pore pressure
$\sigma_1'$	=	effective vertical stress
$\sigma_3'$	=	effective lateral stress
$q$	=	deviatoric stress variable
$p$	=	effective mean normal pressure
$\dot{\epsilon}$	=	deviatoric strain increment
$\dot{v}/v$	=	volumetric strain increment
$\epsilon^e$	=	elastic deviatoric strain increment and
$\epsilon^p$	=	plastic deviatoric strain increment
$\dot{p}$	=	volumetric stress increment
$\dot{q}$	=	deviatoric stress increment

The stress-strain theory has been derived using a power law and a stability criteria and assuming that the soil does not display any recoverable shear strain, as follows:

Energy balance criteria,

$$p\left(\frac{\dot{v}}{v}\right)^P + q(\dot{\epsilon})^P = M p |\dot{\epsilon}^P| \quad (18)$$

Normality concept,

$$\dot{p} \left(\frac{\dot{v}}{v}\right)^P + \dot{q}(\dot{\epsilon})^P = 0 \quad (19)$$

Using Equations 18 and 19, the equation of the yield surface can be derived as follows:

$$\frac{q}{p} = M \log_e \left( \frac{p_0}{p} \right) \quad (20)$$

where  $p_0$  = preconsolidation pressure as defined in Figure 42. The material behavior is elastic if the stress state lies within the yield surface and is plastic if the stress state lies outside. The relationships between  $q$ ,  $p$  and  $v$  for undrained condition are shown in Figure 42.

The expression representing the normally consolidated undrained stress-path can be derived based on the fact that the volume of the sample does not change during the test. This is given by Equation (21)

$$\frac{q}{p} = \frac{M \lambda}{\lambda - \kappa} \log_e \left( \frac{p_0}{p} \right) \quad (21)$$

The undrained stress-strain relationship is given by Equation (22)

$$\dot{\epsilon} = \frac{1}{M - \eta} \frac{\lambda - \kappa}{1 + e} \frac{\dot{p}}{p} + \frac{\dot{\eta}}{MP} \quad (22)$$

where

$$\eta = q/p \quad (22a)$$

$$\dot{\eta} = \frac{\dot{q}}{p} - \eta \frac{\dot{p}}{p} \quad (22b)$$

Using Equation 21,

$$q_u = M p_0 \exp - \left( \frac{\lambda - \kappa}{\lambda} \right) \quad (23)$$

where  $q_u$  is the deviatoric stress of normally consolidated soil at failure.

The undrained stress-strain behavior of a normally consolidated soil under triaxial loading conditions is fully defined by Equations 21 and 22. The information required for the analytical prediction of stress-strain behavior is  $\lambda$ ,  $\kappa$ ,  $M$ ,  $e_0$  and  $p_0$ .

## 6b. The Bounding Surface Plasticity Model for Cohesive Soils

In this section the basic features of the bounding surface plasticity model for cohesive soils will be presented, emphasizing the concepts rather than the analytical formulation which can be found in given references. Particular attention will be given in describing the role of the constitutive constants since these are the final objectives of the effort to correlate mechanical with electrical properties.

### 6b.1. The General Concept

Let us first present the salient features of the bounding surface concept, and in order to be specific the presentation will be associated with the particular formulation for cohesive soils. Assuming plastic isotropy, the analytical expression for the bounding surface in the space of stress invariants is given by

$$F(\bar{I}, \bar{J}, \alpha, e'') = 0 \quad (24)$$

where  $I$ ,  $J$  and  $\alpha$  stand for the first stress invariant, the second deviatoric stress invariant and the Lode angle (depends on the ratio of the second and third deviatoric stress invariants), respectively, a bar over stress quantities imply stress states on  $F=0$  and finally  $e''$  represents the plastic change of the void ratio (the change of the void ratio due to plastic volumetric strains). Exact definitions of the above can be found in [Dafalias et al. 1982]. The  $e''$  is the only plastic internal variable which controls the hardening/softening response. A typical schematic representation of the bounding surface is shown in Fig. 43 by means of 2 ellipses and one hyperbola in the meridional section of the  $I, J$  space, but notice that  $\alpha$  enters also the description assuming a fixed value for each such meridional section, on which the model parameters  $N$ ,  $A$  and  $R$  depend (to be explained subsequently). The influence of  $e''$  appears through the

dependence of  $I_0$  on it,  $I_0$  being the intersection with the positive  $I$  axis. Such a surface could also play the role of a classical yield surface and here is where the concept of the bounding surface is introduced: instead of viewing the surface described by eq. (24) as a locus of points in stress space which sharply delineate the purely elastic (inside the surface) from the elasto-plastic domain (on the surface), it is rather viewed as a bounding envelope of elasto-plastic stress states in or on the surface, with an additional property: the closer is an actual stress state to the surface, the more extensive is the corresponding increment of plastic deformation for a given stress increment.

In order to present a well defined analytical form of the above properties, the following concepts have been developed [Dafalias 1981, Dafalias et al. 1982]. For each actual stress state  $I, J, \alpha$  in or on the surface (observe that for a general development not restricted to isotropy, the stress state should be defined by means of the stress components not just their invariants), Fig. 43, a corresponding unique "image" stress state  $\bar{I}, \bar{J}, \bar{\alpha}$  on  $F = 0$  is defined by means of a properly defined mapping rule. In the present formulation the "radial mapping" rule is employed which is shown in Fig. 43 and which essentially defines the "image" stress state by projecting radially the current state  $I, J, \alpha$  onto  $F = 0$  using a properly defined stress point as the center of projection. Here, such a point  $I_C$  will be chosen to lie always on the  $I$ -axis and given by  $I_C = CI_0$  ( $0 \leq C \leq 1$ ). In Fig. 43 the value  $C = 0$  is used, i.e. the projection center is the stress origin  $0$  itself. Observe that on the basis of the above definition of the mapping rule  $\bar{\alpha} = \alpha$  since they both refer to the same meridional section. For a discussion of the general conditions that any mapping rule must satisfy, the reader is referred to [Dafalias, 1981]. It suffices here to say that when the actual stress point lies on  $F = 0$ , its "image" is identical to it. Obviously this is satisfied by the present "radial mapping" rule.

The definition of the "image" stress serves two purposes. First, at the "image" stress the corresponding gradient  $\nabla F$  defines the loading-unloading direction at the actual stress. In order to visualize this, one may think of the "vector"  $\nabla F$  translated parallel to itself from  $\bar{I}, \bar{J}, \alpha$  or  $F = 0$  where it is defined, to  $I, J, \alpha$  where it acts, Fig. 43. Second, the Euclidean distance  $\delta$  between  $\bar{I}, \bar{J}, \alpha$  and  $I, J, \alpha$  is a measure of the proximity of the actual stress to the bounding surface and its effects on the plastic stiffness is expressed by:

$$K_p = \bar{K}_p + h(\alpha) H(I, J, \alpha, e'') \frac{\delta}{\langle r - s\delta \rangle} \quad (25)$$

- where:
- $K_p$  = The actual plastic modulus.
  - $\bar{K}_p$  = A bounding plastic modulus associated with the "image" stress and obtained from the consistency condition  $\dot{F} = 0$ .
  - $h$  = a shape hardening parameter; a function of  $\alpha$ .
  - $H$  = a function of the state (used to normalize the plastic modulus).
  - $r$  = the Euclidean distance between the projection center and the "image" stress.
  - $\langle \rangle$  = the McCauley brackets defining the operation  $\langle A \rangle = A$  if  $A > 0$  and  $\langle A \rangle = 0$  if  $A \leq 0$ .
  - $s$  = the elastic factor, such that for  $\delta > r/s \Rightarrow \langle r - s\delta \rangle = 0 \Rightarrow K_p = \infty$ .

Indeed the definition of  $F = 0$ , eq. (24), and the corresponding definition of the mapping rule together with eq. (25) are the cardinal elements of a bounding surface formulation. For  $\delta = 0$  (point on the bounding surface), eq. (25) yields  $K_p = \bar{K}_p$ , i.e. the bounding surface behaves like a yield surface. The effect of each of the above parameters, will be considered in the following subsections where all material and model constants are discussed systematically.

#### 6b.2. State Variables and Constitutive Constants

Frequently there is confusion in the literature of constitutive modeling on the meaning attributed to the words material or model constants, parameters and variables. The ultimate goal of a constitutive model for history dependent inelastic deformation is to relate the stress increment to the strain increment (or rates) and vice-versa. To this end a number of other variables enter the formulation which effect the above stress-strain rate relations in each step, embodying basically the effect of past loading history. These are frequently called internal variables and can also be called model parameters in the sense that they must be updated in each step in order to provide the proper stress-strain rate relation. These model parameters are not constants and their number effects greatly the storage requirement and efficiency of a constitutive model. In the present formulation the bounding surface model has only one internal variable or model parameter, the  $e''$  or respectively the  $I_0$  (eq. (24)), recalling that the changes of  $I_0$  and  $e''$  are related. It follows that the state of the material is defined by means of the stress and the internal variables, here the  $I_0$ . The initial values of the state variables must be known before any loading process, but let us carefully avoid confusing these initial values with the constitutive constants.

The constitutive constants, as their name implies, are constants whose values are determined during the calibration process and remain constant (for the given material) throughout any subsequent stress-strain history. Again their number and ease of calibration affect the efficiency of the model. Note that for one and the same material the same values of these constants must be used, inhomogeneity due to the state (not the material) can be described by means of the different values of the state variables (stress state and internal variables). Of course, more general inhomogeneity implies different material from location to location, thus yielding different constitutive constants in addition to possible differences of the state. Expecting, however that large portions of the structure under analysis are made from the same material, only one set of constitutive constants must be stored for each portion, while as many

sets of state variables or model parameters must be stored and updated, as is the number of points used in each portion for a finite element analysis. Thus, having a small number of model parameters is much more important for numerical computations than a small number of constitutive constants.

### 6b.3. Constitutive Constants for the Bounding Surface Model

The constitutive constants for the bounding surface model in its present form can be divided in 3 distinct categories.

#### 6b.3a. The classical material constants

These are constants related to a specific material property which is invariant with respect to loading history, within the limits of approximation and experimental error. As such, they can be determined by classical experiments.

The first is the consolidation index  $\lambda$ , i.e. the slope of the normal consolidation line in the  $e-\ln(p)$  plot.

The second is the rebound or swell index  $\kappa$ , i.e. the slope of the swell and recompression line in the  $e-\ln(p)$  plot, and is directly related to the elastic bulk modulus  $K$  for elastic strain increments. The  $\lambda$  and  $\kappa$  define in combination the change of  $I_0$  with respect to changes of  $e''$ , and more precisely the above relation depends on their difference  $\lambda - \kappa$ . This is expected since  $\lambda$  is a "tangent" modulus encompassing both plastic and elastic deformations, while  $\kappa$  is only reflecting elastic volumetric strains, thus  $\lambda - \kappa$  naturally appears related to the change of plastic strains only and therefore to the hardening process (change of  $I_0$  with respect to  $e''$ ).

The third constant is the elastic shear modulus  $G$  which can be obtained from the initial slope of a deviatoric stress versus deviatoric strain curve divided by three, in a typical triaxial experiment. An alternative way is to consider instead the third constant to be Poisson's ratio  $\nu$  and obtain  $G$  indirectly by mean of  $\nu$  and the bulk modulus  $K$  (depending on  $p$  and  $\kappa$ ). This yields a variable  $G$  with  $p$ , which although giving better results in many cases does not satisfy the requirement that elastic

strain should be obtained from a potential of the stresses and vice-versa. The reason for this apparent inconsistency is that  $K$  and  $G$  are more complex function of the stress state than presently assumed.

The fourth material constant is the critical state line slope  $M_c$  (compression) in  $q$ - $p$  space, related to the friction angle. Although a corresponding  $M_e$  (extension) can be obtained from  $M_c$  by assuming Coulomb criterion, it is more accurate to specify  $M_e$  as an independent material constant by extension experiments. Observe that in the invariant stress space  $N = M/\sqrt{3}$ , Fig. 43.

#### 6b.3b. Model constants associated with the shape of the bounding surface

The model constant considered in this and the following subsection, influence the material response indirectly and are not associated with any distinct scalar material property, thus they are called model constants rather than material constants. Fig. 43 will clarify the contents of this subsection.

The shape of the bounding surface must satisfy certain general requirements such as it must intersect the  $I$  axis at points ( $I_0$  and  $I_1$ ) where the normal to the surface is along the axis (isotropy), and at the intersection with the CSL (Critical State Line) the normal must be parallel to the  $J$  axis (critical failure with zero volumetric strain). Besides these two requirements, there is no definite reason to prefer one shape from another. In the course of the development of this model it was found that one shape which can provide a very good fit of experimental data was obtained by a combination of 2 ellipses and one hyperbola as shown in Fig. 43.

Ellipse #1 is defined by the variable  $R$ , function of  $\alpha$ , by means of its values  $R_c$  in compression and  $R_e$  in extension and an interpolation rule for all other values of  $\alpha$ . The  $R$  determines the  $I_1 = I_0/R$  and hereby the shape of the ellipse, since  $I_0$ - $I_1$  and  $J_1$  are the two principal axes. The values of  $R_c$ , and  $R_e$  can be obtained by curve fitting the equation of the undrained stress path in triaxial compression and extension, respectively. Notice also that  $R$  measures the "distance" between the normal

consolidation and the critical state lines in the  $e$ - $\ln p$  plot. Ellipse  $\alpha 1$  is closely related to the behavior of normally consolidated or slightly overconsolidated samples in the wet side of the CSL, as is obvious from its position with respect to  $I_0$ .

If one now attempts to use the extension of Ellipse  $\alpha 1$  to the left of the point C, Fig. 43, for heavily overconsolidated samples, it will be impossible to properly fit experimental data for this range. Experience shows that a surface closer to the CSL is required, and as such a hyperbola is introduced with an asymptote parallel to CSL. Its proximity to CSL is controlled by the scalar quantity  $A$ , Fig. 43, which in general depends on  $\alpha$  and, therefore, requires two model constants for its determination, i.e. its values  $A_c$ ,  $A_e$  in compression/extension. These model constants can be determined by fitting the stress-strain curves at large OCR, especially by fitting the peak stress. The smaller is the values of  $A$ , the lower is the value of peak stress etc.

Finally, the bounding surface extends into the purely tensile range ( $I < 0$ , compressive stress: positive) as Ellipse #2, requiring one more model constant  $T$  which defines its intersection  $I_t$  with the  $I$  axis by  $I_t = TI_0$ . There is not much experimental evidence to be used for the accurate determination of  $T$  at this stage, but it is expected that  $T$  is proportional to the cohesive strength of the material.

In summary, the following 5 model constants define the shape of the bounding surface:  $R_c$ ,  $R_e$ ,  $A_c$ ,  $A_e$  and  $T$ . It is expected that the use of only three constants  $R = (R_c + R_e)/2$ ,  $A = (A_c + A_e)/2$  and  $T$  can give satisfactory agreement with experimental data. Moreover, often  $A$  and  $T$  may be fixed at typical values of 0.02 and 0.1, respectively, leaving only  $R$  as the only important model constant for the shape of the surface.

#### 6b.3c. Model constants associated with response for $OCR > 1$

The first such constant is  $C$  defining the projection center  $I_C = CI_0$ . In Fig. 43 the particular case for  $C = 0$  is only shown. The determination of  $C$  requires at least two undrained stress paths at small and large OCR, since the position of  $I_C$  essentially determines the shape of these paths in the  $q - p$  (or  $J - I$ ) space. From experience, it is expected to be between 0.3 and 0.5.

The remaining constants are associated with eq. (25). The value of  $s > 1$ , defines a range of purely elastic response within the bounding surface, called the elastic nucleus since for  $\delta > r/s$  one has  $K_p = \infty$  according to the definition of  $\langle \rangle$ . Again its value can be obtained by observing the shape of the undrained stress path, namely when it deviates from a straight-up line in the  $p - q$  space it indicates the boundary of the elastic nucleus. Its value controls also cyclic stabilization. It is possible to fix the value of  $s$  at a typical value between 1.5 and 2.

And finally, 2 additional and perhaps not important constants for  $OCR > 1$  define the values of the shape hardening parameter  $h$  in compression ( $h_c$ ) and extension ( $h_e$ ), thus  $h$  is obtained by interpolation. It is again expected that a single constant  $h = (h_c + h_e)/2$  will provide very good results. The greater is the value of  $h$ , the stiffer is the response within  $F = 0$ , and as a matter of fact as  $h \rightarrow \infty$  one retrieves the classical yield surface formulation since then  $K_p = \infty$  from eq. (25) for points within the bounding surface.

In summary, the following 4 constants are necessary for  $OCR > 1$  :  $C$ ,  $s$ ,  $h_c$  and  $h_e$ .

#### 6b.3d. A final conclusion

Averaging the values of different constants in compression and extension and fixing some of them at typical values, one finally ends up with the following set of 9 material and model constants:  $\lambda$ ,  $\kappa$ ,  $G$ ,  $M$ ,  $R$ ,  $A$ ,  $C$ ,  $s$  and  $h$ .

Even further,  $A$ ,  $C$  and  $s$  can be fixed for classes of typical clay soils, and one is left with only 6 constants:  $\lambda$ ,  $\kappa$ ,  $G$ ,  $M$ ,  $R$  and  $h$ . The effort of this project is to

obtain a correlation between electrical measurements and the above constants, thus enabling us to predict the soil constitutive model by in-situ measurements (the electrical ones) and hence be able to perform analysis of earth structures on the basis of the calibrated bounding surface soil plasticity model.

#### 6b.4. Laboratory Calibration of the Bounding Surface Model

In order to provide checks for the electrical measurement calibration procedure that is being developed as part of this research, means must be available for calibrating the model using standard laboratory, triaxial test data. In this section a brief description of a computer aided semi-automated calibration scheme for using such data is given; greater detail and examples are given in reference (DeNatale, et al. 1983, DeNatale, 1982). If different behavior in extension and compression is to be modeled the scheme requires that data from at least six triaxial tests (three in extension and three in compression) be available, in addition to isotropic consolidation and rebound data. If similar (or average) behavior in compression and extension is assumed then only three test results need be available.

In formulations such as the Bounding Surface model, which employ a small number of constitutive constant whose roles in the constitutive formulation are each well defined, the calibration process becomes systematic and straightforward. However, reliance on user expertise is still high, since all manual curve fitting procedures, by their very nature, require both judgement (in deciding just what constitutes the "best" overall fit) and familiarity (in deciding how much each constants value must be changed to improve a given prediction).

In order to simplify the model calibration process, a computer code has recently been developed by DeNatale (1982) and tested on a variety of real soils. The code employs a Quasi-Newton optimization strategy to locate that set of paramter values which minimizes the discrepancy between the model predictions and the experimental observations included in the calibration data base. Because this new computer aided prcedure greatly reduces the dependence of calibration success on user expertise, it significantly increases the accessibility and usefulness of sophisticated material models to the general engineering community.

#### 6b.4a. Objective function

Since the calibration of a material model involves minimizing the error, or residual, between the observed and predicted soil response, the process can quite naturally be viewed as an optimization problem. Therefore, in order to develop a computer directed calibration procedure, it is necessary to (i) construct an objective function to serve as a scalar measure of the goodness of a particular solution, and (ii) select a search strategy to enable the minimum of this function to be located in an efficient and reliable manner.

For those cases in which all aspects of the soil response can be expressed in terms of a single quantity (by using, for example,  $q$  vs  $\epsilon_1$ ,  $u$  vs  $\epsilon_1$  and  $p'$  vs  $\epsilon_1$  rather than  $q$  vs  $p'$ ,  $q$  vs  $\epsilon_1$  and  $u$  vs  $\epsilon_1$ ), a vertical measure of the residual may be reasonable. However, if the distinction between independent and dependent variables cannot be made clear, there is no more reason to use a vertical measure ( $y=y(x)$ ) than there is to use a horizontal measure ( $x=x(y)$ ). In these cases it is probably more appropriate to use a measure such as the shortest distance between the experimental observation and prediction curve. While there is no reason to suspect that this alternative is theoretically more sound, such a "Euclidean" measure is probably closer to what one intuitively uses when estimating the error between two curves.

The calibration code permits either absolute or squared residuals, to be used to form the objective function. When these two options are combined with the choice of either a vertical or a Euclidean measure (as described above), the user has four possible ways to define the error at a point. Recent research by DeNatale (1982) has shown that the location of the global minimum remains essentially the same, regardless of which options are used. However, preliminary applications to a variety of artificial and real soils indicated that the absolute Euclidean measure results in a more well-behaved objective function that can be most easily minimized.

In order to combine the residuals at various points within a given relation (for example, the  $q$  vs  $\epsilon_1$  relation from a test at OCR=1), or from relations of the same kind obtained from different tests (for example, the  $u$  vs  $\epsilon_1$  relation from tests at OCR=1 and 2), it is necessary to first define what is meant by "equal" error. A given solution could be defined to be equally good at two points A and B if either (i) there was the same absolute error at both A and B, or (ii) there was the same relative error at A as at B. The decision as to which definition of equality should be used is entirely up to the user. The computer code permits the use of either extreme, or any strategy in between. Consequences of the various choices are discussed further in DeNatale (1982). It should be noted that most physical analogies lie somewhere in the middle - a given dial gauge or pore pressure transducer may be accurate to within  $\alpha\%$ , but may fail to register any meaningful readings below a magnitude of  $\beta$ .

The code permits any number of tests, relations and/or individual observations to be included in the calibration data base. Because the various response relations will generally be of different dimensions (such as stress vs stress, stress vs strain, strain vs strain, etc.), all data is nondimensionalized so that the errors from different relations can be properly combined. Different weights may be assigned to specific components of the data base if it is felt that certain tests, relations or observations are more reliable or representative than others, or if it is necessary to have the final model predictions fit some data more closely than others. The consequences and proper role of weighting factors is again discussed in DeNatale (1982).

#### 6b.4b. Optimization strategy

An extremely large number of optimization strategies have been suggested over the last 30 years, with the performance of a given approach being strongly dependent on the particular type of problem to which it is applied. Hence, it is generally agreed that there is no single best algorithm, but, rather only strategies which perform best when applied to certain classes of problems.

In selecting the most suitable approach, a key factor is whether or not first

and second derivative information can be readily obtained. With the Bounding Surface model, as with most sophisticated material models, the governing equations are so complex that it is essentially impossible to directly relate the relevant response parameters (such as  $p$ ,  $q$ ,  $u$ ,  $\epsilon_1$ , etc.) to the constitutive constants employed by the formulation. Thus, the objective function must be formed by summing a series of discrete weighted residuals, and therefore first and second derivative information is not explicitly available.

Under these conditions, the current consensus among those most active in optimization research is that a Quasi-Newton strategy with finite difference approximations to derivatives will, if properly implemented, generally exhibit the most efficient and reliable performance. Hence, a Quasi-Newton strategy was incorporated into the calibration code to direct the search.

Finally, the code permits constraints to be imposed on the various constitutive constants in the form of simple bounds

$$l_i \leq x_i \leq u_i$$

where  $l_i$  and  $u_i$  represent the minimum and maximum values that parameter  $x_i$  can assume. A restriction of this kind would be appropriate if either (i) there were certain theoretical restrictions placed on the value which a given parameter could assume, or (ii) there were certain ranges of parameter values beyond which the numerical implementation of the material model became unstable, or (iii) certain material properties were observed experimentally to vary over some finite range, and there was no overwhelming reason to fix them prior to calibration at any particular values.

#### 6b. 4c Application to the Bounding Surface Model

The search for the optimal set of constitutive constant is directed by the Quasi-Newton strategy previously described. However, in order to evaluate the objective function at some location  $x$ , it is necessary to first generate a corresponding set of model predictions. To accomplish this, the calibration code relies on two subroutines

— EVAL and CLAY — developed by Herrmann et al. (1980, 1982) during previous research with the Bounding Surface model and briefly described in the following section. Subroutine performs, essentially, single element incrementaliterative finite element analyses of bodies under a homogeneous state of stress and/or strain. Subroutine CLAY consists of a numerical implementation of the governing constitutive equations, and thus, when called, provides the appropriate material response to the given stress and/or strain increment.

To verify the viability of the new computer aided calibration procedure, the method was applied to a number of representative soil data bases, both artificial and real. The outcome of these studies is discussed by DeNatale (1982).

#### 6b.5 Numerical Implementation of the Model

As noted in the last section, calibrations of a material model to fit laboratory data requires that means be available for numerically evaluating the model, i.e., means for using the model to predict response to various test conditions. Furthermore if a material model is to be of any practical value numerical means must be available for using the model in analyzing engineering structures. To these ends a numerical analysis procedure has been developed for evaluating the bounding surface plasticity model for cohesive soils. This development is briefly discussed in the following sub-sections.

##### 6b.5a Incremental Stress-Strain Relation

The theoretical formulations previously discussed yield a relationship between the rates of the stress and strain components (Herrmann et al., 1980); expressing this relation in matrix form gives:

$$\{\dot{\sigma}\} = [D] \{\dot{\epsilon}\} \quad (26)$$

where  $[D]$  is a matrix whose dependence on the stress state, the internal variable and the constitutive constants follow simply from the basic equations of the bounding surface model Herrmann et al. (1980).

In general the response of an elasto-plastic body is highly nonlinear and path dependent. Thus a general numerical analysis procedure for elasto-plasticity problems requires an incremental solution and unless the increments are made excessively small, iteration must be conducted in each increment to account for the nonlinear behavior.

To be able to use eq. 26 in an incremental solution procedure, it must be expressed in an incremental form. Consider the  $n^{\text{th}}$  step of an incremental analysis; i.e., the solution has been found at  $n-1$ , and it is desired to calculate the incremental change that will give the solution at  $n$ . Because of the nonlinear behavior, iteration is required to establish the incremental change. In the  $k-1$  iteration of this process, the estimates of the stress and strain states at  $n$  are given by

$$\{\sigma\}_{n,k-1} = \{\sigma\}_{n-1} + \{\Delta\sigma\}_{n,k-1} \quad (27)$$

$$\{\epsilon\}_{n,k-1} = \{\epsilon\}_{n-1} + \{\Delta\epsilon\}_{n,k-1} \quad (28)$$

Even though rate independent behavior is being considered, it is convenient to think in terms of the time history of the quantities involved. Integrating eq. (26) from time  $t_{n-1}$  to  $t_n$  and using the trapezoidal formula to approximate the right hand side gives

$$\{\Delta\sigma\}_{n,k} = [\bar{D}]_{n,k-1} \{\Delta\sigma\}_{n,k} \quad (29)$$

where

$$[\bar{D}]_{n,k-1} = \frac{1}{2} [D]_{n-1} + [D]_{n,k-1} \quad (30)$$

Eq. (29) is the desired incremental stress-strain equation for iteration  $k$  of increment  $n$ .

Because  $[D]_n$  is a function of the stress and strain states at  $n$ , it is necessary to base its value on the estimates of the previous iteration (eqs. (27) and (28)). The resulting value, denoted by  $[D]_{n,k-1}$  do not in fact satisfy eq. (30). In general, the estimates of the stress and strain increments used in the calculation of  $[\bar{D}]_{n,k-1}$  do

not satisfy eq. (30). This inconsistency disappears as iteration (at the global level) continues and convergence occurs. However, to speed up the global convergence process, iteration can be introduced in the calculation of  $[\bar{D}]_{n,k-1}$  (e.g., for finite element applications, iteration when the properties for each integration point are calculated) to eliminate this inconsistency; in light of the additional iteration at the system level a rather loose convergence criterion appears to be justified. Thus, the stress estimate is iteratively modified (in this process  $\{\Delta\epsilon\}_{n,k-1}$  is held constant in order to preserve compatibility of the global strain field) to give a refined incremental stress estimate  $\{\Delta\sigma\}_{n,k}^*$  and a corresponding consistent incremental properties estimate  $[\bar{D}]_{n,k-1}^*$  which satisfy eq. (29).

The developed incremental stress-strain relationship has been used in evaluating simple laboratory test results and research is currently being carried out to use it in finite element analysis of engineering structures; preliminary results indicate that the model is exceedingly easy to implement in finite element analysis and is numerically very well behaved. The application to homogeneous tests is described in the next sub-section.

#### 6b.5b. Application to Homogeneous Tests

As previously noted, the assessment of the characteristics of a material model, and in the fitting of it to experimental measurements, a means must be available for using the model to predict the results of simple homogeneous tests. For cohesive soils, program EVAL has been written for this purpose. EVAL can be used to predict the behavior of homogeneous soil samples subjected to arbitrary homogeneous stress and strain histories for either drained or undrained conditions.

The solution history is broken into "history segments." Within each history segment, a consistent combination of six stress and strain components are prescribed (i.e., the histories of  $\epsilon_x$  or  $\sigma_x$ ,  $\epsilon_y$  or  $\sigma_y$ ,... and  $\gamma_{yz}$  or  $\tau_{yz}$ ). A different combination may be prescribed in each history segment. For example, a uniaxial test might involve

two segments with a specified value of axial strain achieved at the end of the first segment and with unloading to zero axial stress specified in the second. Each history segment is broken into increments with the iteration conducted within each increment. The analysis conducted by EVAL is essentially a one-element finite element analysis of a homogeneous body. The analysis is straightforward and well behaved with only two special features worth noting.

Because the analysis can be used for the extreme case when either all the stress or all the strain components are specified, both the stress and strain vectors are checked for convergence. The convergence check on the stress increment, however, must be done with some care. The problem is that the relative measure of error,  $L_1(\Delta\sigma_{n,k} - \Delta\sigma_{n,k-1})/L_1(\Delta\sigma_{n,k})$ , used for the check is meaningless when applied for near failure conditions (because  $\Delta\sigma_i \approx 0$ ,  $L_1(\Delta\sigma_{n,k}) \approx 0$ ). To avoid this difficulty, the denominator of the error measure is limited to a minimum value of  $L_1(\sigma_{n-1})/10$ . In the above, the  $L_1$  norm is the sum of absolute values.

The second feature involves the starting estimate for the strain increment. For the first iteration of the first increment of all history segments beyond the first, special precautions are used to avoid a problem of non-uniqueness that may occur for unstable soil behavior. With strain-controlled loading it is possible to predict soil response for the falling portion of a stress-strain curve. Having arrived at some point in the unstable region, at the end of a particular history segment, a user might switch to stress-control to unload the sample in the next history segment. However, starting from a point on a descending stress-strain curve (or its equivalence for a multi-axial event) the strain may either increase (loading) or decrease (unloading) for a specified reduction in stress; thus, the subsequent behavior is non-unique. Because such a stress controlled specification (from a point on a descending stress-strain curve) is only meaningful for an unloading situation, the analysis must select this path. The selection of the unloading path is assured by using for the initial estimates of the components of the strain increment, for the first iteration of the first increment of each new

history segment, the negative (reduced by the multiple .01 in order to reckon with the stiffer behavior encountered for unloading) of the calculated values for the last increment of the previous history segment.

As previously noted, program EVAL is an integral part of the recently developed model calibration algorithm; it is used for evaluating the residuals (differences between modal predictions and experimental observations) needed to define the objective function in the optimization procedure. It has also been used extensively in verification studies where model predictions are compared to experimental observations, e.g. see Herrmann et al., 1981.

#### 6c. Application to In Situ Prediction of Stress-Strain Behavior

The values of the slope of the critical state line were obtained both from Cam-clay theory and the bounding surface plasticity theory and correlated with an electrical index as described earlier. It can be observed from Equation (21) that a plot of  $q/p$  vs.  $\lambda \log_e p$  would be linear and the slope of the line is  $M/(\lambda - \kappa)$ . The variables  $q$  and  $p$  are the experimentally determined values during the undrained test. Knowing  $\lambda$  and  $\kappa$ , the slope of the critical state line,  $M$ , can then be computed. An example of a plot of  $\lambda \log_e p$  vs.  $q/p$  is shown in Figure 39. The slope is 28.0 and  $\lambda = 0.09918$  and  $\kappa = 0.016399$  for this soil. From this the "M" value is computed to be 2.318. The values of "M" plotted in Figure 40 were obtained in this manner.

The model parameters defining the bounding surface plasticity model can be obtained using a set of triaxial test data by a trial and error procedure, i.e., the model parameters should be chosen so that the predicted and measured stress-strain relationships are close to each other. A computer program was developed Herrmann et al. (1982) as described in the earlier section incorporating the bounding surface theory in order to predict the stresses and strains. This program was used to obtain the value of  $M$  which predicts the relationships of  $q$  vs.  $\epsilon_1$  and  $q$  vs.  $p$  ( $\epsilon_1$  = axial

strain) as close to the corresponding experimental relationships as possible. The values of "M" obtained in this manner are correlated with the electrical index,  $A^2/\bar{f}$  as shown in Figure 41.

It could be observed from Figures 40 and 41 that the values of "M", required by these theories to predict the experimental stress-strain behavior to best of their ability, are different. This could be ascribed mainly to the differences in the shape and size of the yield surface in the Cam-clay theory and the bounding surface in the bounding surface theory. These surfaces are used as plastic potential to define the direction of the plastic strain increment vectors assuming the associated flow rule, as discussed below.

From Equations 23 and 26, the undrained strength of the soil depends on  $\lambda$ ,  $\kappa$ , M, R, and the initial effective confining pressure,  $p_0$ . Since  $R = 2.72$  was used in the bounding surface theory, the undrained strengths predicted by Cam-clay theory would be different from the ones predicted by the bounding surface theory by the ratios of "M". The undrained strengths normalized with respect to the initial effective confining pressures are presented in Table 14.

In order to see how realistic these predictions are, the stress-strain relationships predicted by these theories were compared with the experimental relationships Anandarajha (1982) as shown in Figure 44 for the soil type Snow Cal (60%) + Illite (40%). The comparisons are made on the  $q - \epsilon_1$  space and the  $q - p$  space. It could be noted from Figure 44 that the overall deviations of these predictions from the experimental results are larger in the case of Cam-clay theory.

From this, the bounding surface plasticity theory developed by Dafalias et al. (1980) is considered to be desirable because of its realistic predictions and the generality of the theory for use under various conditions.

Comparison of the experimental stress-strain relationships and the bounding surface predictions for three other soils, Snow Cal (95%) + Bentonite (5%), Marysville Red soil, and Illite are shown in Figures 45-47.

A reasonably good agreement between the experimental and theoretical predictions of stress-strain behavior of fine grained soils is seen from the results presented in Figures 44-47. It is therefore possible to predict the stress-strain behavior of normally consolidated fine grained soils using bounding surface plasticity model if model parameters can be determined by in situ tests. In situ model parameters could be predicted from in situ electrical measurements. Therefore it can be concluded that if in situ electrical measurements (i.e., apparent dielectric constants and conductivity in the radio frequency range along with conductivity of the solution extract) are made in situ, stress-strain behavior of normally consolidated fine grained soils could be predicted.

#### **7. Current Work in Progress**

The work reported above were for the prediction of stress strain behavior of fine grained soils. Current study is concerned with the stress strain behavior of mixed soils (a mixture of sands, silts, natural and artificial clays up to 10 percent).

It should also be noted that the study presented in this report is limited to the prediction of stress strain behavior of normally consolidated soils. Prediction of the in situ stress strain behavior of over-consolidated soils needs to be investigated.

#### **8. Future Work**

It is proposed to investigate the possibility of the prediction of initial in situ stress state using the electrical method. The prediction of in situ stress-strain behavior of over consolidated soils requires a knowledge of O.C.R. or preconsolidation pressure ( $P_c$ ) and the value of  $K$ . It is proposed to establish correlations between the mechanical parameters  $K_o$ ,  $P_c$  and  $K$  and electrical parameters in order to enable the prediction of  $K_o$ ,  $P_c$  and  $K$  in situ.

## 9. Summary and Conclusions

The feasibility of quantifying the inter and intra cluster void ratios by characterizing the soils by electrical methods is investigated. The mechanical properties of fine grained soils related to the stress-strain behavior are quantified by a fundamental characterization of soils by electrical methods. The Cam-clay constitutive model and a bounding surface model were used to predict the stress-strain behavior of the normally consolidated fine grained soils. The bounding surface theory was found to yield more realistic predictions compared to the Cam-clay theory. This study shows that:

1. The inter and intra cluster void ratios can be quantified by characterizing the soils by electrical methods.
2. The mechanical properties required to predict the stress-strain behavior of soils can be determined by electrical methods.
3. Stress-strain behavior of normally consolidated fine grained soils can be determined by electrical methods.
4. Since the electrical properties can be measured in situ, stress-strain behavior of normally consolidated fine grained soils can be determined by the in situ measurements of electrical properties.

## REFERENCES

1. Anandarajha, A., (1982) "In Situ Prediction of Stress-Strain Relationships of Clays Using a Boundary Surface Plasticity Model and Electrical Methods". Dissertation Presented to the University of California, Davis, California in 1982, in partial fulfillment of the requirements for the degree of Doctor of Philosophy, 1982.
2. Arulanandan, K., Smith, S.S., and Linkhart, T.A., "Characterization of Clays by Electrical Methods," Proceedings of the Sixth Annual Meeting of Clays and Clay Minerals Society, 1969.
3. Arulanandan, K. and Mitra, S.K., "Soil Characterization by Use of Electrical Network," Proceedings of the 4th Asilomar Conference on Circuits and Systems, November 1970, pp. 480-485.
4. Arulanandan, K., Smith, S.S., and Spiegler, K.S., "Radio Frequency Properties of Polyelectrolyte Systems," Proceedings, NATO Advanced Study Institute, Forges-les-Eaux, June, 1972.
5. Arulanandan, K. and Smith, S.S., "Electrical Dispersion in Relation to Soil Structure," Journal of the Soil Mechanics and Foundation Division, ASCE, Vol. 99, No. SM12, Proc. Paper 10235, December 1973, pp. 1113-1133.
6. Arulanandan, K., "Fundamental Aspects of Erosion of Cohesive Soils" Journal of the Hydraulics Division, Proceedings of the American Society of Civil Engineers, Vol. 101, No. HYS, May 1975.
7. Arulanandan, K., "Relationship Between Electrical and Mechanical Properties of Soils," Patent Disclosure to Regents of the University of California, Davis, January 1981.
8. Basu, R. and Arulanandan, K., "A New Approach for the Identification of Swell Potential of Soils" Proceedings of the Third International Conference on Expansive Soils, Technion-Israel Institute of Technology, July 1973. Also in Bulletin of the Association of Engineering Geologists Vol. XI, No. 4, 1974.
9. Bolt, G.H., "Physico-Chemical Analysis of the Compressibility of Pure Clays," Geotechnique, Vol. 6, pp. 86-93, 1956.
10. Castel, A.K. and Arulanandan, K., "New Approach to Predict Lime Reactivity of Soils" Journal of the Geotechnical Engineering Division, Proceedings of the American Society of Civil Engineers, Vol. 105, No. GT4, April 1979.
11. Dafalias, Y.F. and Arulanandan, K., "The Formation Factor Tensor in Relation to Structural Characteristics of Anisotropic Granular Soils," Proc. Colloque International du C.N.R.S., Euromech Colloquium 115, Villard-de-Laus, France, June 1979.

12. Dafalias, Y.F. and Arulanandan, K., "Electrical Characterization of Transversely Isotropic Sands," *Archives of Mechanics*, 31, 5, pp. 723-739, Warszawa, 1979.
13. Dafalias, Y.F. and Herrmann, L.R., "A Bounding Surface Soil Plasticity Model," *Int. Symp. on Soils under Cyclic and Transient Loading*, Swansea, U.K., 1980, pp. 335-345.
14. Dafalias, Y.F., "The Concept and Application of The Bounding Surface in Plasticity Theory", *IUTAM Symp. on Physical Non-Linearities in Structural Analysis*, Senlis France, 1980, J. Halt and J. Lemaitre eds, Springer, Berlin, 1981.
15. Dafalias, Y.F. and L.R. Herrmann, "A Generalized Bounding Surface Constitutive Model for Clays", in *Application of Plasticity and Generalized Stress-Strain in Geotechnical Engineering*, R.N. Yong and E.T. Selig Eds, ASCE publishers, 1982.
16. Dafalias, Y.F. and L.R. Herrmann, "Bounding Surface Formulation of Soil Plasticity," Chapter 10 in *Soil Mechanics-Transient and Cyclic Loads*, G.N. Pande and O.C. Zienkiewicz eds, J. Wiley and Sons publs., 1982.
17. DeNatale, J.S. "Calibration of the Bounding Surface Plasticity Model by Multivariate Optimization," Ph.D. Thesis, Department of Civil Engineering, University of California, Davis, 1982.
18. DeNatale, J.S. and L.R. Herrmann, Y.S. Dafalias, "Calibration of the Bounding Surface Plasticity Model by Multivariate Optimization" *International Conference on Constitutive Laws for Engineering Materials Theory and Applications*, Tucson, Arizona, January 1983.
19. Di Maggio, F.L. and Sandler, I.S., "Material Model for Granular Soils," *J. Eng. Mech. Div., ASCE*, 97, 1971, pp. 935-950.
20. Fernando, J., Smith, R. and Arulanandan, K., "New Approach to Determination of Expansion Index" *Journal of the Geotechnical Engineering Division, Proceeding of the American Society of Civil Engineers*, Vol. 101, No. GT9, September 1975.
21. Heinzen, R.T. and Arulanandan, K., "Factors Influencing Erosion, Dispersive Clays and Methods of Identification" *Proceedings of the Paris Symposium on Erosion and Solid Matter Transport in Inland Waters*, International Association of Hydrological Sciences - Association Internationale des Sciences Hydroloiques, No. 122, pp. 75-81 1977.
22. Herrmann, L.R. and Dafalias, Y.F., and DeNatale, J.S., "Bounding Surface Plasticity for Soil Modelling," Department of Civil Engineering, University of California, Davis, Final Report to the Civil Engineering Laboratory of the Naval Construction Battalion Center, Port Hueneme, California, 1980.
23. Herrmann, L.R., C.K. Shen, S. Jafroudi, J.S. DeNatale and Y.F. Dafalias, "A Verification Study for the Bounding Surface Plasticity Model for Cohesive Soils" *Final Report to Civil Engineering Laboratory, Naval Construction Battalion Center, Port Hueneme, California*, Order No. USN N62583-81MR320, December 1981.

24. Herrmann, L.R., Dafalias, Y.F. and DeNatale, J.S., "Numerical Implementation of a Bounding Surface Soil Plasticity Model," Proceedings of the International Symposium on Numerical Models in Geomechanics (in press), 1982.
25. Lambe, T.W., "A Mechanistic Picture of Shear Strength in Clay," Research Conference on Shear Strength on Cohesive Soils, ASCE, University of Colorado, Boulder, Colorado, June, 1960.
26. Michaels, A.S. and Lin, C.S., "The Permeability of Kaolinite," Ind. and Eng. Cheml, Vol. 46, pp. 1239-1246, 1954.
27. Mitchell, J.K. "The Application of Collodial Theory to the Compressibility of Clays," Proceedings, Seminar on Interparticle Forces in Clay-Water-Electrolyte System, Commonwealth Scientific and Industrial Research Organization, Melbourne, Australia, pp. 2.92-2.97, 1960.
28. Olsen, H.W., "Hydraulic Flow Through Saturated Clays," Submitted in Partial Fulfillment of the Requirements for the Degree of Doctor of Science in Civil Engineering, M.I.T., 1961.
29. Olson, R.E. and Mitronovas, F., "Shear Strength and Consolidation Characteristics of Calcium and Magnesium Illite," Proc. 9th Nat. Conf. Clays and Clay Minerals, pp. 185-209, 1962.
30. Prevost, J.H., "Plasticity Theory for Soil Stress Strain Behavior," J. Eng. Mech. Division, ASCE, 1978, 104, 1177-1196.
31. Quigley, R.M. and Thompson, C.D., "The Fabric of Anisotropically Consolidated Sensitive Marine Clay," Canadian Geotechnical Journal 3, Vol. 2, pp. 61-73, 1966.
32. Quirk, J.P., "Permeability of Porous Media," Nature, Vol. 183, pp. 387-388, 1959.
33. Roscoe, K.H. and Burland, J.B., "On the Generalized Stress-Strain Behavior of "Wet Clay", Engineering Plasticity, ed. J. Heyman and F.A. Leckie, Cambridge University Press, 1968, pp. 535-609.
34. Rosenqvist, Th., "Physico-Chemical Properties of Soils: Soil Water Systems," Proc. ASCE, Vol. 85, No. SM2, pp. 31-54, 1959.
35. Schofield, A.N. and Wroth, C.P., "Critical State Soil Mechanics," McGraw-Hill, London, 1968.
36. Sharlin, J.R., "A New Approach to Soil Classification," M.S. Thesis, University of California, Davis, California, 1972.
37. Smith, S.S., "Soil Characterization by Radio Frequency Electrical Dispersion," Dissertation presented to the University of California, Davis, California, in 1971, in partial fulfillment of the requirements for the degree of Doctor of Philosophy.
38. Smith, S.S. and Arulanandan, K., "Relationship of Electrical Dispersion to Soil Properties," J. of Geotechnical Engineering Division, ASCE, Vol. 107, No. GT5, May 1981.
39. Valanis, K.C., "A Theory of Viscoplasticity without a Yield Surface, Part I: General Theory, Part II: Application to Mechanical Behavior of Metals," Arch. of Mech. 1971, 23, 517-551.

## APPENDIX 1

DERIVATION OF THE PROPOSED THREE ELEMENT  
ELECTRICAL MODEL DISPERSION EQUATIONS

Three current paths considered and the associated three elements are described in Fig. 2.8 in the text. The equivalent admittance of each element is derived below.

Element 1

$$\text{Solid path: Resistance } R = \frac{l}{k_r} \cdot \frac{L_{1e}}{A_{1e}}$$

$$\text{Capacitance } C = \alpha \cdot \frac{A_{1e}}{L_{1e}} \cdot \epsilon_r$$

$$\text{Equivalent impedance } Z_1' = \frac{L_{1e}}{A_{1e} k_r (1 + j\omega \frac{\alpha}{k_r} \cdot \epsilon_r)}$$

Similarly, equivalent impedance of the solution part,

$$Z_1'' = \frac{L_{2e}}{A_{1e} k_s (1 + j\omega \frac{\alpha}{k_s} \epsilon_s)}$$

Equivalent impedance of Element 1,

$$Z_1 = Z_1' + Z_1''$$

Equivalent admittance of Element 1,

$$\begin{aligned}
 Y_1 &= Z_1^{-1} \\
 &= (Z_1' + Z_1'')^{-1} \\
 &= \left[ \frac{L_{1e}}{A_{1e}k_r + j\omega\alpha A_{1e}\epsilon_r} + \frac{L_{2e}}{A_{1e}k_s + j\omega\alpha A_{1e}\epsilon_s} \right]^{-1} \\
 &= \frac{A_{1e}[(k_s k_r - \omega^2 \alpha^2 \epsilon_s \epsilon_r) + j(\omega\alpha \epsilon_s k_r + \omega\alpha \epsilon_r k_s)]}{L_{2e} L_{1e} \left[ \frac{k_r}{L_{1e}} + \frac{k_s}{L_{2e}} + j\omega\alpha \left( \frac{\epsilon_r}{L_{1e}} + \frac{\epsilon_s}{L_{2e}} \right) \right]} \\
 &= \frac{A_{1e}}{L_{1e} L_{2e} S'} \{ (k_s k_r - \omega^2 \alpha^2 \epsilon_s \epsilon_r) + j\omega\alpha (\epsilon_s k_r + \epsilon_r k_s) \} \\
 &\times \left\{ \frac{k_r}{L_{1e}} + \frac{k_s}{L_{2e}} - j\omega\alpha \left( \frac{\epsilon_r}{L_{1e}} + \frac{\epsilon_s}{L_{2e}} \right) \right\}
 \end{aligned}$$

$$\text{in which } S' = \left( \frac{k_r}{L_{1e}} + \frac{k_s}{L_{2e}} \right)^2 + \omega^2 \alpha^2 \left( \frac{\epsilon_r}{L_{1e}} + \frac{\epsilon_s}{L_{2e}} \right)^2$$

Real part,

$$(Y_1)_{\text{real}} = \frac{A_{1e}}{L_{1e} L_{2e} S'} \left[ \frac{k_s k_r^2}{L_{1e}} + \frac{k_s^2 k_r}{L_{2e}} + \omega^2 \alpha^2 \left( \frac{\epsilon_r^2 k_s}{L_{1e}} + \frac{\epsilon_s^2 k_r}{L_{2e}} \right) \right]$$

Imaginary part,

$$(Y_1)_{\text{imag.}} = \frac{A_{1e} \omega \alpha}{L_{1e} L_{2e} S'} \left[ \frac{\epsilon_s k_r^2}{L_{1e}} + \frac{\epsilon_r k_s^2}{L_{2e}} + \omega^2 \alpha^2 \left( \frac{\epsilon_s \epsilon_r^2}{L_{1e}} + \frac{\epsilon_s^2 \epsilon_r}{L_{2e}} \right) \right]$$

### Element 2

Following the same procedure as in element 1,

$$Y_2 = \left[ \frac{L_e}{A_{2e} k_r + j \omega \alpha A_{2e} \epsilon_r} \right]^{-1}$$

$$= \frac{A_{2e}}{L_e} (k_r + j \omega \alpha \epsilon_r)$$

### Element 3

$$Y_3 = \frac{A_{3e}}{L_e} (k_s + j \omega \alpha \epsilon_s)$$

### Soil Sample

$$\text{Resistance: } R = \frac{1}{\sigma_{\text{theor.}}} \cdot \frac{L}{A}$$

$$\text{Capacitance: } C = \alpha \cdot \frac{A}{L} \cdot \epsilon'_{\text{theor.}}$$

Equivalent admittance:

$$Y = \frac{A}{L} (\sigma_{\text{theor.}} + j \omega \epsilon'_{\text{theor.}})$$

Now since  $I = I_1 + I_2 + I_3$

$$\text{i.e. } VY = VY_1 + VY_2 + VY_3$$

$$Y = Y_1 + Y_2 + Y_3$$

Equating the imaginary parts,

$$\begin{aligned} \epsilon'_{\text{theor.}} = & \frac{L}{A} \frac{A_{1e}}{L_{1e} L_{2e} S'} \left\{ \frac{\epsilon_s k_r^2}{L_{1e}} + \frac{\epsilon_r k_s^2}{L_{2e}} + \omega^2 \alpha^2 \left( \frac{\epsilon_s^2 \epsilon_r^2}{L_{1e}} + \frac{\epsilon_s^2 \epsilon_r^2}{L_{2e}} \right) \right\} \\ & + \frac{L}{A} \cdot \frac{A_{2e}}{L_e} \epsilon_r + \frac{L}{A} \cdot \frac{A_{3e}}{L_e} \epsilon_s \end{aligned}$$

Equating the real parts,

$$\begin{aligned} \sigma_{\text{theor.}} = & \frac{L}{A} \cdot \frac{A_{1e}}{L_{1e} L_{2e} S'} \left\{ \frac{k_s k_r^2}{L_{1e}} + \frac{k_s^2 k_r}{L_{2e}} + \omega^2 \alpha^2 \left( \frac{\epsilon_r^2 k_s^2}{L_{1e}} + \frac{\epsilon_s^2 k_r^2}{L_{2e}} \right) \right\} \\ & + \frac{L}{A} \frac{A_{2e}}{L_e} k_r + \frac{L}{A} \frac{A_{3e}}{L_e} k_s \end{aligned}$$

### Assumptions

- 1) Assuming that the volume of soil sample = volume of element 1 of electrical model:

$$A L = A_{1e} L_e$$

$$\frac{L_e}{L} = \frac{A}{A_{1e}} = t$$

- 2) Assuming that the volume of solution part of element 1 = volume of element 3;

$$A_{1e} L_{2e} = A_{3e} L_e$$

$$\frac{A_{3e}}{A_{1e}} = \frac{L_{2e}}{L_e}$$

Define,  $\frac{L_{1e}}{L_e} = d$

then  $\frac{L_{2e}}{L_e} = 1 - d$  since  $L_{1e} + L_{2e} = L_e$

Defi ,  $a = \frac{1}{t^2}$ ,  $b = \frac{A_{2e}}{A_{1e} t^2}$  and  $c = \frac{A_{3e}}{A_{1e} t^2}$

then,

$$\begin{aligned} \sigma_{\text{theor.}} = & \frac{L}{L_e} \cdot \frac{A_{1e}}{A} \cdot \frac{1}{\frac{L_{1e} L_{2e}}{L_e^2} (S' L_e^2)} \left\{ \frac{k_s^2 k_r}{L_{2e}/L_e} + \frac{k_s k_r^2}{L_{1e}/L_e} \right. \\ & + \alpha^2 \left( \frac{\epsilon_s^2 k_r}{L_{2e}/L_e} + \frac{\epsilon_r^2 k_s}{L_{1e}/L_e} \right) \} + \frac{L}{L_e} \cdot \frac{A_{1e}}{A} \cdot \frac{A_{2e}}{A_{1e}} \cdot k_r \\ & + \frac{L}{L_e} \cdot \frac{A_{1e}}{A} \cdot \frac{A_{3e}}{A_{1e}} \cdot k_s \end{aligned}$$

$$\begin{aligned}
\sigma_{\text{theor.}} &= \frac{L}{L_e} \cdot \frac{A_{1e}}{A} \frac{1}{\frac{L_{1e} L_{2e}}{L_e^2} (S' L_e^2)} \left[ \frac{k_s^2 k_r}{L_{2e}/L_e} + \frac{k_s k_r^2}{L_{1e}/L_e} \right. \\
&\quad + \omega^2 \alpha^2 \left( \frac{\epsilon_s^2 k_r}{L_{2e}/L_e} + \frac{\epsilon_r^2 k_s}{L_{1e}/L_e} \right) \left. \right] + \frac{L}{L_e} \cdot \frac{A_{1e}}{A} \cdot \frac{A_{2e}}{A_{1e}} \cdot k_r \\
&\quad + \frac{L}{L_e} \cdot \frac{A_{1e}}{A} \cdot \frac{A_{3e}}{A_{1e}} \cdot k_s \\
&= \frac{a}{(1-d)dS} \left[ \frac{k_s^2 k_r}{1-d} + \frac{k_s k_r^2}{d} + \omega^2 \alpha^2 \left( \frac{\epsilon_s^2 k_r}{1-d} + \frac{\epsilon_r^2 k_s}{d} \right) \right] + b k_r + c k_s
\end{aligned}$$

in which

$$\begin{aligned}
S &= L_e^2 S' \\
&= \left( \frac{k_s}{L_{2e}/L_e} + \frac{k_r}{L_{1e}/L_e} \right)^2 + \omega^2 \alpha^2 \left( \frac{\epsilon_s}{L_{2e}/L_e} + \frac{\epsilon_r}{L_{1e}/L_e} \right)^2 \\
&= \left( \frac{k_s}{1-d} + \frac{k_r}{d} \right)^2 + \omega^2 \alpha^2 \left( \frac{\epsilon_s}{1-d} + \frac{\epsilon_r}{d} \right)^2
\end{aligned}$$

Similarly,

$$\sigma'_{\text{theor.}} = \frac{a}{(1-d)dS} \left[ \frac{\epsilon_r k_s^2}{1-d} + \frac{\epsilon_s k_r^2}{d} + \epsilon_s^2 \left( \frac{\epsilon_s^2 \epsilon_r}{1-d} + \frac{\epsilon_s \epsilon_r^2}{d} \right) \right] + b \epsilon_r + c \epsilon_s$$

Observe that the expressions for  $\epsilon_{\text{theor.}}^l$ ,  $\sigma_{\text{theor.}}$ , and  $S$  are the same as those given by equations 2.30, 2.31, and 2.32 in the main text, with

$$a = 1/t^2, \quad b = \frac{A_{2e}}{A_{1e}t^2}, \quad c = \frac{A_{3e}}{A_{1e}t^2}, \quad \frac{L_{1e}}{L_e} = d, \quad \frac{L_{2e}}{L_e} = 1-d \quad \text{and} \quad t = \frac{L_e}{L}.$$

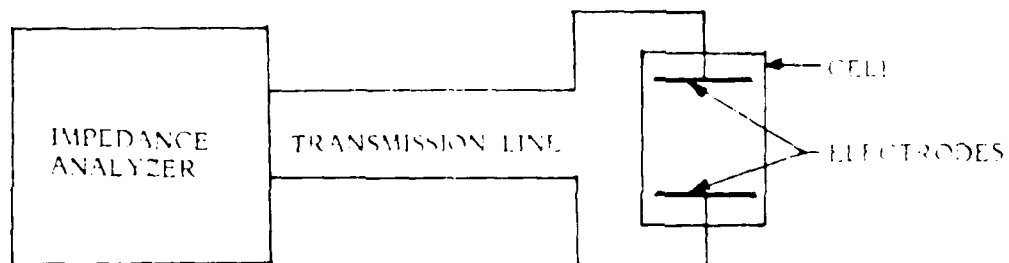
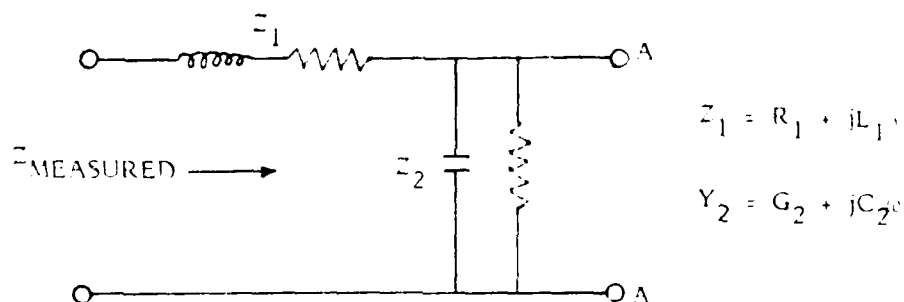
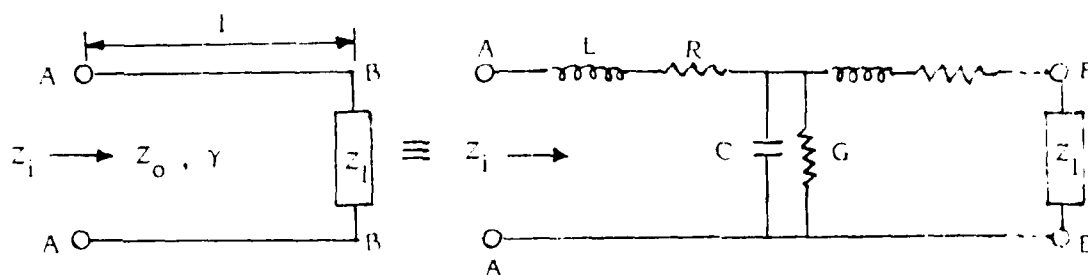
From these,

$$c = \frac{A_{3e}}{A_{1e}t^2} = \frac{L_{2e}}{L_e t^2} = (1-d)a$$

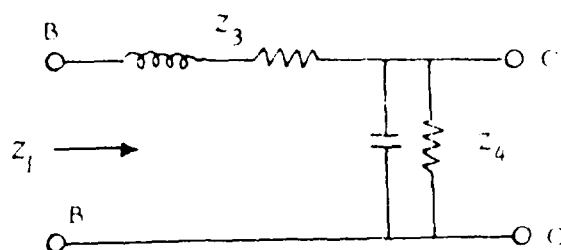
## APPENDIX 2

## CALIBRATION OF ELECTRICAL CELLS

Representation of the system by an equivalent electrical network:

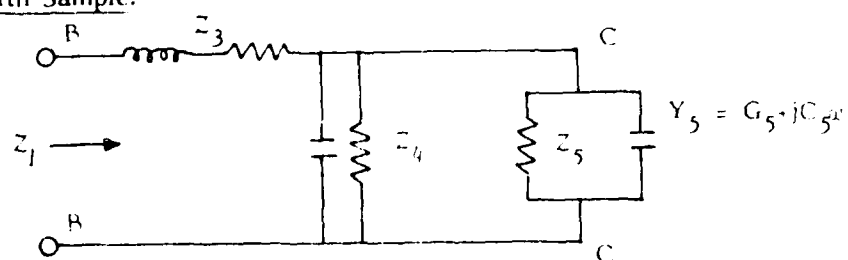
Impedance Analyzer:Transmission Line:

- $L$  = distributed inductance per unit length
- $R$  = distributed resistance per unit length
- $C$  = stray capacitance per unit length
- $G$  = stray conductance per unit length
- $Z_0$  = characteristic impedance of the line
- $\gamma$  = propagation constant of the line

Cell without Sample:

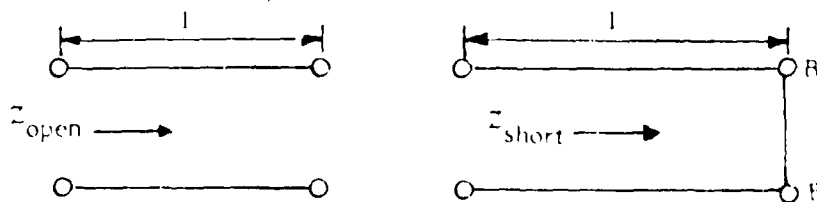
$$Z_3 = R_3 + jL_3\omega$$

$$Y_4 = G_4 + jC_4\omega$$

Cell with Sample:

By knowing  $Z_1$ ,  $Z_2$ , characteristic impedance of the transmission line,  $Z_0$ , propagation constant of the line,  $\gamma$ , impedances of the cells  $Z_3$  and  $Z_4$ , the resistance and the capacitance of the sample ( $Z_5$ ) can be reduced from the measured value of the impedance at a required frequency. They are determined as follows:

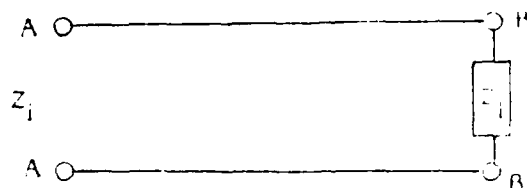
1. The values of  $R_1$ ,  $L_1$ ,  $G_2$ , and  $C_2$  are given in the impedance analyzer operating manual.
2. Characteristic impedance of the transmission line:



$$Z_0 = \sqrt{Z_{\text{open}} Z_{\text{short}}}$$

$$\gamma = \frac{1}{l} \tanh^{-1} \sqrt{\frac{Z_{\text{short}}}{Z_{\text{open}}}}$$

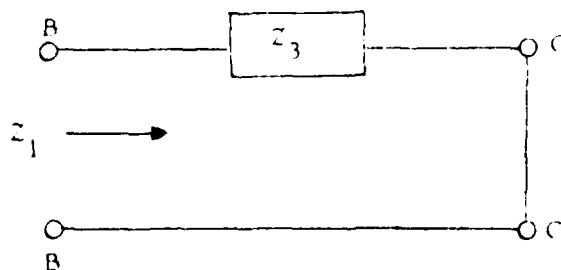
## 3. Impedance of the cell:



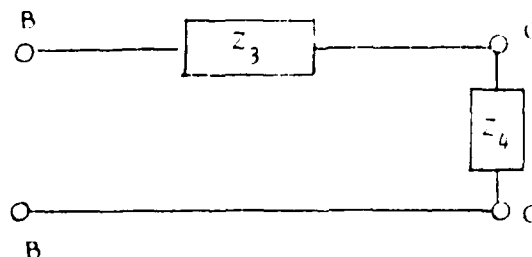
$$Z_1 = Z_0 \frac{Z_0 \tanh \gamma l - Z_1}{Z_1 \tanh \gamma l - Z_0}$$

Thus by measuring the impedances with CC short and open, without sample, and accounting for the impedance of the impedance analyzer, cell impedances  $Z_3$  and  $Z_4$  can be computed using the above expression.

Cell without the sample with CC short:



Cell without the sample with CC open:



Now by measuring the impedances with the sample in the cell, resistance and the capacitance of the sample can be computed since the impedances of the rest of the system are known.

#### Calibration results:

The procedure described in the preceding section was followed in determining the impedance characteristics of the system. This procedure, along with the known values of the system impedance parameters were incorporated in a computer program, written in BASIC, which computes the dielectric constant and the conductivity of the sample when the length of the sample, measuring frequency, resistive part of the measured impedance and the reactive part of the measured impedance are used as input parameters. The cell impedance was determined at different heights of the samples. A listing of the program is attached at the end of Appendix 2.

Water with known values of conductivity was used in the cells, and the measurements were made in order to check the validity of the equivalent electrical network representation of the transmission line and the cell and the accuracy of the measurement of the parameters concerned. The water is found to have a dielectric constant of 79, and it is not supposed to exhibit dispersion in the radio frequency range. But the measured values of dielectric constant and conductivities were found to vary slightly with the frequency. This was suspected to be due to the inaccurate determination of the impedances with the electrodes CC short, since the electrodes had to be shorted using a length of wire, and this has a certain unknown value of inductance.

Utilizing the fact that the water does not exhibit dispersion and its electrical properties are known, cell impedance values were adjusted slightly by trial and error to obtain the expected results. A typical example of the computed dielectric constant and conductivity of water is given in Table A.1.

The determined characteristic impedance and the propagation factor of the transmission line with frequency are shown in Figures A.1 and A.2. The inductance and the capacitance of the cells for 5 different heights of the sample are presented in Table A.2. The resistance of the cell is plotted against the frequency for different heights of the sample as shown in Figure A.3. The typical example of the behavior of the conductance with frequency is shown in Figure A.4.

Table A.1

COMPUTED DIELECTRIC CONSTANT AND CONDUCTIVITY OF WATER;  
 HEIGHT OF SAMPLE = 2.564 inch.  
 CONDUCTIVITY OF WATER AT 100 KHZ =  $5.05 \times 10^{-4}$  mho/cm

Frequency (MHZ)	Measured impedance		Computed dielectric constant of water	Computed Conductivity of water $\times 10^{-4}$ (mho/cm)
	R( $\Omega$ )	X( $\Omega$ )		
4	560.0	-605.0	81.3	5.402
6	317.0	-537.0	82.6	5.303
10	140.8	-383.9	80.0	5.313
16	60.8	-253.0	80.2	5.299
20	41.2	-202.6	82.2	5.363
26	26.26	-152.8	79.5	5.432
30	20.00	-128.74	80.6	5.293
36	15.42	-102.46	80.5	5.383
40	13.21	-88.23	79.0	5.277
50	10.33	-60.10	78.2	5.329
60	9.56	-37.91	77.5	5.419
70	9.68	-17.17	77.9	5.384
80	11.40	6.50	81.9	5.311

Table A.2  
INDUCTANCE AND CAPACITANCE OF THE CELL

Vertical			Horizontal		
Height of Sample (inch)	L3 (MH)	C4 (PF)	Height of Sample (inch)	L3 (MH)	C4 (PF)
3.564	155	8.9	4.142	93	6.4
3.144	145	9.1	3.292	93	6.4
2.374	145	9.3	2.627	94	6.4
1.969	145	9.3	1.917	95	6.4
1.229	145	9.9	1.517	94	6.4

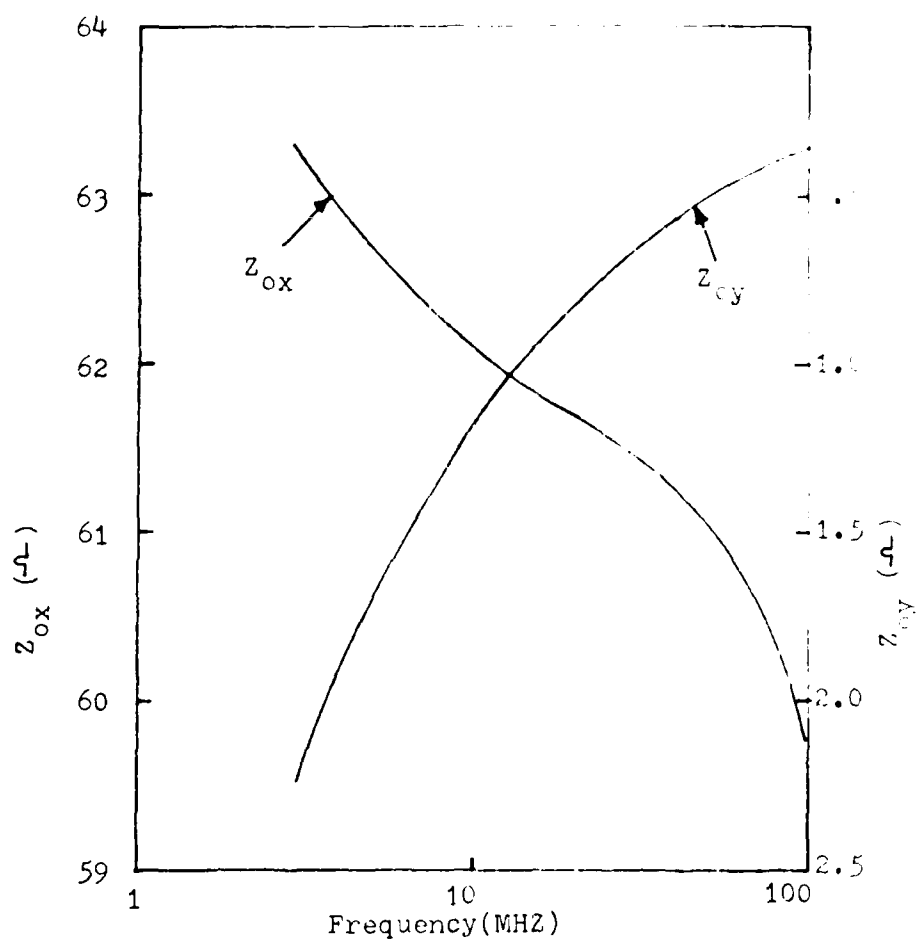


Fig. A.1 The Characteristic Impedence of The Transmission Line With Frequency.

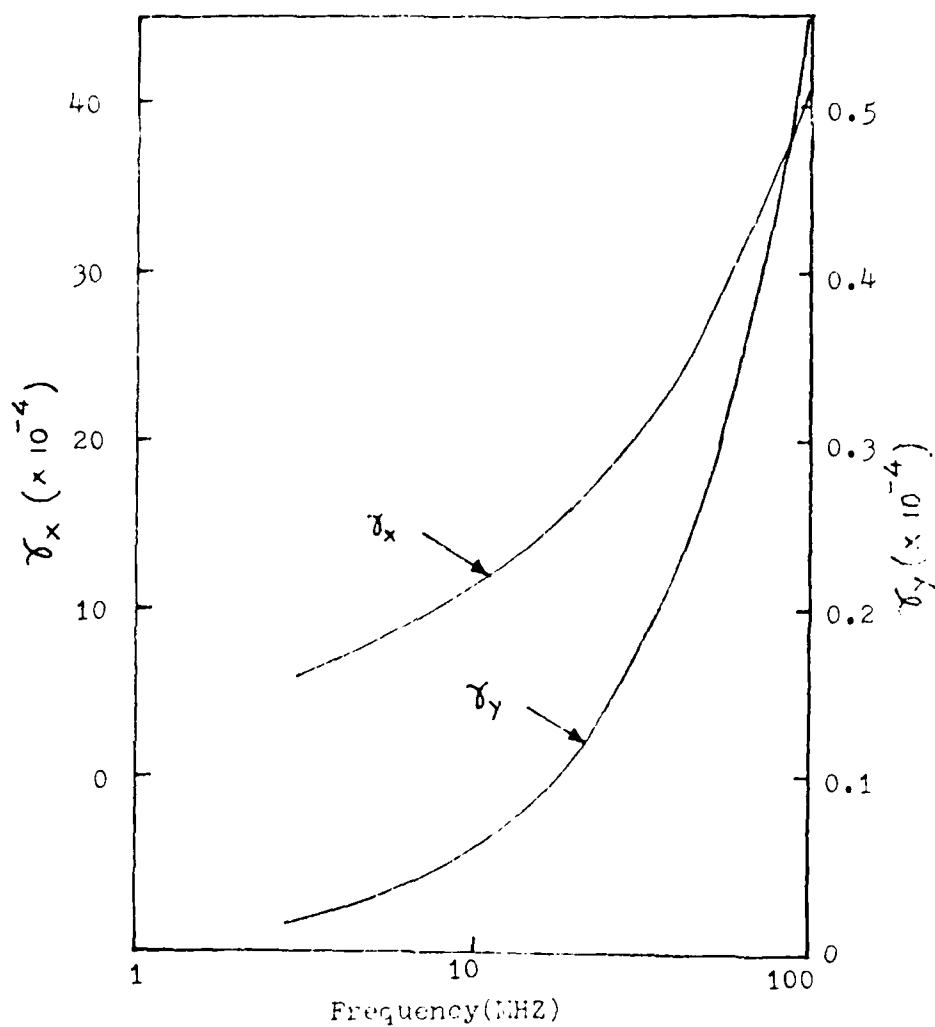


Fig. A.2 The Propagation Factor of The Transmission.  
Line with Frequency.

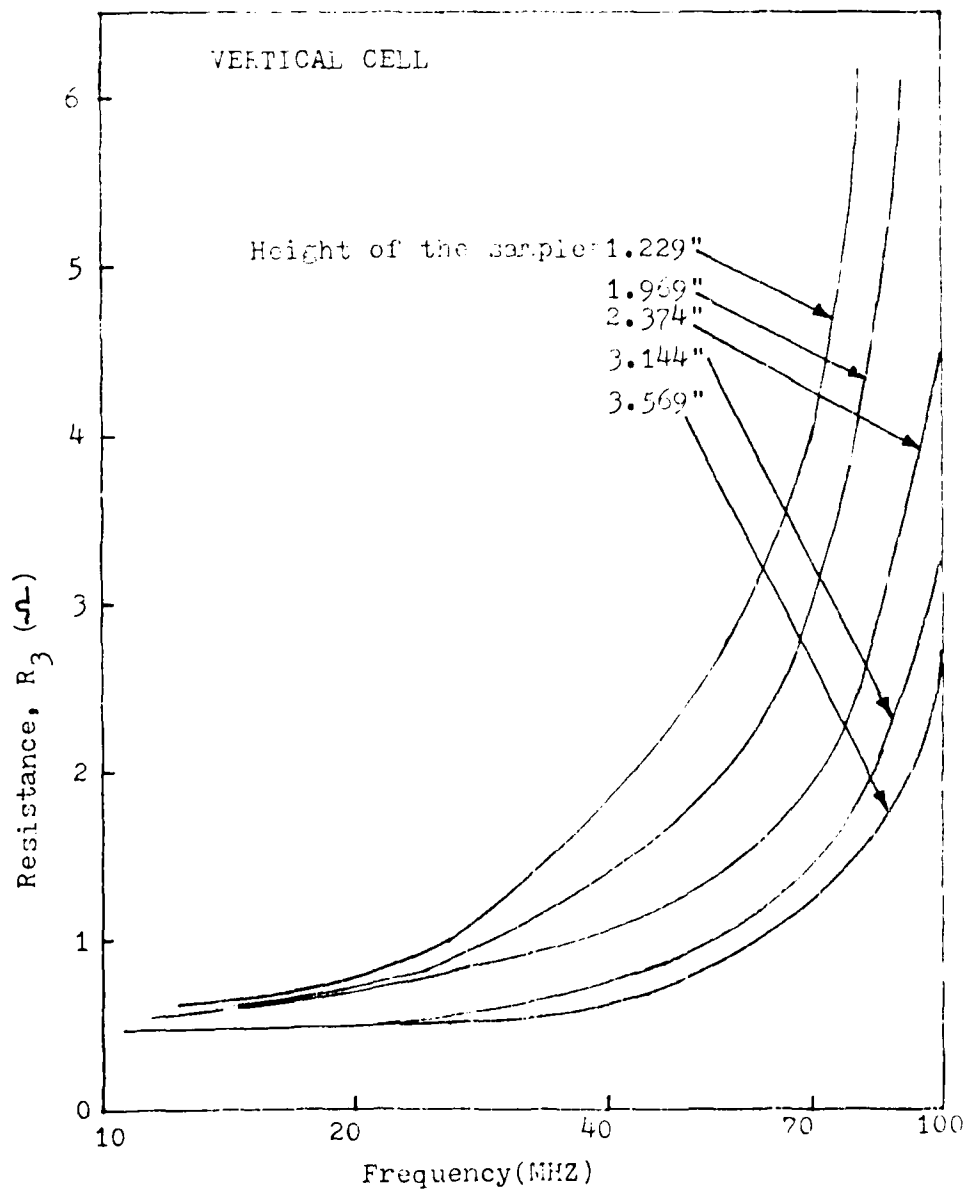


Fig. A.3 The resistance of the square cell corresponding to different sample heights.

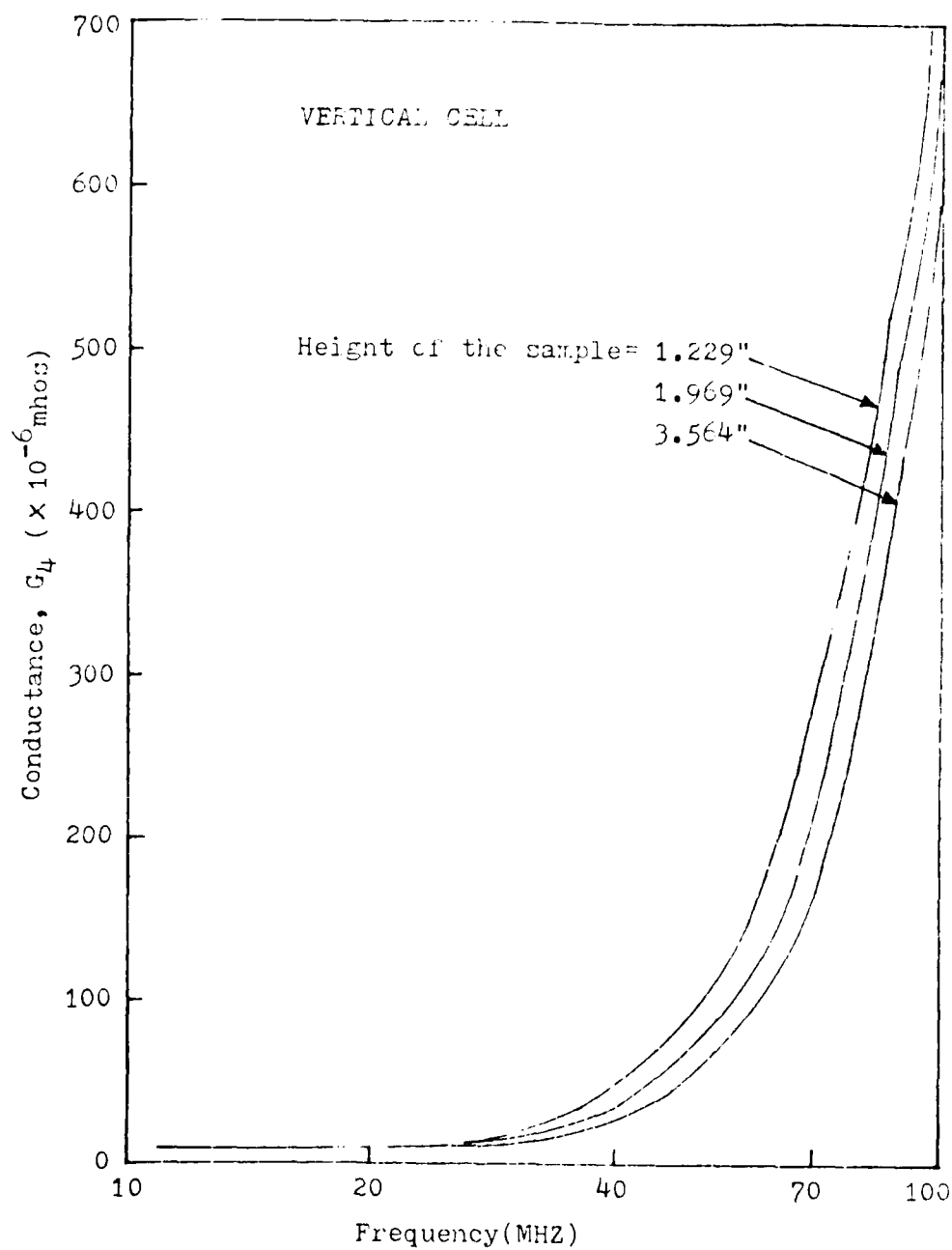


Fig. A.4 The conductance of the square cell corresponding to different sample heights.

LISTING OF THE COMPUTER PROGRAM WHICH COMPUTES THE DIELECTRIC  
CONSTANT AND CONDUCTIVITY OF THE SAMPLE FROM THE MEASURED  
IMPEDENCE AT ANY REQUIRED FREQUENCY.

```

10 DIM F(20),R(20),B(20),C(20),D(20)
20 DIM E(20),G(20),H(20),L(5),M(5)
30 DIM P(20),U(20),V(20),Q(20)
40 DIM R(5,20),C(5,20),V(5,20)
50 DIM M(20),N(20)
60 DIM Q(20),J(20),W(20)
70 INPUT M9,L3
80 IF M9=2 THEN 130
90 PRINT "    HORIZONTAL"
100 PRINT
110 PRINT
120 GOTO 160
130 PRINT "    VERTICAL"
140 PRINT
150 PRINT
160 N5=19
170 PRINT "    L3=",L3
180 IF M9=2 THEN 250
190 M(1)=3.325
200 M(2)=2.475
210 M(3)=1.81
220 M(4)=1.1
230 M(5)=0.7
240 GOTO 300
250 M(1)=2.995
260 M(2)=2.575
270 M(3)=1.805
280 M(4)=1.4
290 M(5)=0.66
300 FOR I=1 TO N5
310 READ F(I),R(I)
320 B(I)=1.8+2*PI+F(I)+.01E-03
330 C(I)=0
340 D(I)=-1/(1.8+2*PI+F(I)+.01E-03)
350 NEXT I
360 DATA 1.0,2.0,3.0,0.001,4.0,0.001,5.0,0.002,6.0,0.0025
370 DATA 10,0.005,16,0.006,20,0.008,26,0.009,30,0.009
380 DATA 36,0.009,40,0.009,50,0.01,60,0.012,70,0.014
390 DATA 80,0.018,90,0.02,100,0.025
400 FOR I=1 TO 10
410 READ S(I)
420 NEXT I
430 DATA 1.4,1.4,1.4,1.385,1.368
440 DATA 1.086,1.076,1.068,1.066,1.066
450 FOR I=1 TO N5
460 READ E(I),Q(I),G(I),H(I)
470 NEXT I
480 DATA 63.4,-2.33,0.0001,0.017
490 DATA 63.35,-2.3,0.0005,0.0171
500 DATA 63.305,-2.2329,0.0006,0.0172

```



```

1010 READ T(1)
1020 NEXT I
1030 DATA 5.4,6.4,6.4,6.4,6.4
1040 RESTORE 1140
1050 DATA 8.9,9.1,9.3,9.3,9.3
1060 IF N9=1 THEN 1060
1070 RESTORE 1240
1080 FOR I=1 TO 5
1090 FOR J=1 TO N5
1100 READ C(I,J)
1110 C(I,J)=C(I,J)+1E-06
1120 NEXT J
1130 NEXT I
1140 DATA 0.0,0.0,0.5,1.2,4.5,5.9,9.5,10.10,5.12,15
1150 DATA 35.30,30.15,100.240,410
1160 DATA 0.0,0.0,0.5,1.2,4.5,5.9,9.5,10.10,5.12,15
1170 DATA 25.30,30.35,100.240,410
1180 DATA 0.0,0.0,0.5,1.2,4.5,5.9,9.5,10.10,5.12,15
1190 DATA 25.30,30.35,100.240,410
1200 DATA 0.0,0.0,0.5,1.2,4.5,5.9,9.5,10.10,5.12,15
1210 DATA 25.30,30.35,100.240,410
1220 DATA 0.0,0.0,0.5,1.2,4.5,5.9,9.5,10.10,5.12,15
1230 DATA 25.30,30.35,100.240,410
1240 DATA 0.0,0.0,0.5,1.2,4.5,5.9,9.5,10.10,5.12,15
1250 DATA 30.50,100.150,100.450,500
1260 DATA 0.0,0.0,0.5,1.2,4.5,5.9,9.5,10.10,5.12,15
1270 DATA 30.70,120.220,150.500,700
1280 DATA 0.0,0.0,0.5,1.2,4.5,5.9,9.5,10.10,5.12,15
1290 DATA 40.70,120.180,100.550,700
1300 DATA 0.0,0.0,0.5,1.2,4.5,5.9,9.5,10.10,5.12,15
1310 DATA 40.50,120.320,150.500,700
1320 DATA 0.0,0.0,0.5,1.2,4.5,5.9,9.5,10.10,5.12,15
1330 DATA 50.90,160.250,400.100,1000
1340 FOR I=2 TO 5
1350 L3=X(I)-L3
1360 L4=X(I)-L3
1370 IF ABS(L3) < 0.01 THEN 1400
1380 IF ABS(L4) < 0.01 THEN 1400
1390 L5=L3+L4
1400 IF L5 = 0 THEN 1490
1410 NEXT I
1420 GOTO 1520
1430 I5=I
1440 I6=I
1450 GOTO 1520
1460 I5=I-1
1470 I6=I-1
1480 GOTO 1520
1490 I5=I
1500 I6=I-1

```

```

1510 GOTO 1580
1520 IF L3=0 THEN 1560
1530 L5=4
1540 L6=5
1550 GOTO 1580
1560 L5=1
1570 L6=2
1580 FOR I=1 TO N5
1590 IF L5=L6 THEN 1620
1600 N5=(L2-N5)*50+(N5*50-N5*50)
1610 GOTO 1620
1620 N5=0
1630 FC(I)=FC(L5,I)+FC(L6,I)-FC(L5,I)+N5
1640 IF N5=2 THEN 1670
1650 F6=SC(L5)+SC(L6)-SC(L5)+N5
1660 GOTO 1680
1670 F6=SC(L5+50)+SC(L6+50)-SC(L5+50)+N5
1680 O7=LC(L5)+LC(L6)-LC(L5)+N5
1690 UC(I)=UC(L5,I)+UC(L6,I)-UC(L5,I)+N5
1700 W7=TC(L5)+TC(L6)-TC(L5)+N5
1710 NEXT I
1720 N3=0
1730 INPUT F8,N8,Y8
1740 IF F8=0 THEN 2080
1750 N3=N3+1
1760 FOR I=1 TO N5
1770 IF FC(I)=F8 THEN 1790
1780 NEXT I
1790 N8=I
1800 X6=EXP(GC(L8)) * EXP(-GC(L8))
1810 Y6=EXP(GC(L8)) * EXP(-GC(L8))
1820 X1=Y6+COS(HC(L8))
1830 Y1=X6+SIN(HC(L8))
1840 X2=X6+COS(HC(L8))
1850 Y2=Y6+SIN(HC(L8))
1860 X3=X2+X2+Y2+Y2
1870 T5=(X1+X2+Y1+Y2)/N3
1880 T6=(X1+Y2+Y1+X2)/N3
1890 GOSUB 2150
1900 I=N3
1910 X1=UC(I)-FC(I)
1920 X2=HC(I)-FC(I)
1930 Y3=HC(I)-X2+P1+FC(I)+O7*(1E-03)
1940 Z6=X2+X2+Y2+Y2
1950 G1=UC(I)
1960 G2=X2+Z6
1970 G3=G2-G1
1980 F3=1/G3
1990 G3=-Y2/X3+P1+FC(I)+Z6*(1E-06)
2000 C4=C3-W7

```

```

2010 G6=G1*(1E+06)
2020 IF M9=1 THEN 2070
2030 Q(N3)=F(I)
2040 J(N3)=C4+(L2+0.569)/(F6+0.44046)
2050 W(N3)=(L2+0.569)/(F6+4.977*R3+1E-04)
2060 GOTO 2100
2070 Q(N3)=F(I)
2080 J(N3)=C4+3.7905/F6
2090 W(N3)=0.33614/(R3+F6+1E-04)
2100 WRITE (15,2110)N3,F(I),J(N3),W(N3)
2110 FORMAT (2F10.0,2F15.3)
2120 GOTO 1730
2130 STOP
2140 END
2150 T1=A(I*8)-X8
2160 T2=B(I*8)-Y8
2170 D1=C(I*8)+T1-D(I*8)+T2
2180 D2=C(I*8)+T2-D(I*8)+T1
2190 T1=X8-A(I*8)-C(I*8)
2200 T2=Y8-B(I*8)-D(I*8)
2210 T3=T1+T1+T2+T2
2220 P8=(D1*T1+D2*T2)/T3
2230 Q8=(-D1+T2+D2*T1)/T3
2240 X1=E(I*8)+T5-C(I*8)+T6
2250 Y1=E(I*8)+T6+C(I*8)+T5
2260 X1=X1-P8
2270 Y1=Y1-Q8
2280 X2=P8+T5-Q8+T6
2290 Y2=P8+T6+Q8+T5
2300 X2=X2-E(I*8)
2310 Y2=Y2-D(I*8)
2320 X4=X2+X2+Y2+Y2
2330 X3=(X1+X2+Y1+Y2)/X4
2340 Y3=(-X1+Y2+Y1+X2)/X4
2350 M(I*8)=E(I*8)+X3-C(I*8)+Y3
2360 N(I*8)=E(I*8)+Y3+C(I*8)+X3
2370 RETURN
2380 INPUT J1,J2,J3,J4,J5,J6
2390 INPUT N4
2400 IF N4=2 THEN 2510
2410 SCALE 0.2,J1,J2
2420 XAXIS J1,1
2430 YAXIS 0,J3
2440 FOR I=1 TO N3
2450 F2=LOG(Q(I))
2460 F3=J(I)
2470 PLOT F2,F3
2480 PLOT F2,F3,2
2490 NEXT I
2500 GOTO 2390
2510 SCALE 0.2,J4,J5
2520 XAXIS J4,1
2530 YAXIS 0,J5
2540 FOR I=1 TO N3
2550 F2=LOG(Q(I))
2560 F3=W(I)
2570 PLOT F2,F3
2580 PLOT F2,F3,2
2590 NEXT I
2600 GOTO 2390
2610 END

```

Table 1  
DIFFERENT FEASIBLE OPTIMIZED MODEL PARAMETERS

No.	Soil Type	a	b	c	d	$\epsilon_r$	$\epsilon_s$	$k_r \times 10^{-4}$ (mho/cm)
1 (a)	Illite	.5640	.0053	.3396	.3974	39.9	79	29
(b)		.5575	.0058	.2903	.4792	58.3	79	34
2 (a)	Illite	.5885	.0060	.2834	.5184	21.8	79	16
(b)		.5078	.0027	.1965	.6129	42.9	79	26
(c)		.4916	.0052	.1836	.6265	47.4	79	28
3 (a)	Yolo Loam	.5376	.0053	.1873	.6516	26.1	79	21
(b)		.5820	.0061	.2252	.6130	18.5	79	17

Table 2  
COMPARISON OF WATER CONTENTS CORRESPONDING  
TO THE RESULTS GIVEN IN TABLE 2.1

No.	Soil Type	$e_l$	$e_p$	Water Content (%) -Calculated	Water Content (%) -Measured
1 (a)	Illite	.904	2.887	137.9	159.0
(b)		2.592	3.904	236.2	159.0
2 (a)	Illite	0.301	1.209	54.9	60.0
(b)		1.068	1.306	86.4	60.0
(c)		1.357	1.405	100.4	60.0
3 (a)	Yolo Loam	0.408	0.753	42.2	45.0
(b)		0.230	0.777	26.6	45.0

Table 3

OPTIMIZED MODEL PARAMETERS TO PREDICT  
WATER CONTENT OF THE SOILS

No.	Soil Type	a	b	c	d	$\epsilon_r$	$\epsilon_s$	$k_r \times 10^{-4}$ (mho/cm)
1	Illite	.5635	.0053	.3396	.3974	39.9	79	29
2	Illite	.7130	.0032	.2576	.6386	30.7	79	17
3	Illite	.6249	.0070	.2507	.5988	23.9	79	19
4	Illite	.6369	.0049	.2593	.5929	15.8	79	17
5	K-Illite	.5661	.0047	.2194	.6125	35.8	79	21
6	Li-Illite	.5885	.0060	.2834	.5184	21.8	79	16
7	Illite	.5614	.0064	.3254	.4203	22.6	79	11
8	Kaolinite	.5869	.0044	.3327	.4332	18.7	79	5
9	Yolo Loam	.5376	.0053	.1873	.6516	26.1	79	21
10	Kaolinite	.6678	.0001	.2788	.5824	9.8	79	78
11	Kaolinite	.8695	.0261	.2542	.7076	12.3	79	6

Table 4

COMPARISON OF WATER CONTENTS CORRESPONDING  
TO THE RESULTS GIVEN IN TABLE 2.3

No.	Soil Type	$c_1$	$c_p$	Water Content (%) -Calculated	Water Content (%) -Measured
1	Illite	.904	2.887	137.8	159
2	Illite	.542	.873	51.5	54
3	Illite	.353	.906	45.8	42
4	Illite	.179	.809	35.9	32
5	K-Illite	.724	1.091	65.9	61
6	Li-Illite	.301	1.209	54.9	60
7	Illite	.322	1.823	77.9	77
8	Kaolinite	.235	1.616	67.3	60
9	Yolo Loam	.408	.753	42.2	45
10	Kaolinite	.772	.077	32.2	29
11	Kaolinite	.461	.116	21.9	25

Table 5

THE VALUES OF VERTICAL AND HORIZONTAL FORMATION  
FACTORS AT DIFFERENT VOID RATIOS

MARYSVILLE RED SOIL								
No.	e	n	$F_V$	$F_H$	$A^2 = \frac{F_V}{F_H}$	$\bar{F}$	Log $\bar{F}$	-LOG n
1	2.187	.6865	2.409	1.850	1.14	2.04	.309	.164
2	1.753	.6363	2.695	2.07	1.14	2.28	.358	.196
3	1.579	.6124	2.781	2.09	1.15	2.32	.366	.213
4	1.418	.5868	3.056	2.23	1.17	2.51	.399	.232
5	1.239	.5534	3.320	2.40	1.17	2.71	.432	.257

Table 6

THE VALUES OF VERTICAL AND HORIZONTAL FORMATION  
FACTORS AT DIFFERENT VOID RATIOS

ILLITE (100%)								
No.	e	n	$F_V$	$F_H$	$A^2 = \frac{F_V}{F_H}$	$\bar{F}$	Log $\bar{F}$	-LOG n
1	1.182	.542	2.84	2.67	1.03	2.73	.436	.266
2	1.066	.514	3.19	2.82	1.06	2.94	.469	.289
3	.944	.486	3.42	2.92	1.08	3.09	.489	.314
4	.821	.451	4.00	3.40	1.08	3.60	.556	.346

Table 7

THE VALUES OF VERTICAL AND HORIZONTAL FORMATION  
FACTORS AT DIFFERENT VOID RATIOS

SNOW CAL (95%) + BENTONITE (5%)								
No.	e	n	$F_V$	$F_H$	$A^2 = \frac{F_V}{F_H}$	$\bar{F}$	$\log \bar{F}$	$-\log n$
1	1.594	.614	2.17	1.90	1.07	1.98	.299	.212
2	1.458	.593	2.34	2.07	1.06	2.16	.335	.227
3	1.350	.575	2.59	2.17	1.09	2.31	.364	.241
4	1.234	.552	2.71	2.28	1.09	2.42	.385	.258
5	1.123	.529	2.69	2.28	1.09	2.42	.383	.277
6	0.998	.499	3.11	2.53	1.10	2.72	.435	.302
7	.0778	.438	3.37	3.06	1.10	3.16	.499	.359

Table 8  
THE VALUES OF VERTICAL AND HORIZONTAL FORMATION  
FACTORS AT DIFFERENT VOID RATIOS

SNOW CAL (60%) + ILLITE (40%)								
No.	e	n	$F_V$	$F_H$	$A = \frac{F_V}{F_H}$	$\bar{F}$	Log $\bar{F}$	-LOG n
1	1.430	.589	2.68	2.29	1.08	2.42	.384	.230
2	.996	.499	3.41	2.82	1.09	3.02	.479	.302
3	.834	.455	3.59	3.25	1.05	3.36	.527	.342
4	.748	.428	4.34	3.72	1.08	3.93	.594	.369

Table 9  
OPTIMIZED MODEL PARAMETERS AT DIFFERENT WATER CONTENTS - SNOW CAL (60%) + ILLITE (40%)

HORIZONTAL

No.	Water Content (%)	a	b	c	d	$\epsilon_r$	$k_r \times 10^{-4}$ (mho/cm)	$k_s \times 10^{-4}$ (mho/cm)	$\epsilon_l$	$e_p$	e	$e_l/e_p$
1	51.94	.7162	.073	.0466	.9349	45.4	22.9	6.9	1.213	.154	1.37	7.89
2	39.58	.7016	.092	.0569	.9188	39.4	20.4	6.7	.879	.166	1.05	5.30
3	35.41	.7404	.043	.0647	.9126	36.8	18.9	6.6	.765	.169	.934	4.53
4	31.76	.7411	.037	.0736	.9007	33.9	17.5	6.6	.656	.183	.838	3.59
5	27.84	.7532	.042	.0765	.8985	31.2	17.0	6.5	.565	.176	.736	3.18
6	24.20	.7659	.037	.0958	.8749	27.1	14.8	6.2	.435	.205	.639	2.12

VERTICAL

No.	Water Content (%)	a	b	c	d	$\epsilon_r$	$k_r \times 10^{-4}$ (mho/cm)	$k_s \times 10^{-4}$ (mho/cm)	$\epsilon_l$	$e_p$	e	$e_l/e_p$
1	41.75	.7224	.063	.0882	.8779	38.6	21.4	6.9	.845	.257	1.102	3.29
2	37.72	.7076	.059	.0966	.8635	35.8	20.3	6.9	.723	.272	.995	2.66
3	31.58	.7195	.030	.1064	.8521	31.3	18.8	6.8	.562	.322	.834	2.07
4	28.35	.6946	.032	.1279	.8157	26.8	16.4	6.5	.426	.335	.749	1.33
5	24.54	.6478	.082	.1315	.7969	22.3	15.4	6.2	.314	.343	.648	0.94
6												

Table 10

OPTIMIZED MODEL PARAMETERS AT DIFFERENT WATER  
CONTENTS - SNOW CAL (95%) + BENTONITE (5%)

## HORIZONTAL

No.	Water Content (%)	a	b	c	d	$\epsilon_r$	$k_r \times 10^{-4}$ (mho/cm)	$k_s \times 10^{-4}$ (mho/cm)	$e_l$	$e_p$	e	$e_l/e_p$
1	64.61	.6782	.050	.0820	.8791	47.68	15.71	5.23	1.379	.327	1.706	4.21
2	58.14	.6478	.058	.0803	.8761	45.45	15.56	5.17	1.220	.314	1.534	3.88
3	53.97	.6949	.021	.0863	.8758	43.93	15.03	5.24	1.120	.301	1.425	3.73
4	49.81	.6231	.080	.0952	.8472	41.00	13.88	4.93	.961	.354	1.314	2.72
5	45.93	.6731	.046	.0985	.8536	39.56	13.59	5.01	.889	.324	1.213	2.75
6	41.76	.6967	.056	.0998	.8567	37.62	13.45	5.11	.850	.301	1.101	2.66
7	37.77	.6833	.043	.1079	.8420	34.79	12.32	4.83	.685	.316	1.002	2.17
8	33.62	.6930	.088	.1092	.8424	32.15	12.36	5.02	.590	.298	.888	1.38
9	29.64	.6114	.041	.1119	.8169	27.85	11.63	4.79	.456	.326	.783	1.39

## VERTICAL

No.	Water Content (%)	a	b	c	d	$\epsilon_r$	$k_r \times 10^{-4}$ (mho/cm)	$k_s \times 10^{-4}$ (mho/cm)	$e_l$	$e_p$	e	$e_l/e_p$
1	66.11	.6372	.084	.0816	.8719	47.88	16.59	4.79	1.391	.352	1.746	3.97
2	60.36	.6481	.063	.0842	.8700	45.99	16.19	4.79	1.250	.337	1.594	3.73
3	55.21	.6542	.074	.0940	.8563	43.59	15.09	4.67	1.104	.353	1.457	3.13
4	51.15	.6249	.049	.0916	.8533	41.85	15.04	4.61	1.006	.345	1.348	2.92
5	46.74	.6373	.015	.0932	.8537	39.94	14.79	4.66	.903	.327	1.234	2.78
6	42.57	.6225	.045	.0942	.8487	37.63	14.55	4.63	.801	.321	1.122	2.79
7	37.80	.6136	.016	.1041	.8303	34.09	13.31	4.33	.654	.339	.997	1.94
8	33.51	.6045	.076	.1074	.8224	30.94	13.02	4.47	.500	.335	.885	1.60
9	29.50	.5915	.042	.1167	.8027	26.71	12.12	4.34	.420	.350	.775	1.21

Table II  
OPTIMIZED MODEL PARAMETERS AT DIFFERENT WATER CONTENTS - YOLO LOAM

HORIZONTAL

No.	Water Content (%)	a	b	c	d	$\epsilon_r$	$k_r \times 10^{-4}$ (mho/cm)	$k_s \times 10^{-4}$ (mho/cm)	$e_l$	$e_p$	e	$e_l/e_p$
2	38.78	.6839	.019	.2658	.6113	18.77	13.08	6.88	.237	.787	1.023	.351
3	35.32	.6920	.054	.2706	.6089	16.23	11.38	6.14	.187	.762	.949	.245
4	31.36	.7339	.051	.2773	.6222	14.08	10.98	6.39	.148	.697	.844	.212
5	28.28	.7545	.001	.2752	.6352	12.96	10.62	6.35	.128	.648	.776	.198
6	25.08	.8025	.030	.2747	.6577	12.30	10.50	6.42	.117	.582	.599	.291

VERTICAL

No.	Water Content (%)	a	b	c	d	$\epsilon_r$	$k_r \times 10^{-4}$ (mho/cm)	$k_s \times 10^{-4}$ (mho/cm)	$e_l$	$e_p$	e	$e_l/e_p$
2	42.51	.6215	.029	.2430	.6098	21.43	16.28	7.11	.294	.828	1.122	.355
3	39.16	.6216	.051	.2425	.6098	19.60	14.52	6.19	.254	.802	1.556	.317
4	34.24	.6615	.001	.2633	.6019	14.46	13.56	7.03	.154	.763	.913	.202
5	29.37	.7040	.001	.2845	.5957	10.72	11.15	6.43	.091	.741	.832	.123
6	26.61	.7291	.047	.2770	.6201	10.36	10.84	6.32	.086	.665	.751	.129

Table 12  
OPTIMIZED MODEL PARAMETERS AT DIFFERENT WATER CONTENTS - ILLITE

HORIZONTAL

No.	Water Content (%)	a	b	c	d	$\epsilon_r$	$k_r \times 10^{-4}$ (mho/cm)	$k_s \times 10^{-4}$ (mho/cm)	$e_l$	$e_p$	e	$e_l/e_p$
1	61.44	.6429	.0499	.0159	.9152	49.86	55.83	7.53	1.556	.565	1.621	23.94
2	51.88	.6503	.077	.0235	.9639	46.38	46.43	7.30	1.284	.586	1.369	15.52
3	41.84	.7328	.053	.0303	.9586	42.97	49.76	7.28	1.017	.587	1.104	11.68
4	36.27	.7993	.033	.0357	.9554	39.15	37.35	7.25	.869	.587	.957	9.96
5	31.29	.7869	.088	.0532	.9323	35.24	30.39	6.88	.753	.124	.526	5.69

VERTICAL

No.	Water Content (%)	a	b	c	d	$\epsilon_r$	$k_r \times 10^{-4}$ (mho/cm)	$k_s \times 10^{-4}$ (mho/cm)	$e_l$	$e_p$	e	$e_l/e_p$
1	59.85	.5955	.042	.0123	.9793	49.51	58.79	7.03	1.527	.553	1.579	28.69
2	49.64	.5795	.096	.0188	.9675	45.66	47.94	6.76	1.236	.575	1.311	16.47
3	39.98	.6335	.031	.0219	.9653	41.45	44.24	6.79	.984	.571	1.556	13.85
4	35.77	.5823	.046	.0263	.9548	38.88	40.44	6.56	.857	.588	.945	9.76
5	31.11	.5354	.071	.0296	.9446	35.73	37.81	6.31	.722	.101	.822	7.16

Table 13

THE VALUES OF 'M' AND THE ELECTRICAL  
INDEX FOR DIFFERENT SOILS

Soil Type	M (Obtained for Cam-Clay)	M (Obtained for Bounding Surface)	$\Lambda$	$\bar{l}$	$\Lambda^2/\bar{l}$
Illite	2.55	1.85	1.97	1.60	.716
Snow Cal (60%) + Illite (40%)	2.32	1.80	1.98	1.60	.729
Marysville Red Soil	1.85	1.62	1.15	1.73	.763
Snow Cal (95%) + Bentonite	1.19	1.45	1.10	1.43	.847

Table 14

THE UNDRAINED SHEAR STRENGTH OF NORMALLY CONSOLIDATED SOILS  
PREDICTED BY CAM-CLAY THEORY AND BOUNDING SURFACE THEORY

Soil Type	$q_u/p_o$ By Cam-Clay Theory	$q_u/p_o$ By Bounding Surface Theory
Illite	1.11	0.81
Snow Cal (95%) + Bentonite (5%)	0.49	0.38
Snow Cal (60%) + Illite (40%)	1.03	0.90
Marysville Red Soil	0.76	0.93

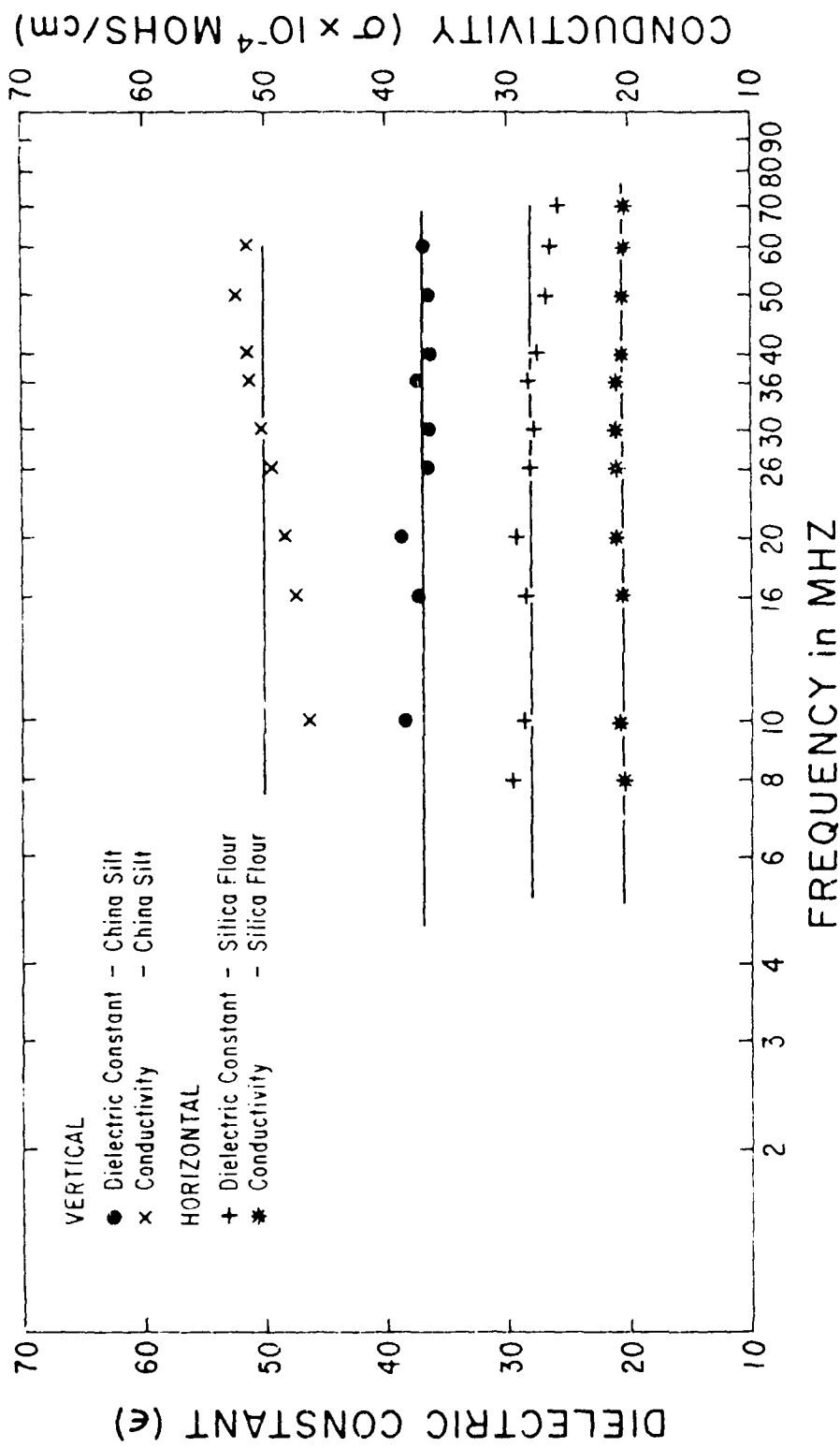


FIG. 1 Variation of Dielectric Constant and Conductivity as a function of frequency for Sands and Silts

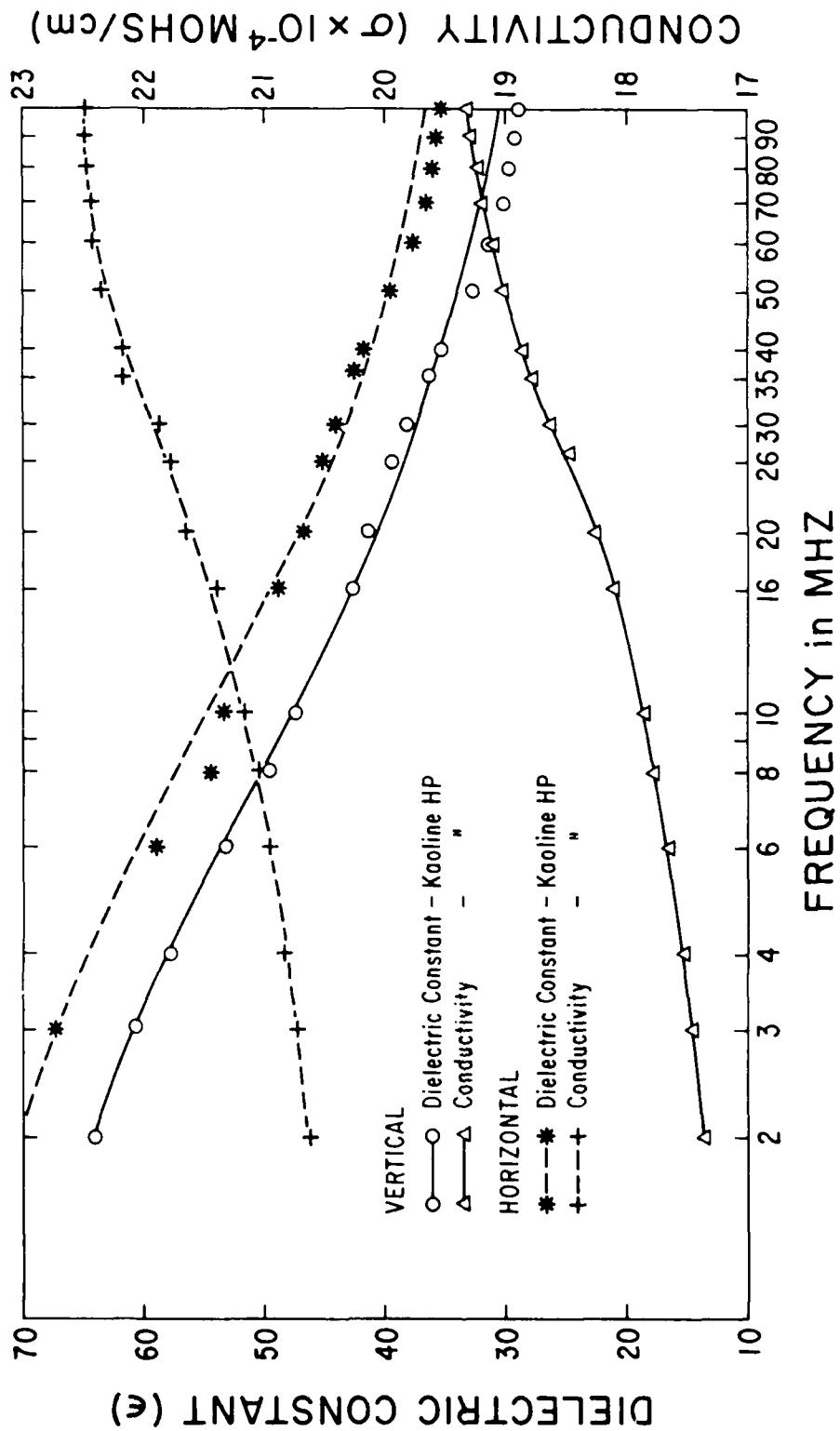


FIG. 2 Variation of Dielectric Constant and Conductivity as a Function of Frequency for Cohesive Soils

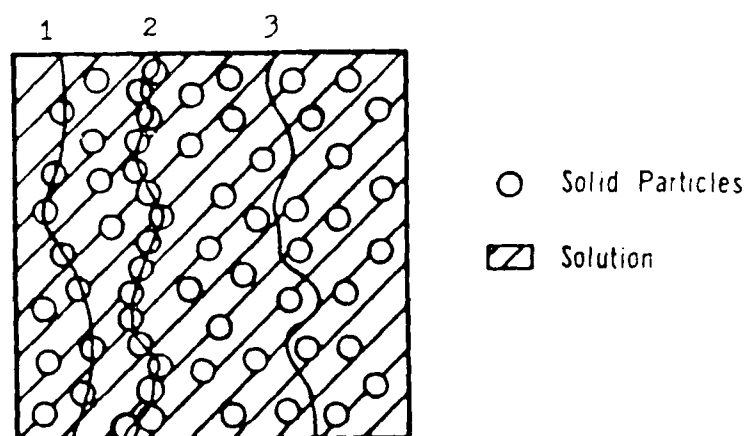


Fig. 3 Three components of the current paths through the soil sample.

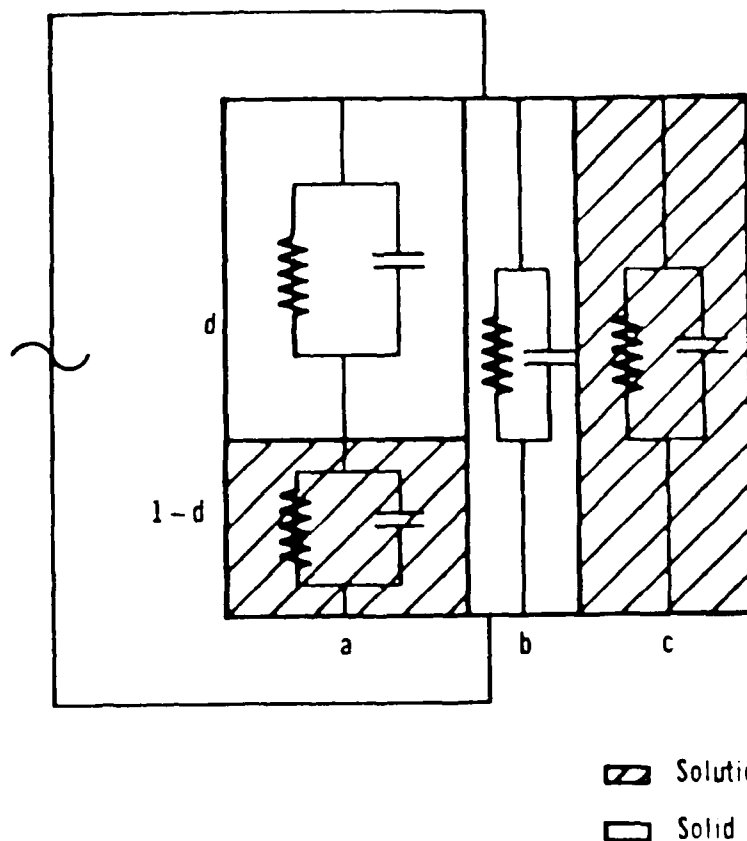


Figure 4 Three Element Electrical Model  
 Each Zone is Represented by a Parallel Circuit of Resistor and Capacitor. Impedance of Each Zone is Determined by its Dimension (a, b, c, d) and Specific Conductivity and Dielectric Constant of Material Forming the Zone ( $k_s$ ,  $k_r$ ,  $\epsilon_s$ ,  $\epsilon_r$ ).

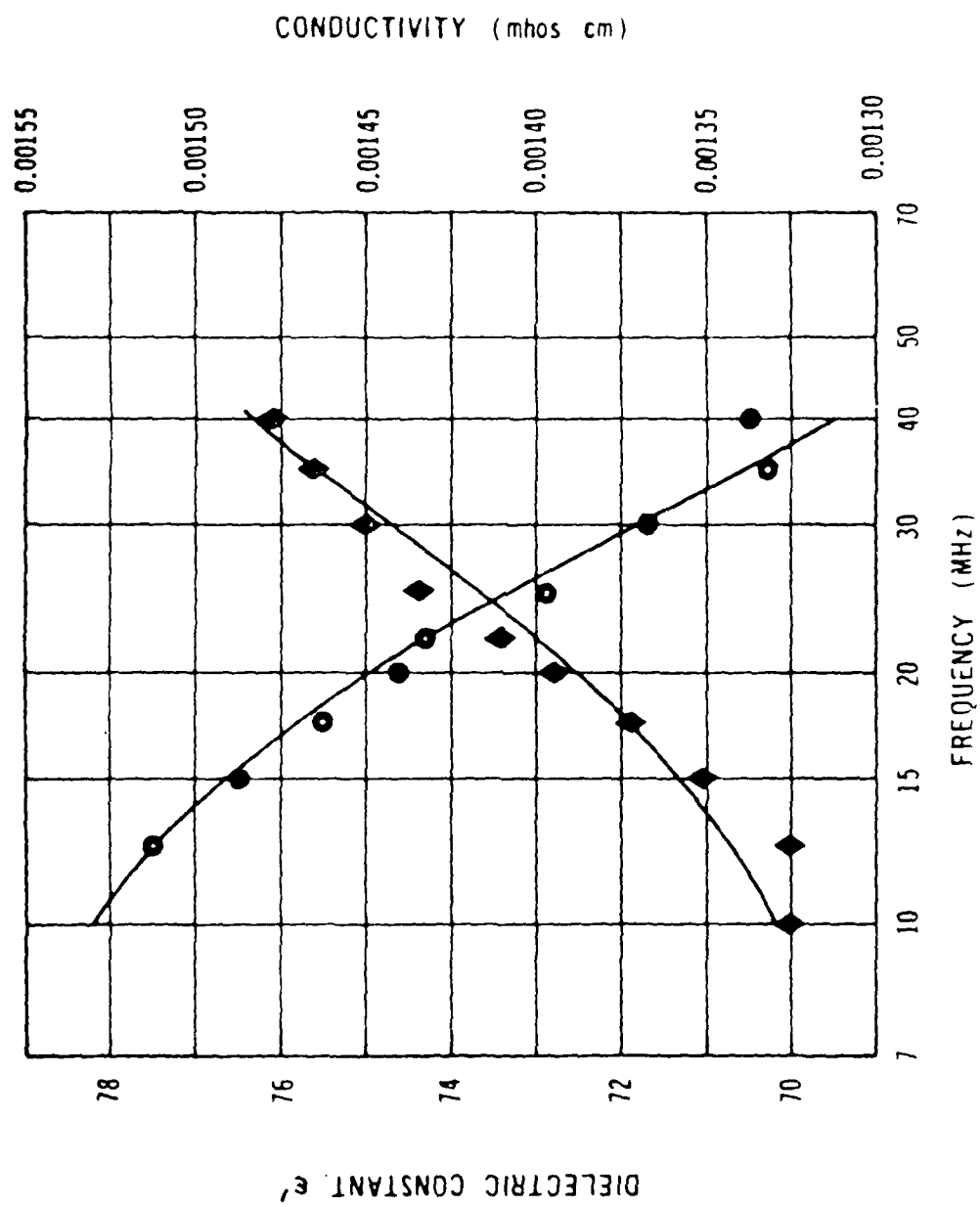


Figure 5 Water Content: w/c = 159%, Comparison of Model and Experimental Dispersions

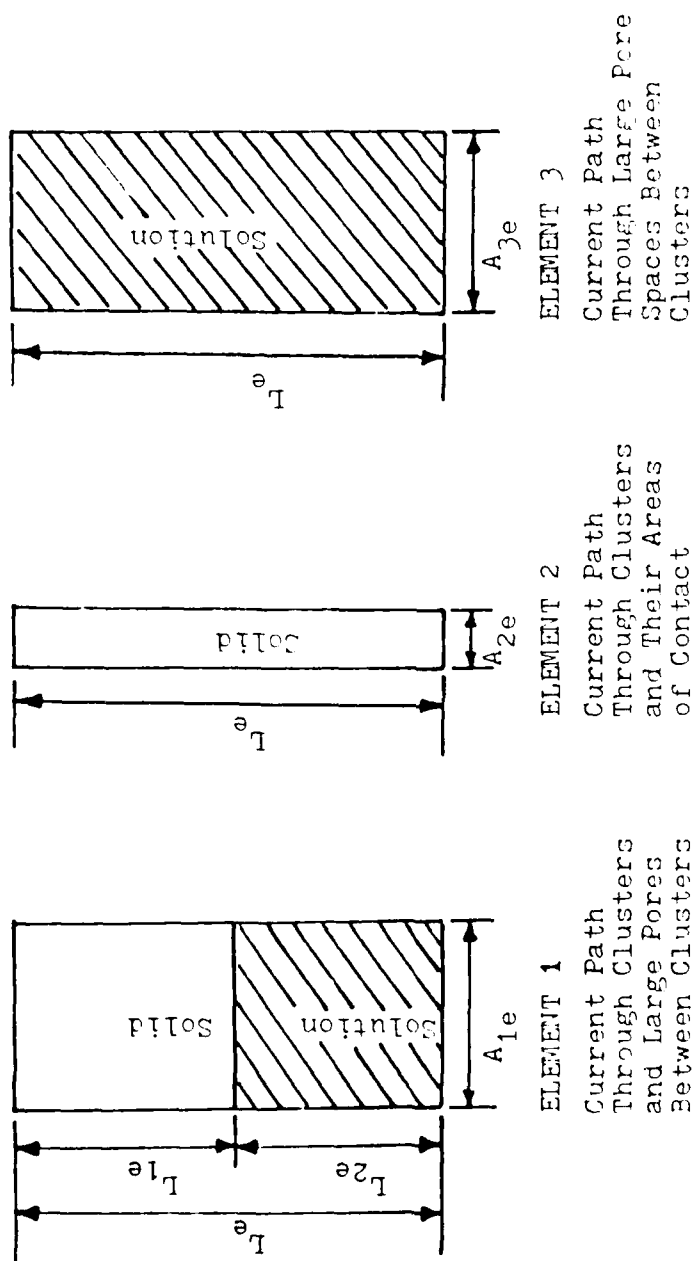
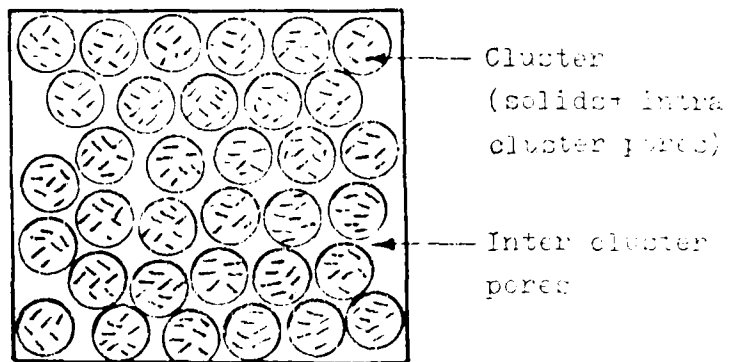
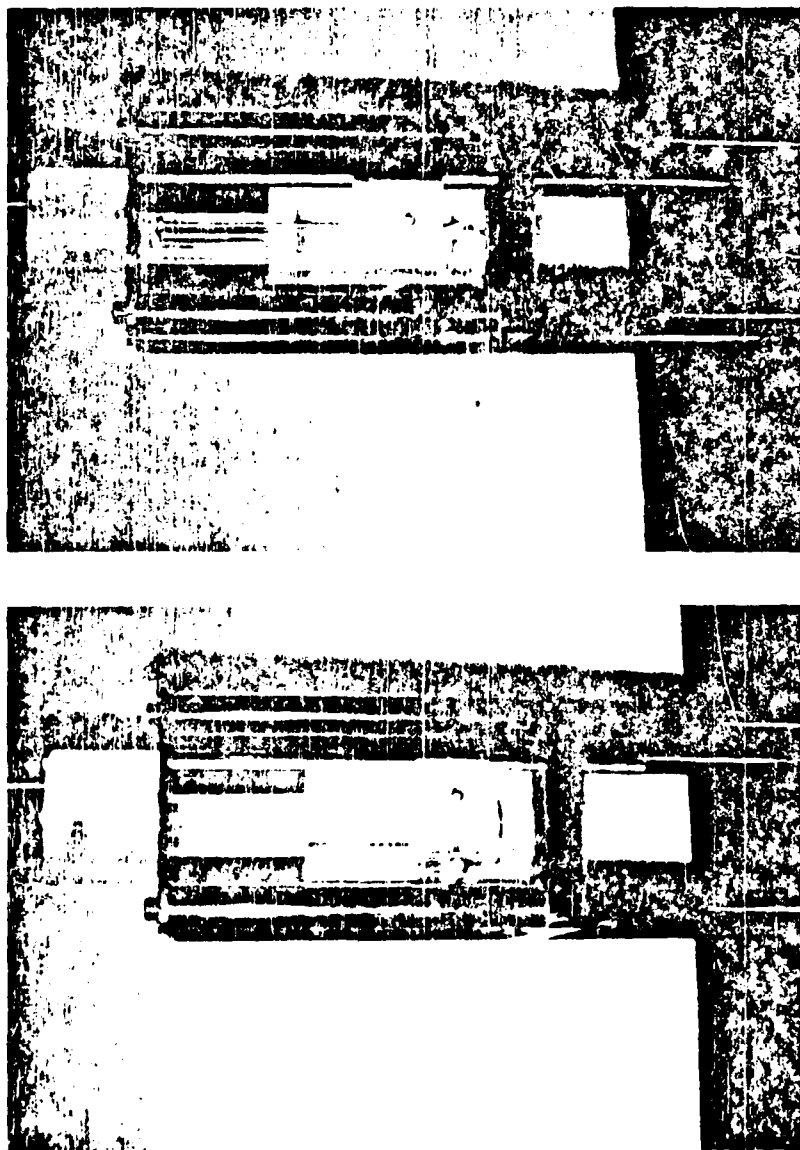


Fig. 6 ELEMENTS REPRESENTING CURRENT PATHS THROUGH CLUSTER MODEL



$V$  = Total Volume  
 $V_s$  = Volume of Solids  
 $V_p$  = Volume of Large Pores  
 $V_c$  = Volume of Clusters  
 $V_i$  = Volume of Intra Cluster Pores  
 $e_i$  = Intra Cluster Void Ratio  
 $e_p$  = Inter Cluster Void Ratio  
 $e$  = Total Void Ratio  
 $n_i$  = Intra Cluster Porosity Considering a Single Cluster  
 $n_p$  = Inter Cluster Porosity  
 $N$  = Number of Clusters Assuming all Clusters are identical

Fig. 7 CLUSTER MODEL (OLSEN , 1961)



VERTICAL

HORIZONTAL

Fig. 8 Square Electrical Cells and the consolidation frames used for the determination of electrical properties at different water contents.

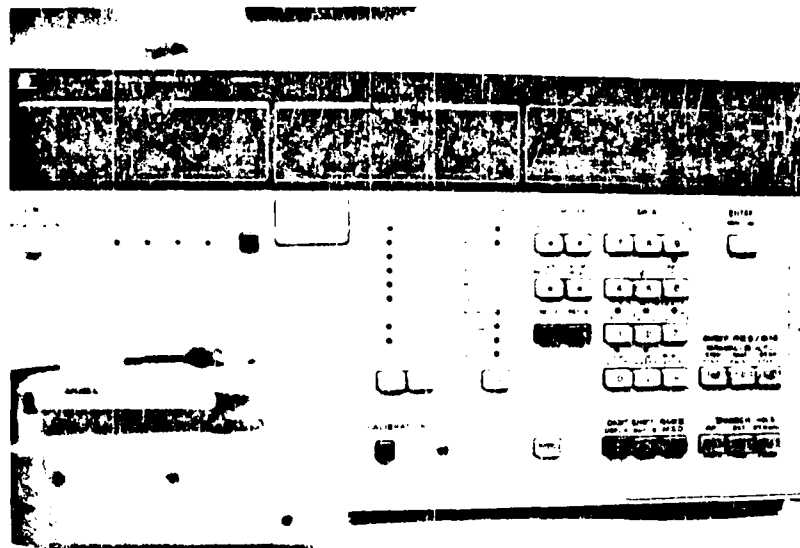


Fig. 9 The impedance analyzer used for the measurement of electrical properties in the radio frequency range.



Fig. 10 The impedance comparator used for the measurement of electrical properties at low frequencies ( $\approx 1$  kHz).

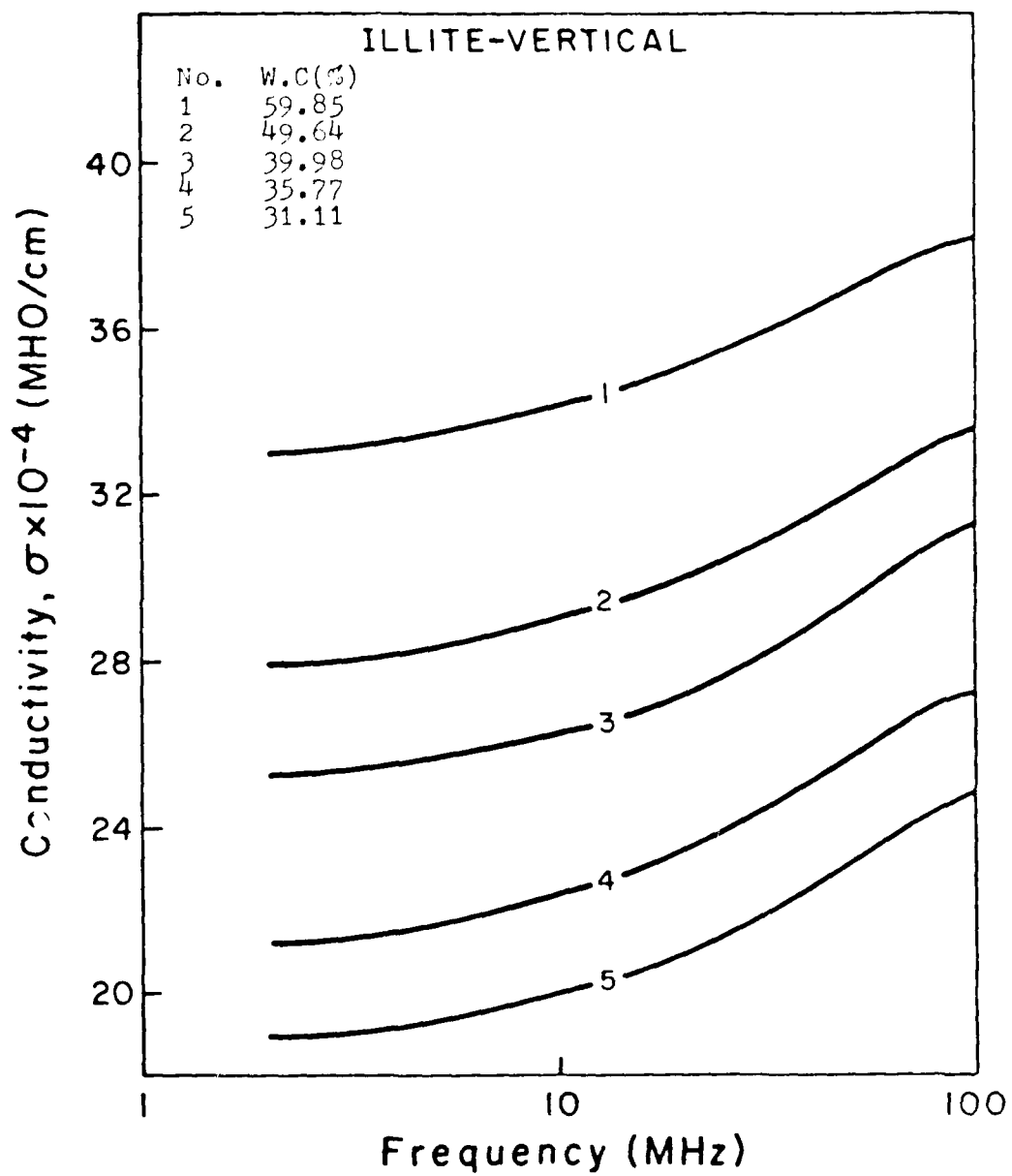


Fig. II Conductivity as a function of frequency at different water contents

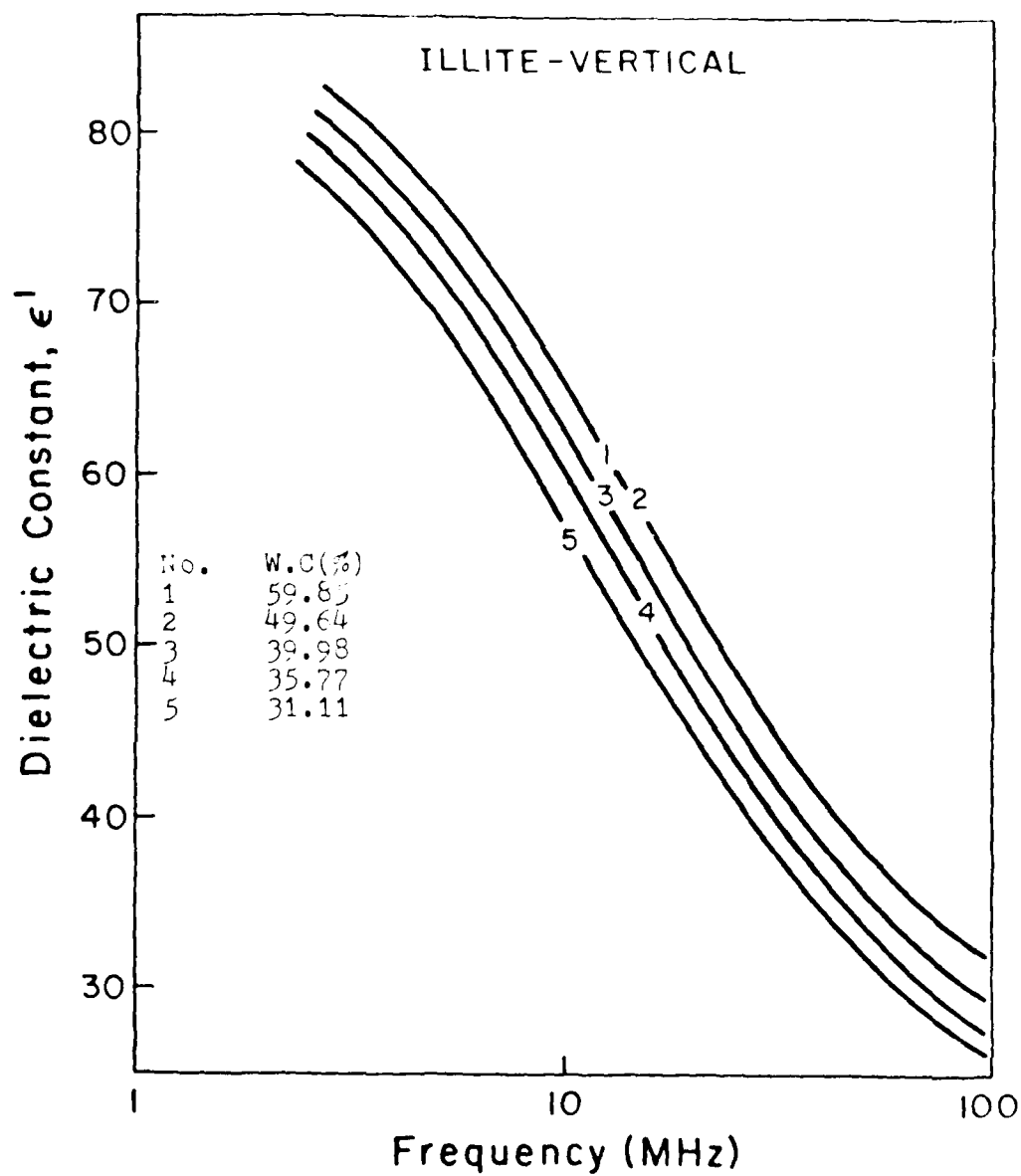


Fig. 12 Dielectric constant as a function of frequency  
at different water contents

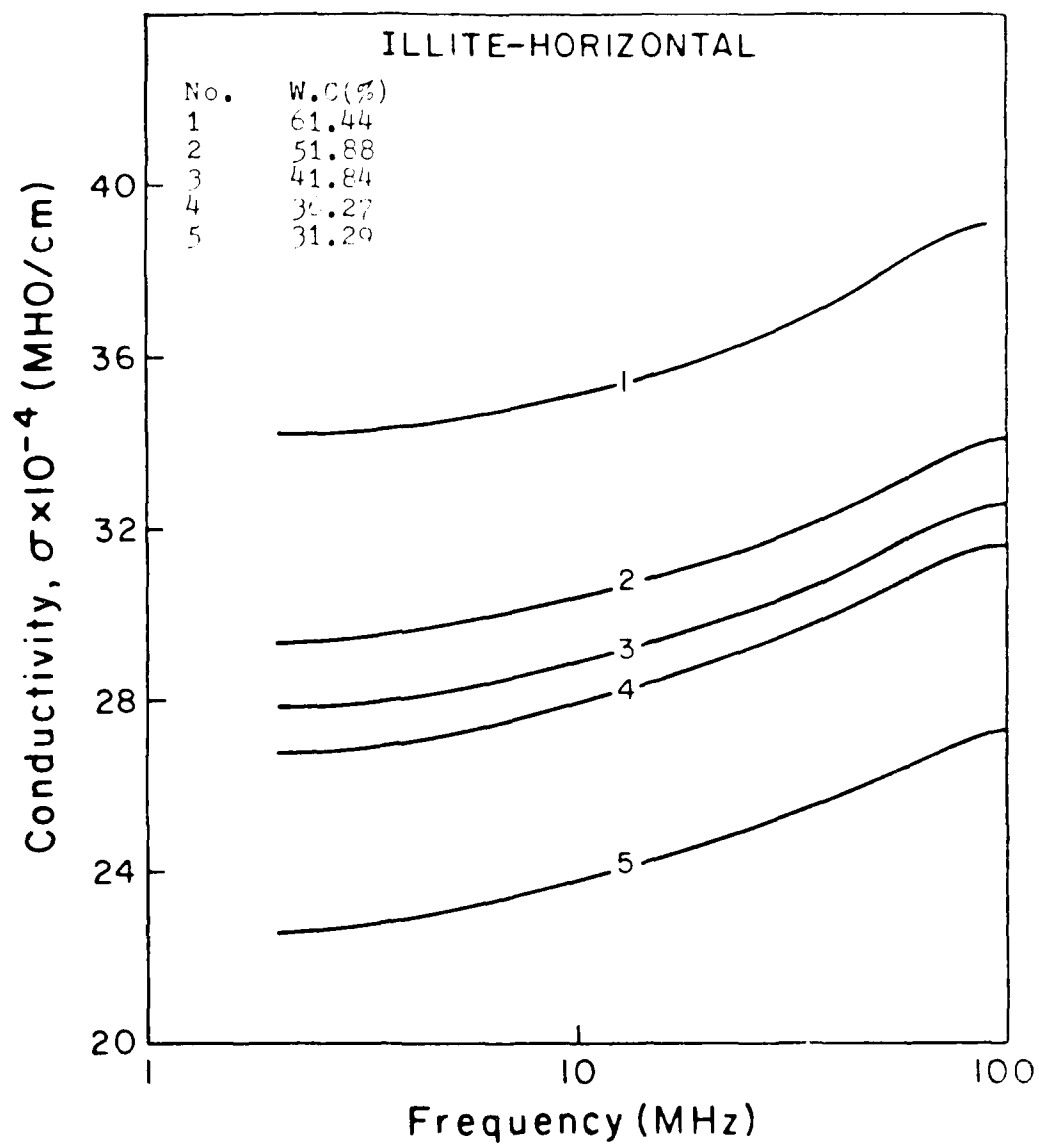


Fig. 13 Conductivity as a function of frequency at different water contents.

AD-A131 650

IN SITU CHARACTERIZATION OF SOILS FOR PREDICTION OF  
STRESS STRAIN RELATIO..(U) CALIFORNIA UNIV DAVIS DEPT  
OF CIVIL ENGINEERING K ARULANANDAN ET AL. 10 NOV 82  
AFOSR-TR-83-0680 AFOSR-81-0216

2/2

UNCLASSIFIED

F/G 8/13

NL

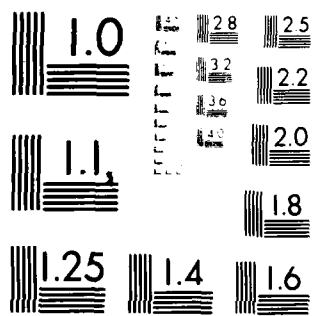
END

DATE

FILED

9 83

DTIC



MICROCOPY RESOLUTION TEST CHART  
NATIONAL BUREAU OF STANDARDS-1963-A

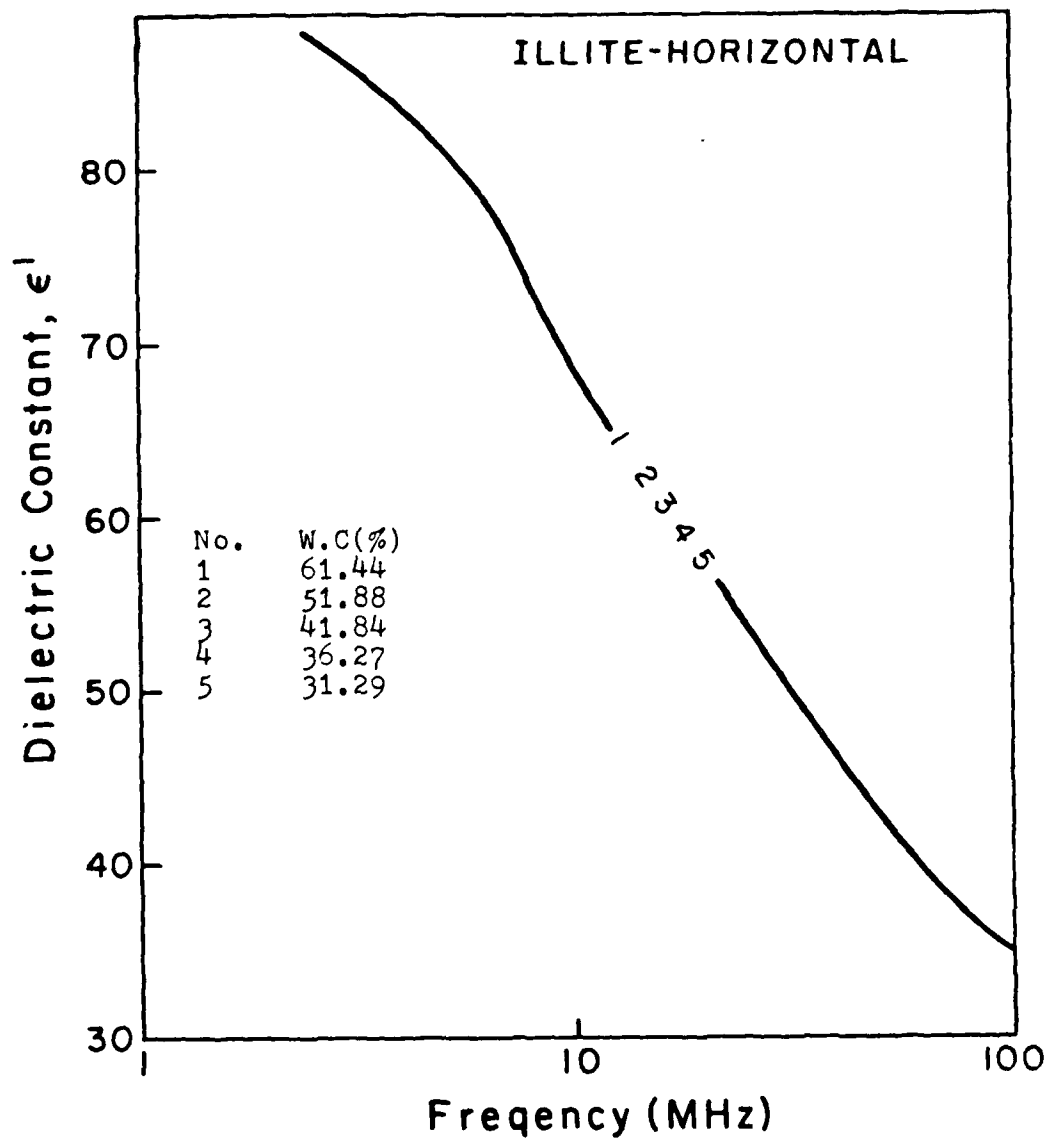


Fig. 14 Dielectric constant as a function of frequency at different water contents.

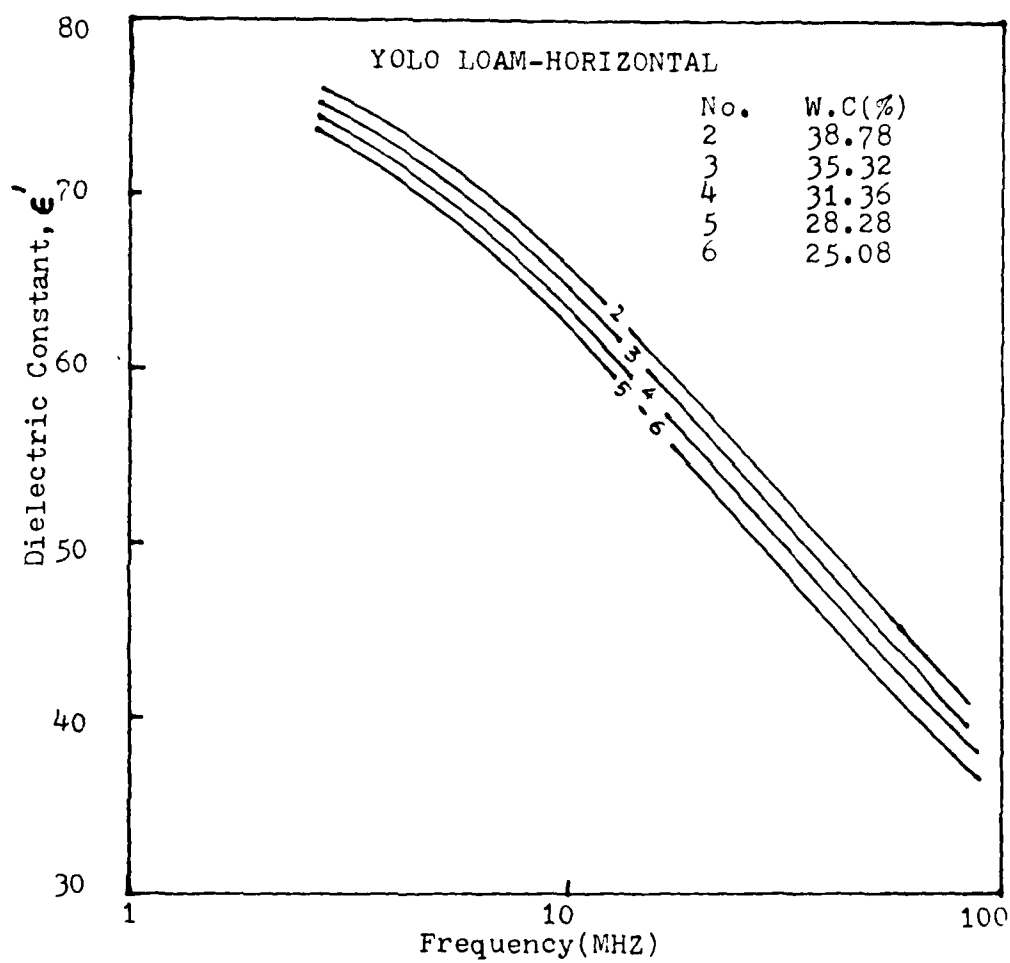


Fig. 15 Dielectric constant as a function of frequency at different water contents.

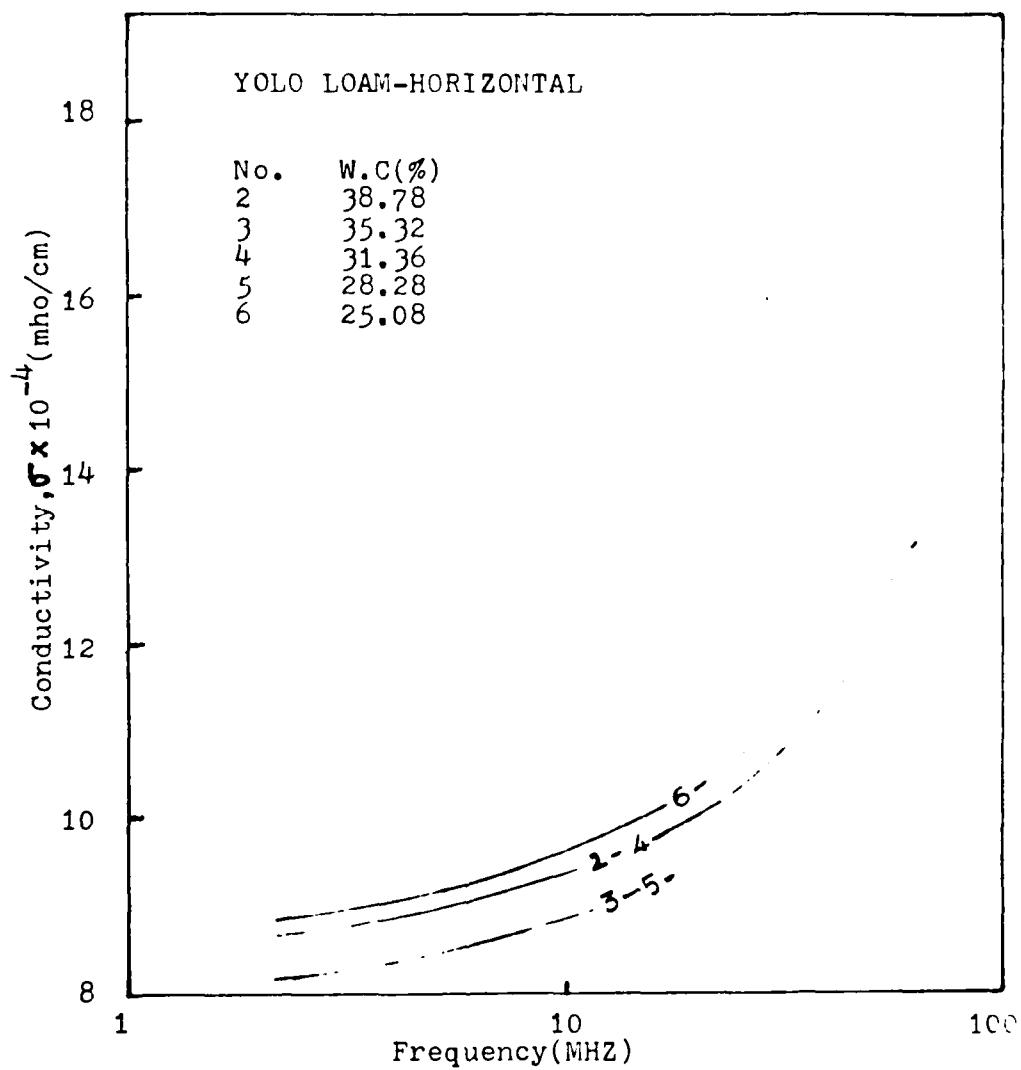


Fig. 16 Conductivity as a function of frequency at different water contents.

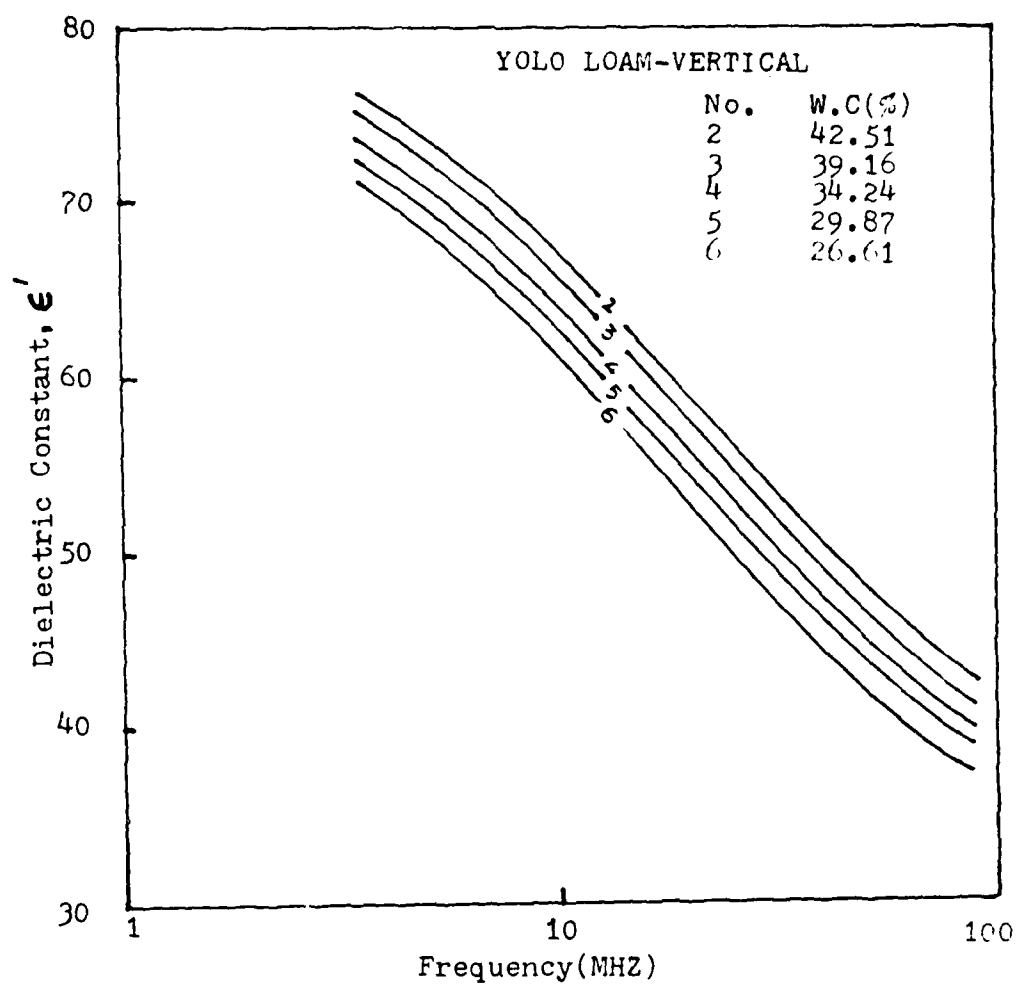


Fig. 17 Dielectric constant as a function of frequency at different water contents.

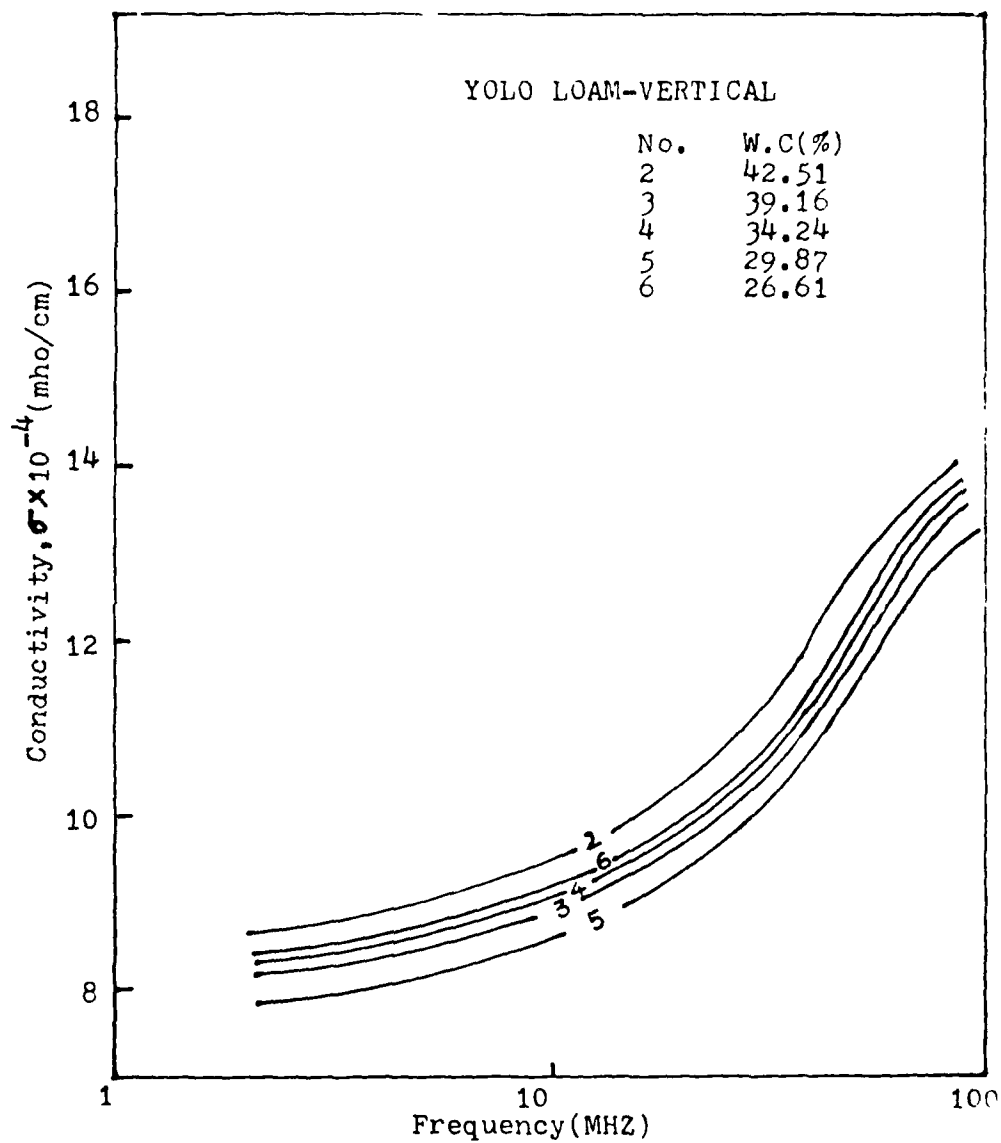


Fig. 18 Conductivity as a function of frequency at different water contents.

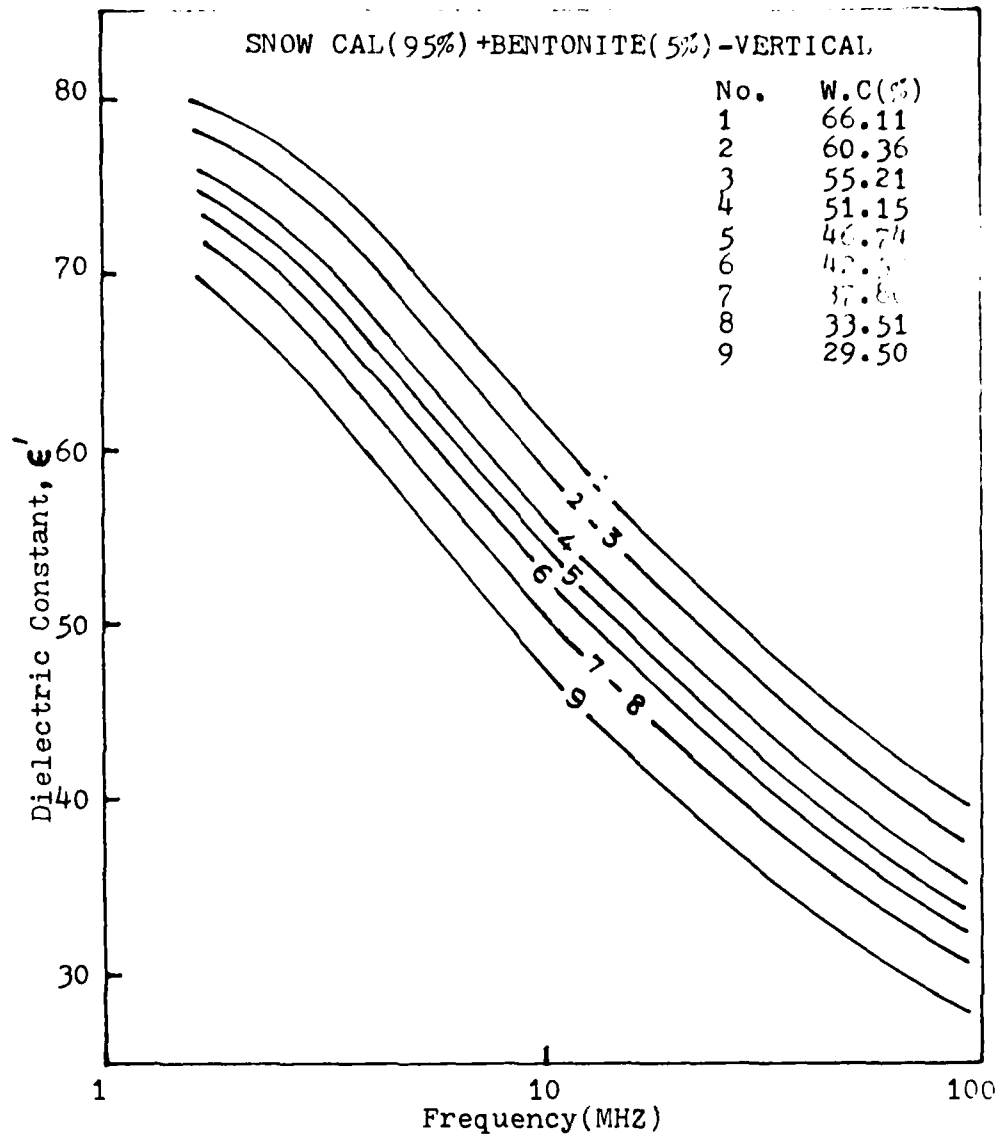


Fig. 19 Dielectric constant as a function of frequency at different water content.

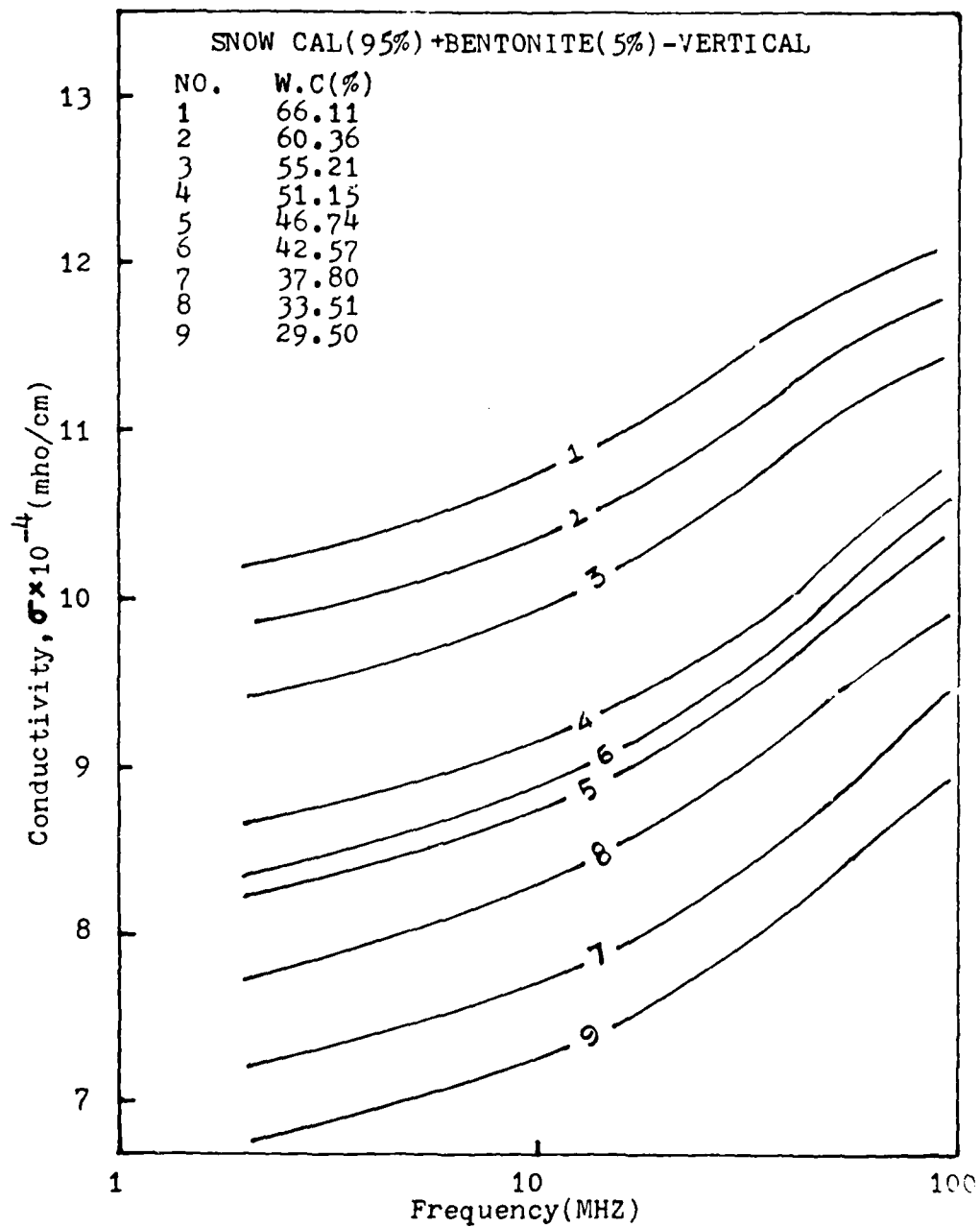


Fig. 20 Conductivity as a function of frequency at different water content.

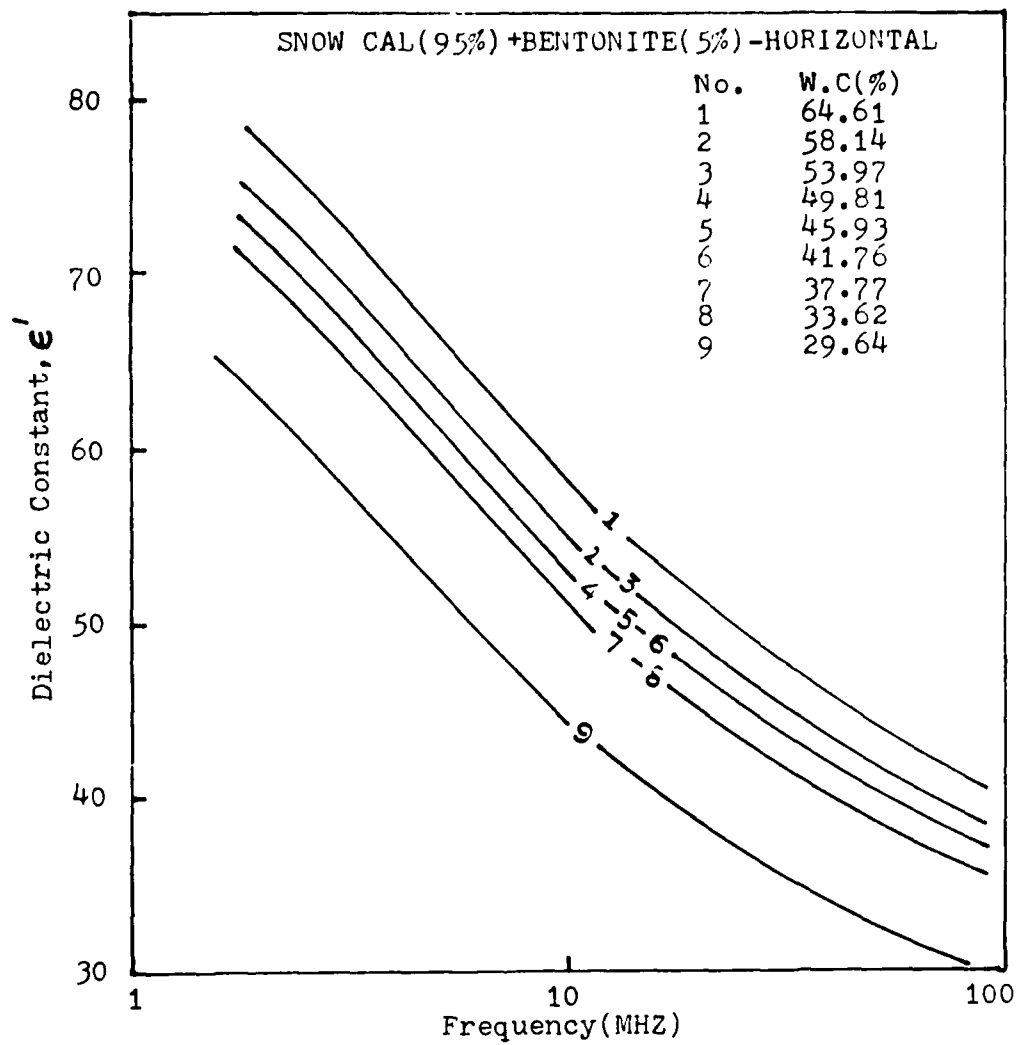


Fig. 21 Dielectric constant as a function of frequency at different water content.

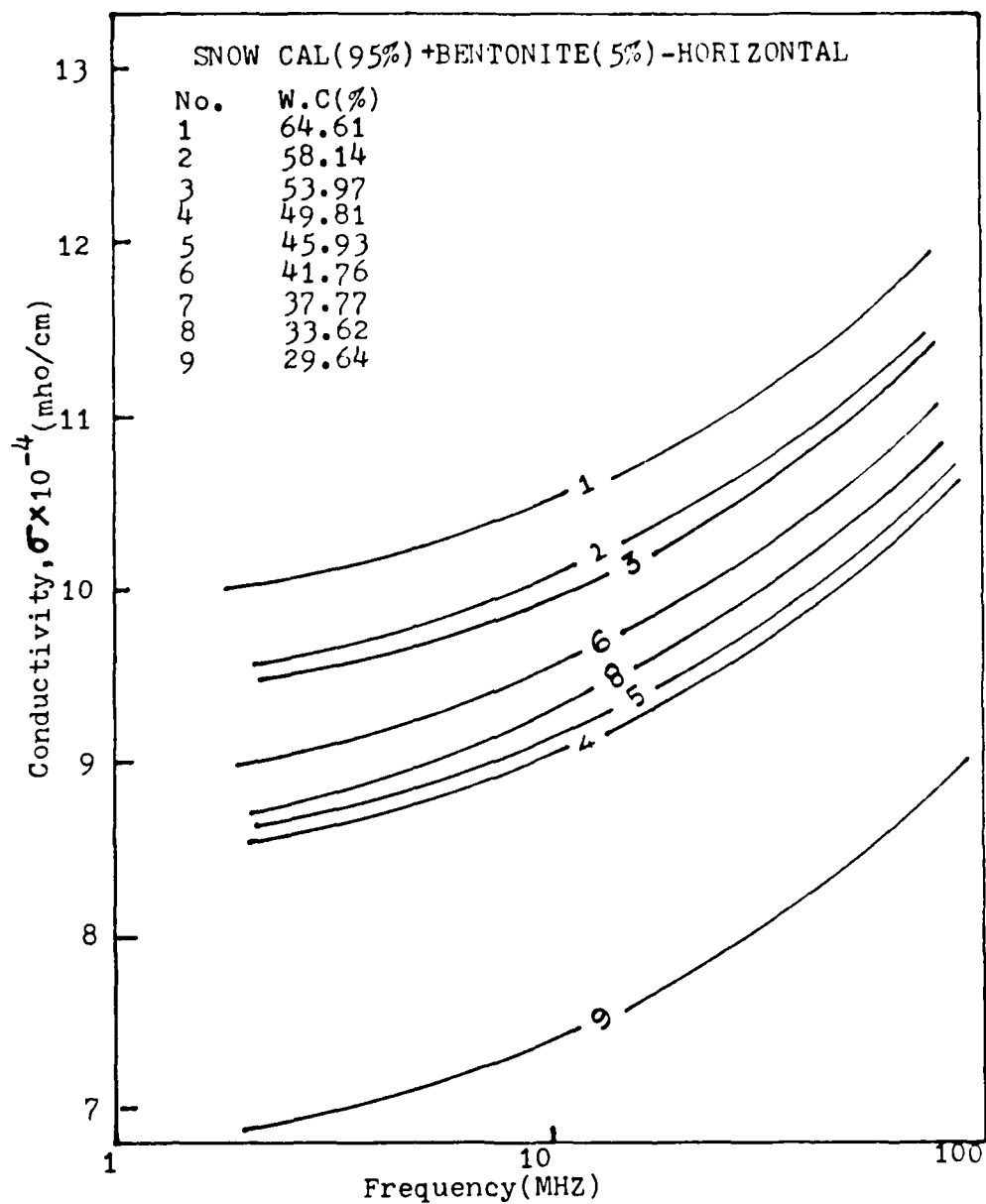


Fig. 22 Conductivity as a function of frequency at different water content.

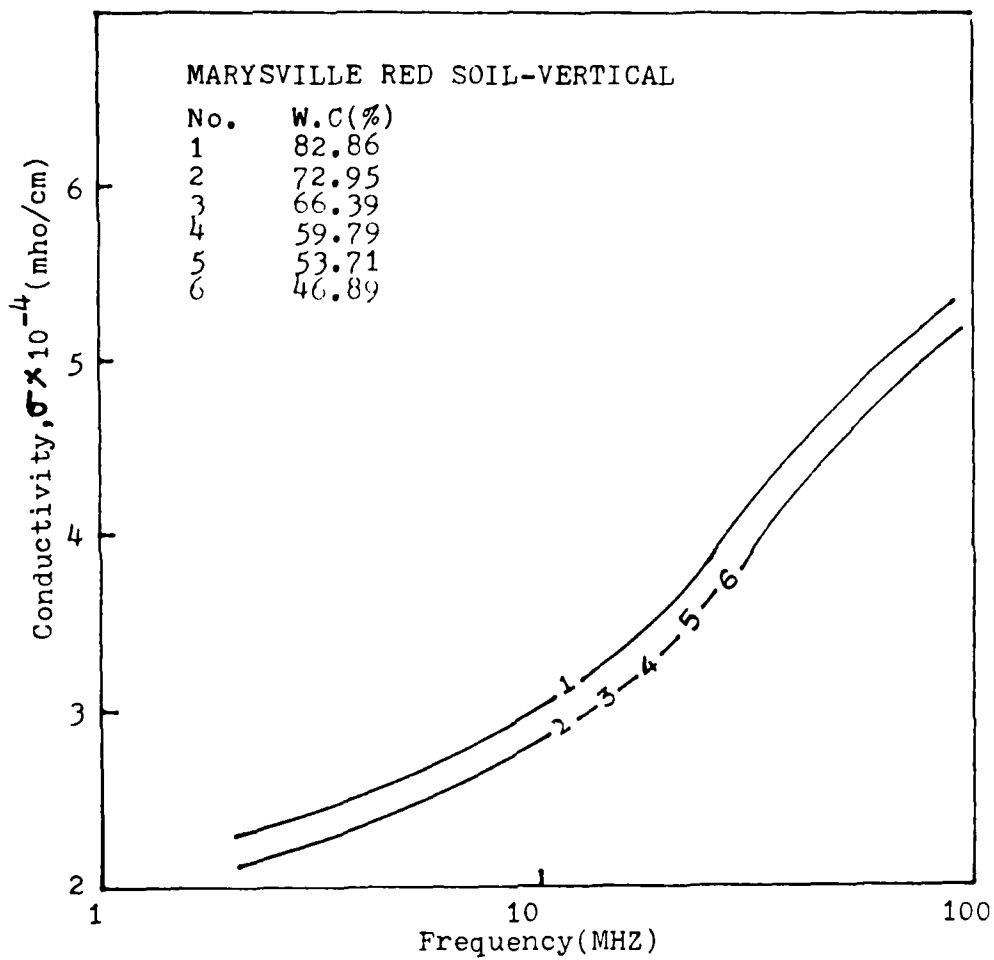


Fig. 23 Conductivity as a function of frequency at different water contents.

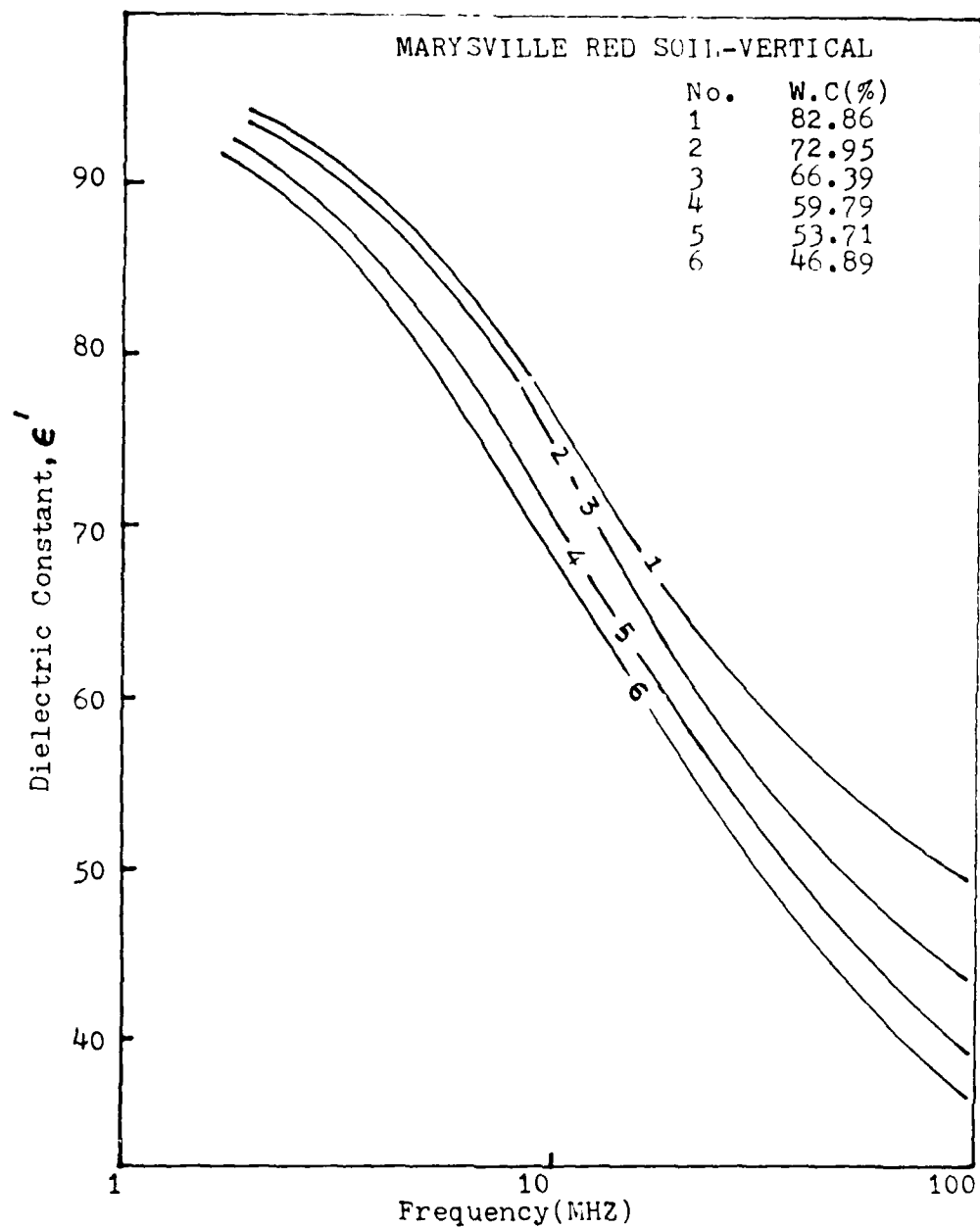


Fig. 24 Dielectric constant as a function of frequency at different water contents.

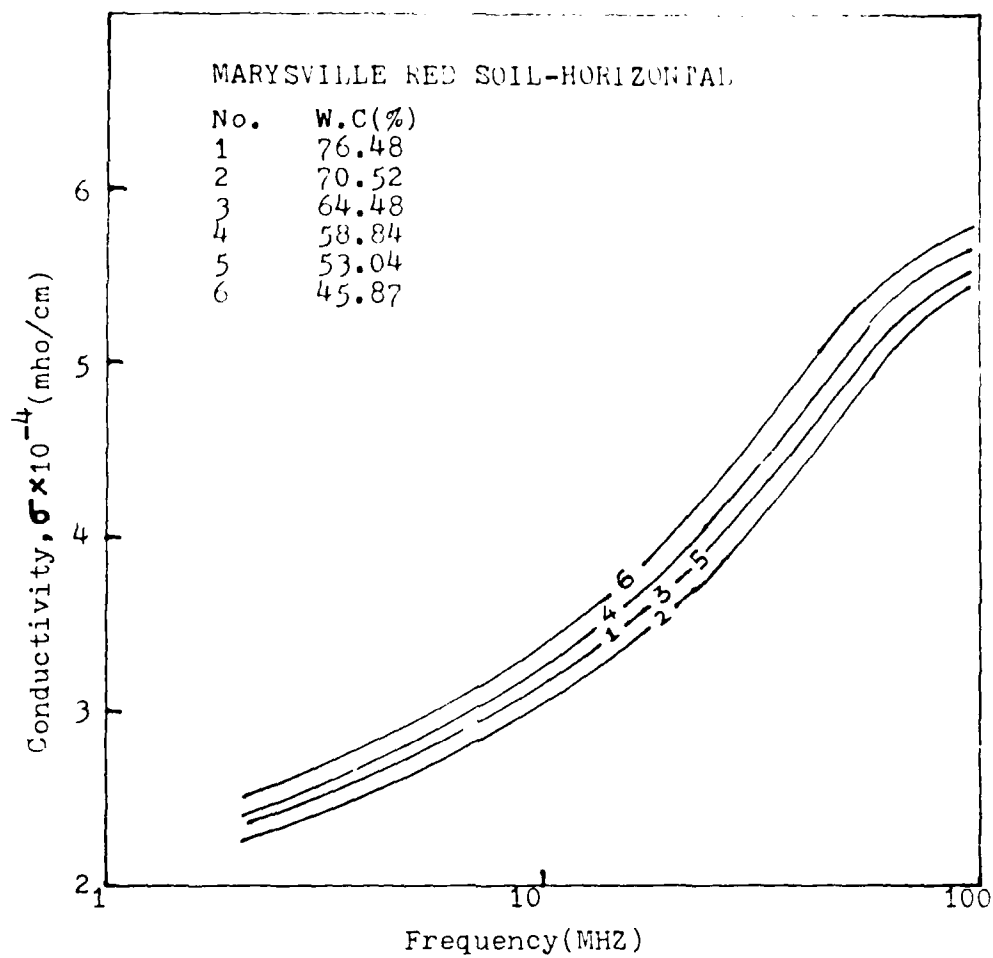


Fig. 25 Conductivity as a function of frequency at different water contents.

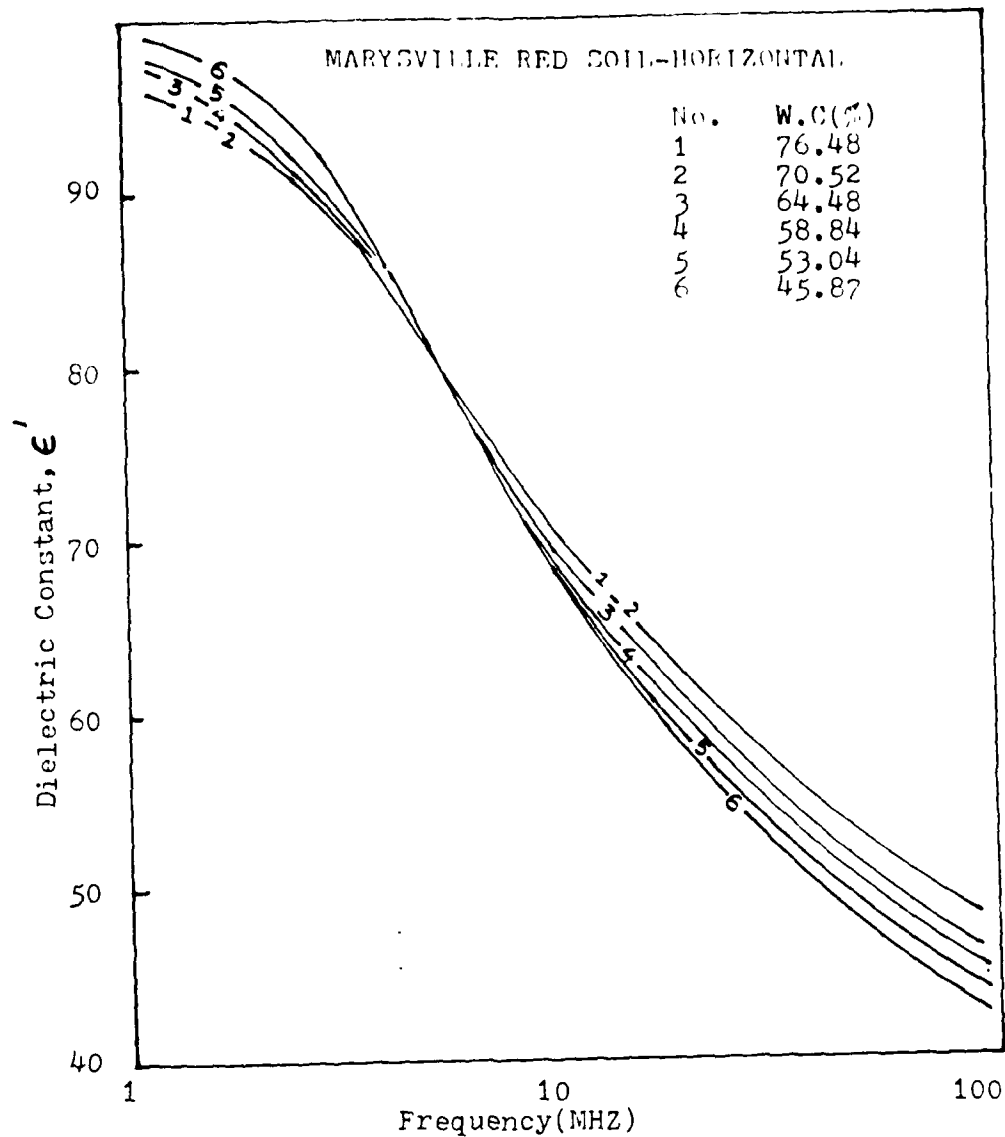


Fig. 26 Dielectric constant as a function of frequency at different water contents.

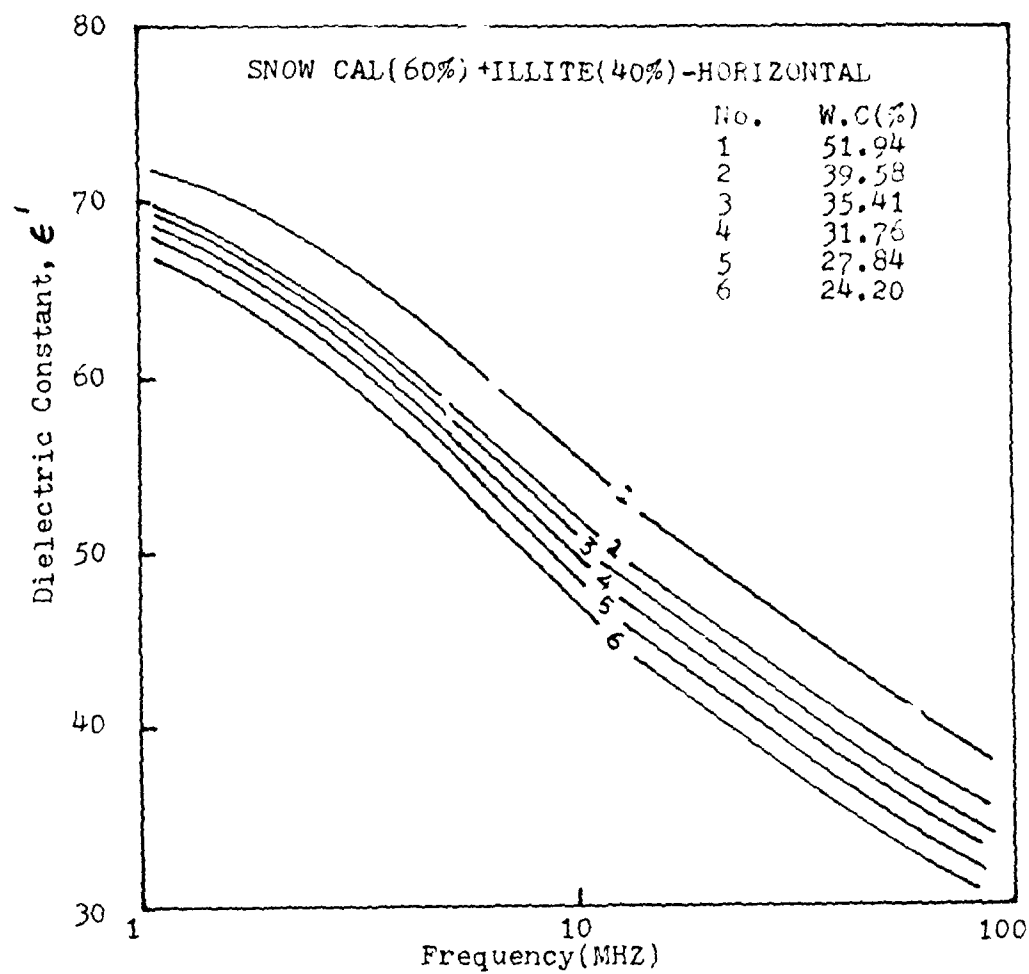


Fig. 27 Dielectric constant as a function of frequency at different water contents.

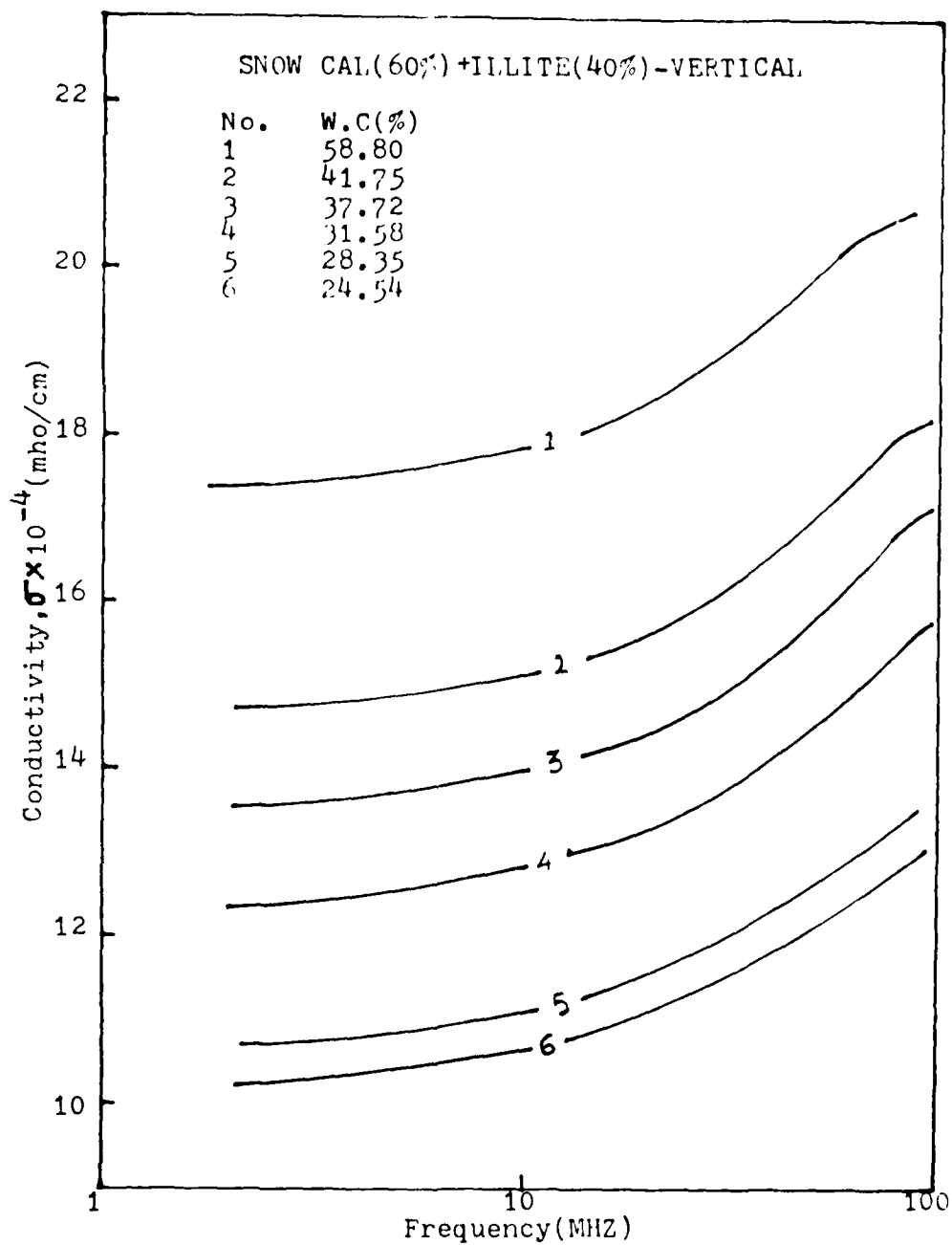


Fig.28 Conductivity as a function of frequency at different water contents.

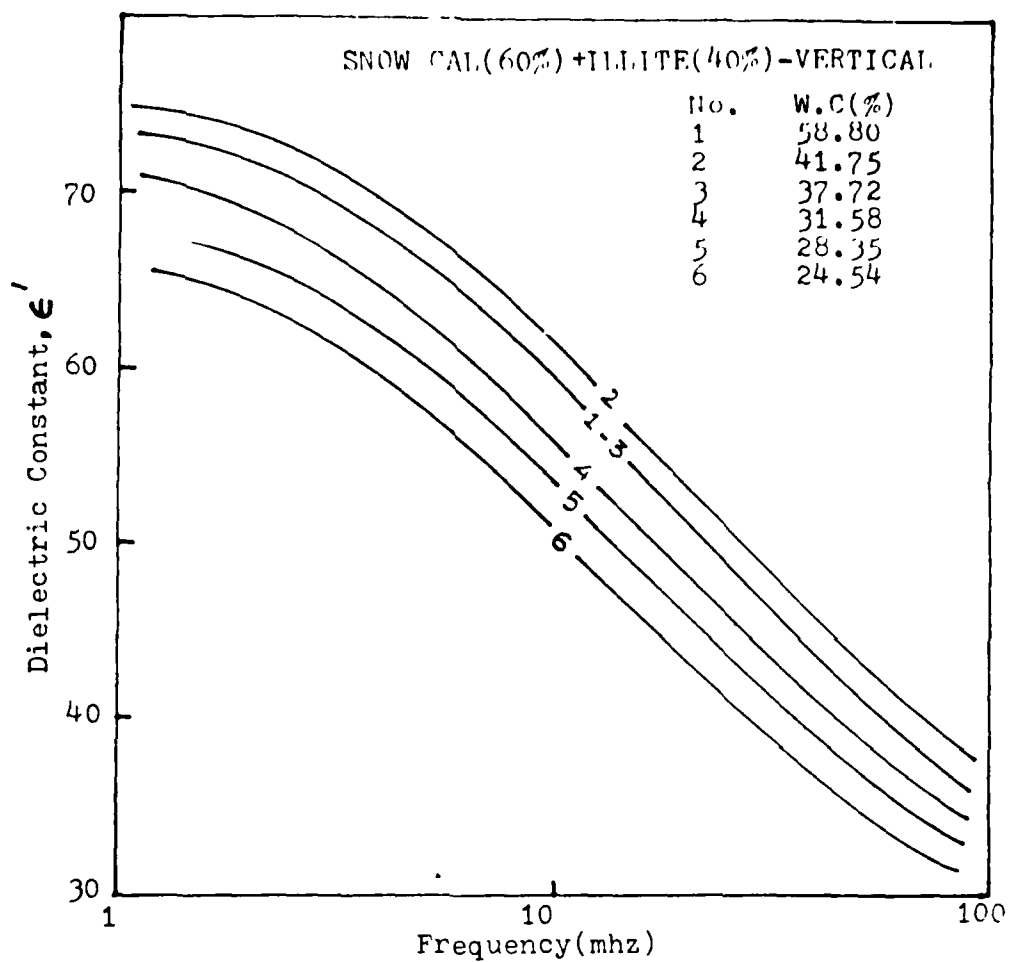


Fig. 29 Dielectric constant as a function of frequency at different water contents.

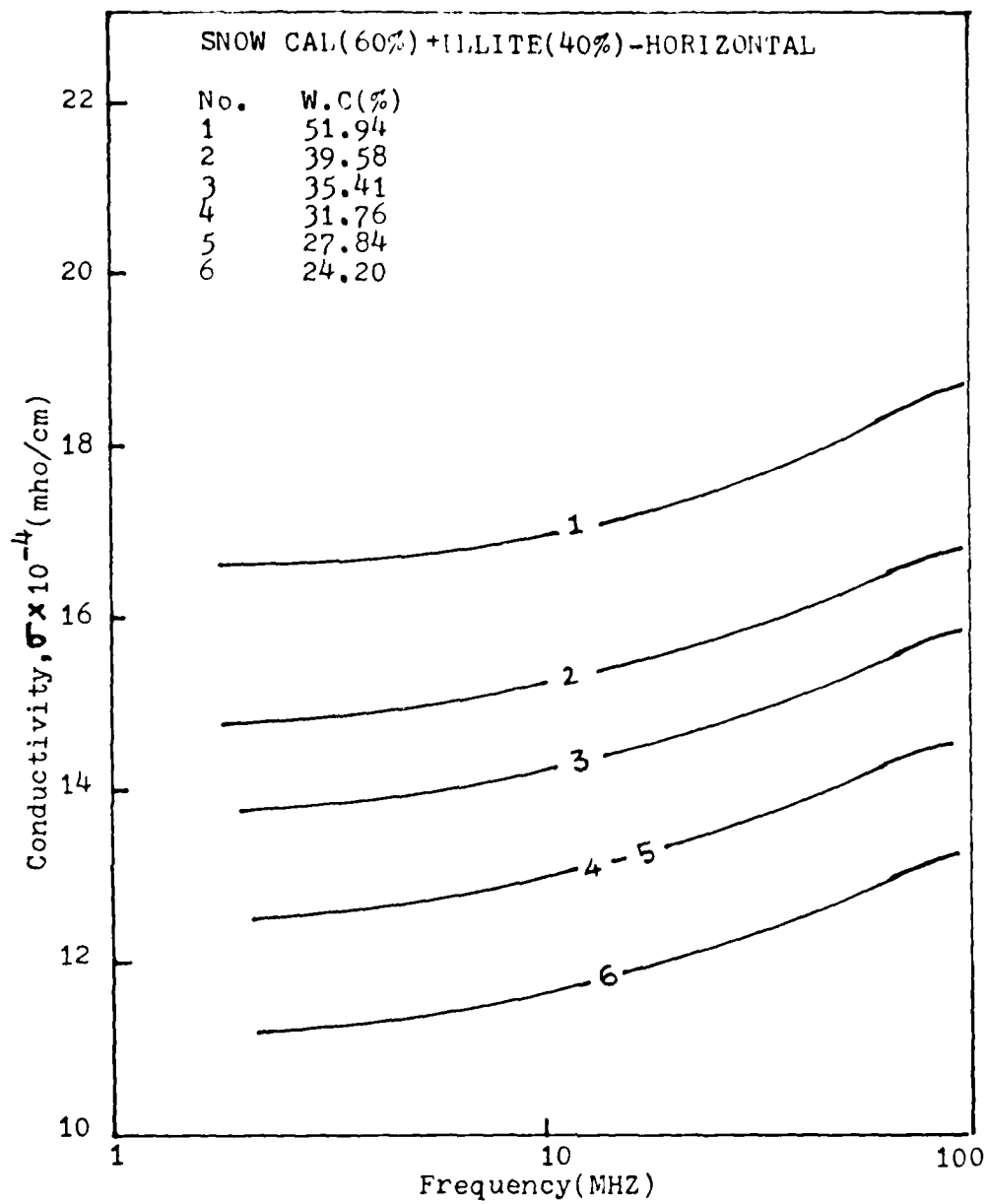


Fig. 30 Conductivity as a function of frequency at different water contents.

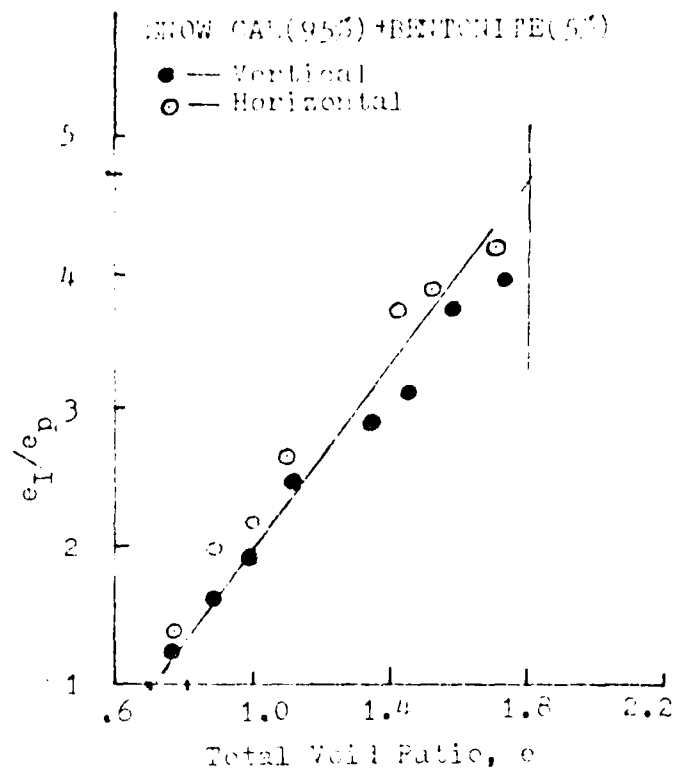


Fig. 31 The relationship between the ratio of intra and inter cluster void ratio,  $e_I/e_p$ , and the total void ratio,  $e$ .

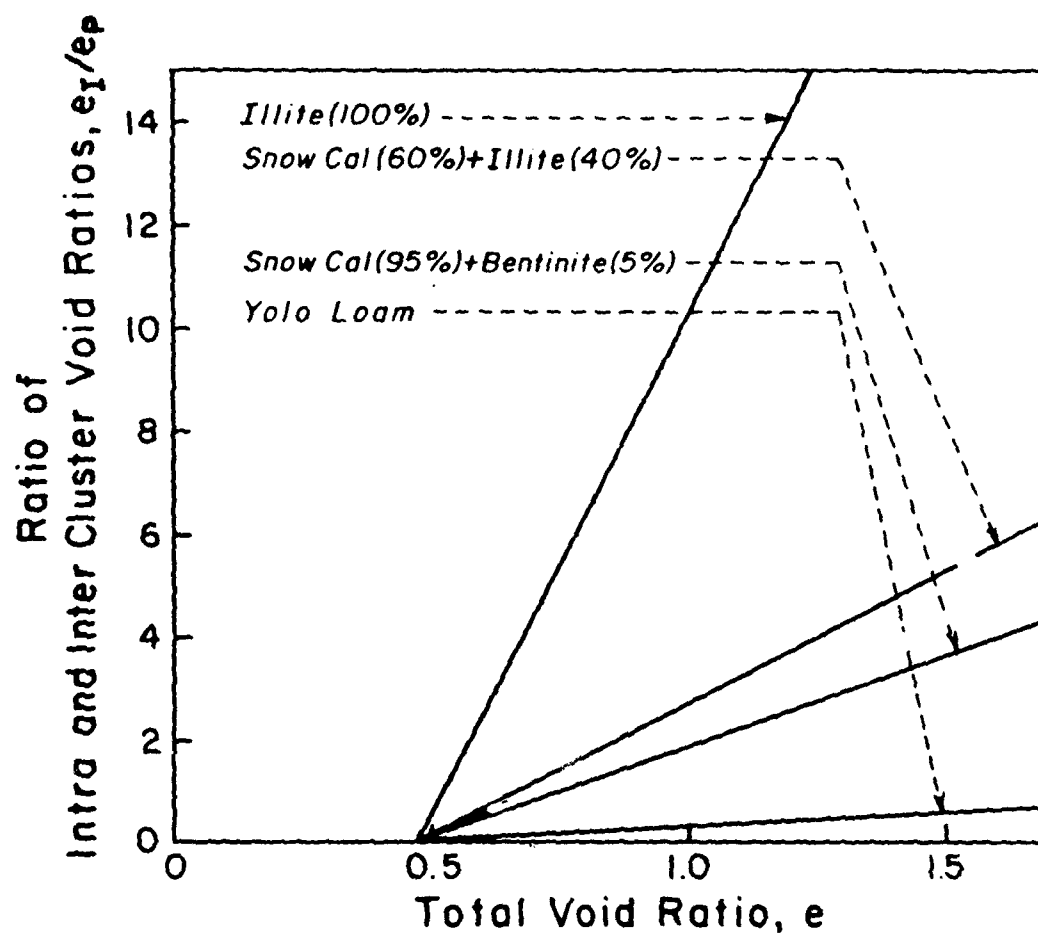


Fig. 32 The relationship between the ratios of intra and inter cluster void ratios and the total void ratios.

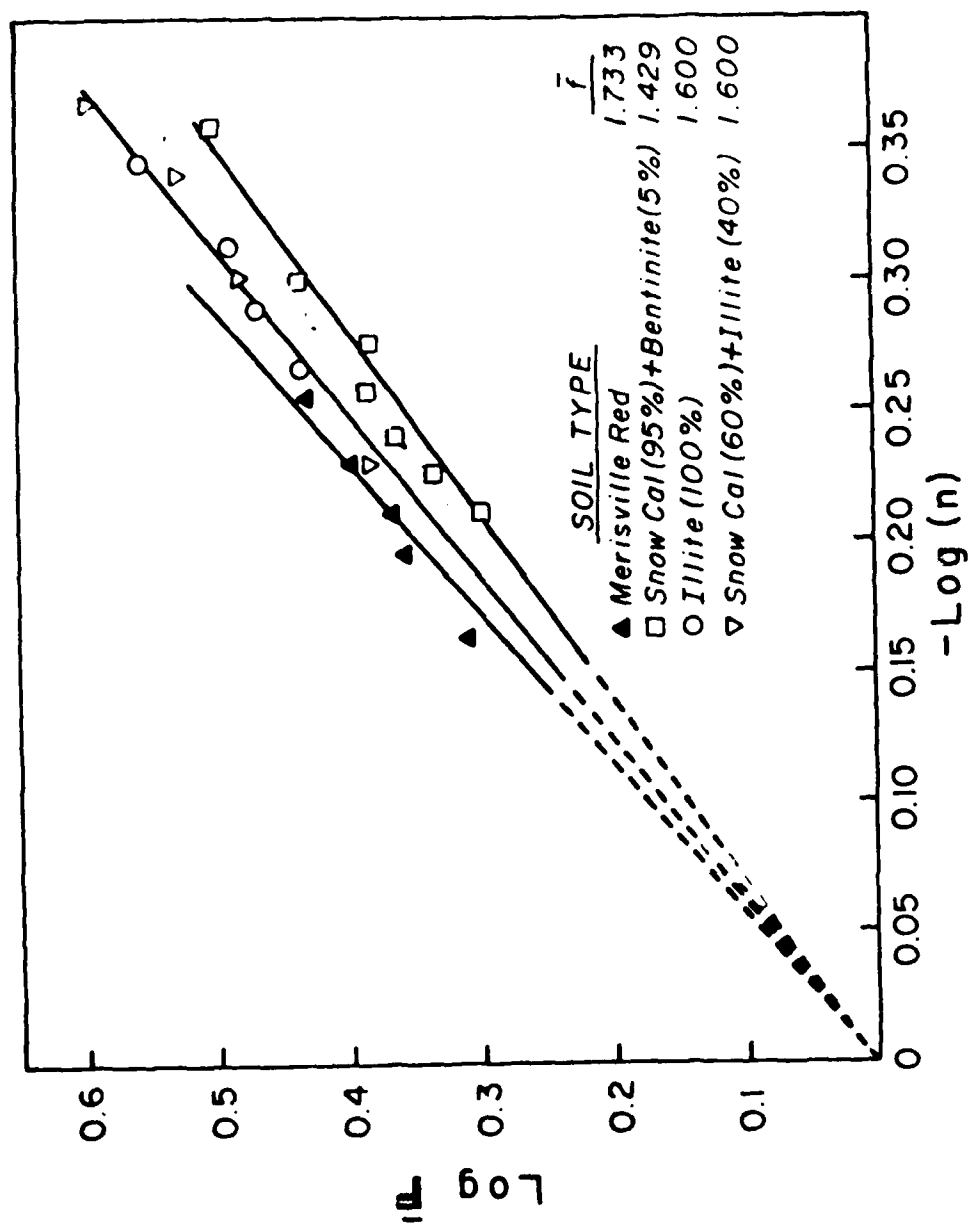


Fig. 33 The relationship between the average formation factor,  $\bar{F}$ , and the total porosity,  $n$

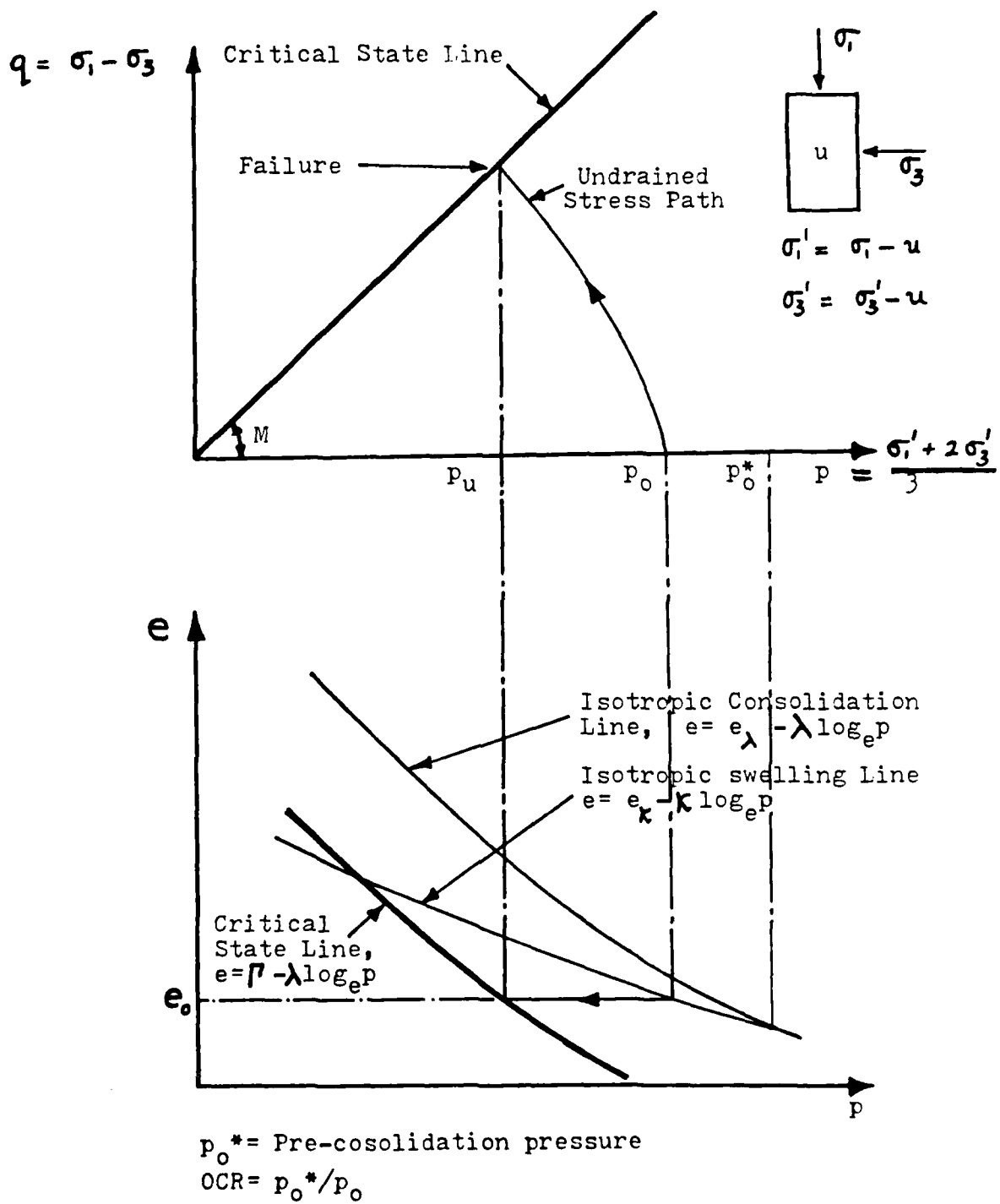


Fig. 34 Schematic Illustration of the definition of  $\lambda, \kappa, M, e_0$  and OCR

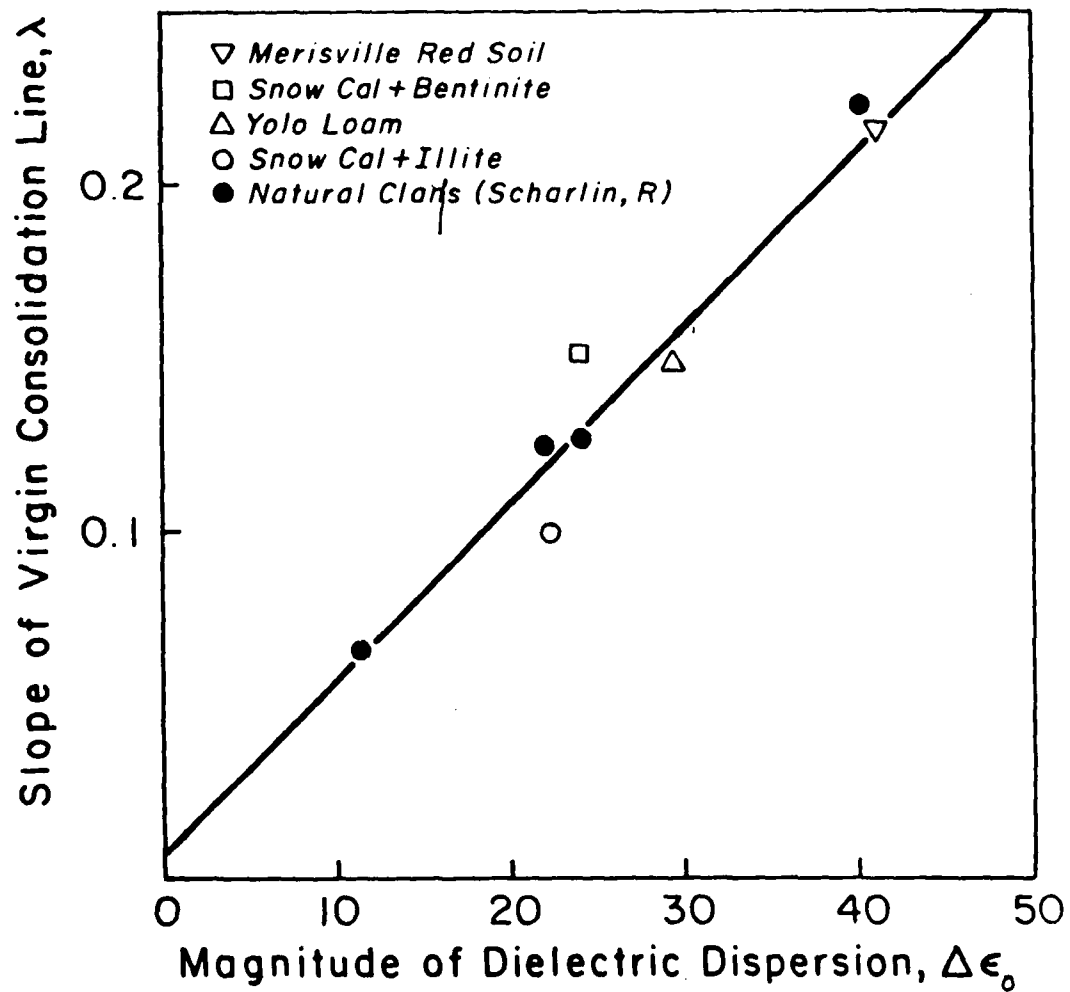


Fig. 35 The relationship between the slope of the isotropic consolidation line,  $\lambda$ , and the magnitude of dielectric dispersion,  $\Delta\epsilon_0$ .

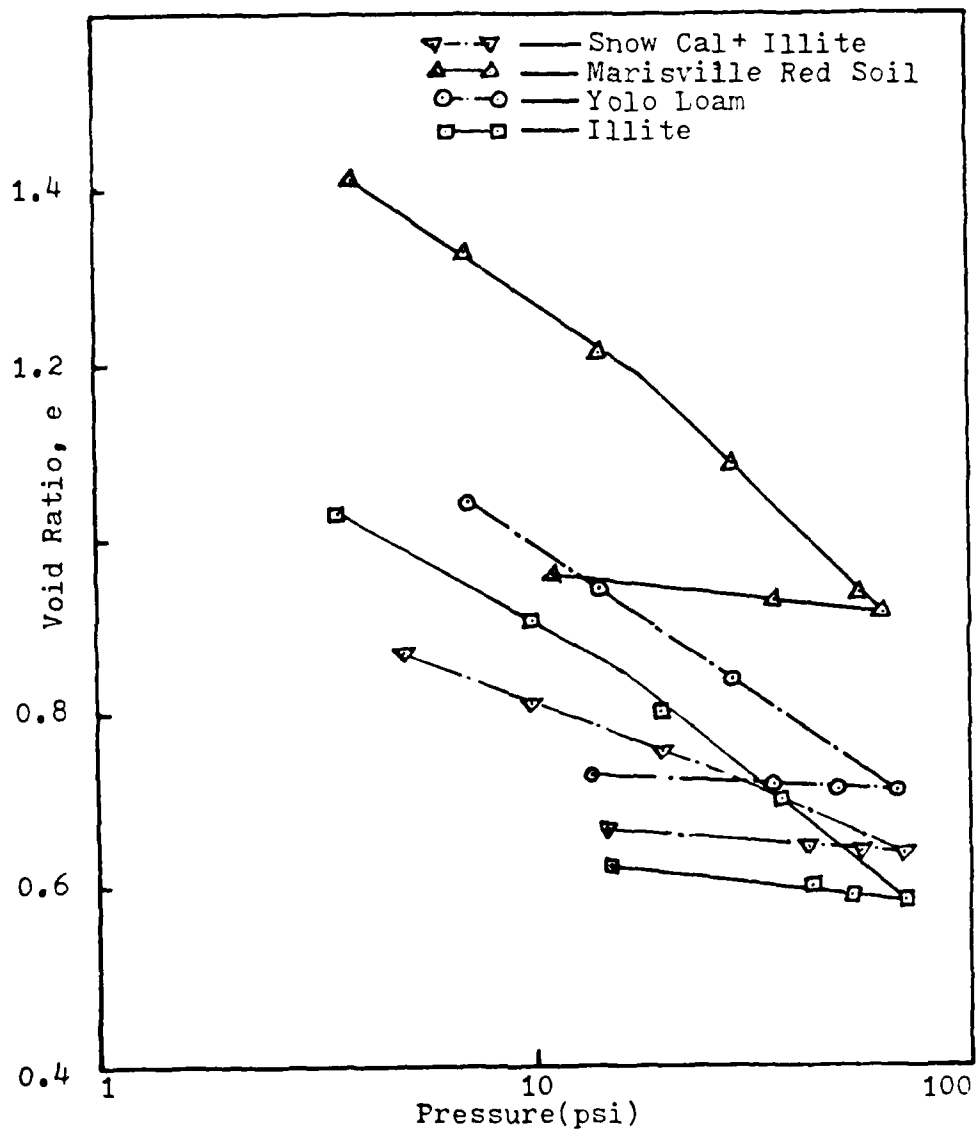


Fig. 36 The relationship between the pressure and the void ratio during an isotropic consolidation test.

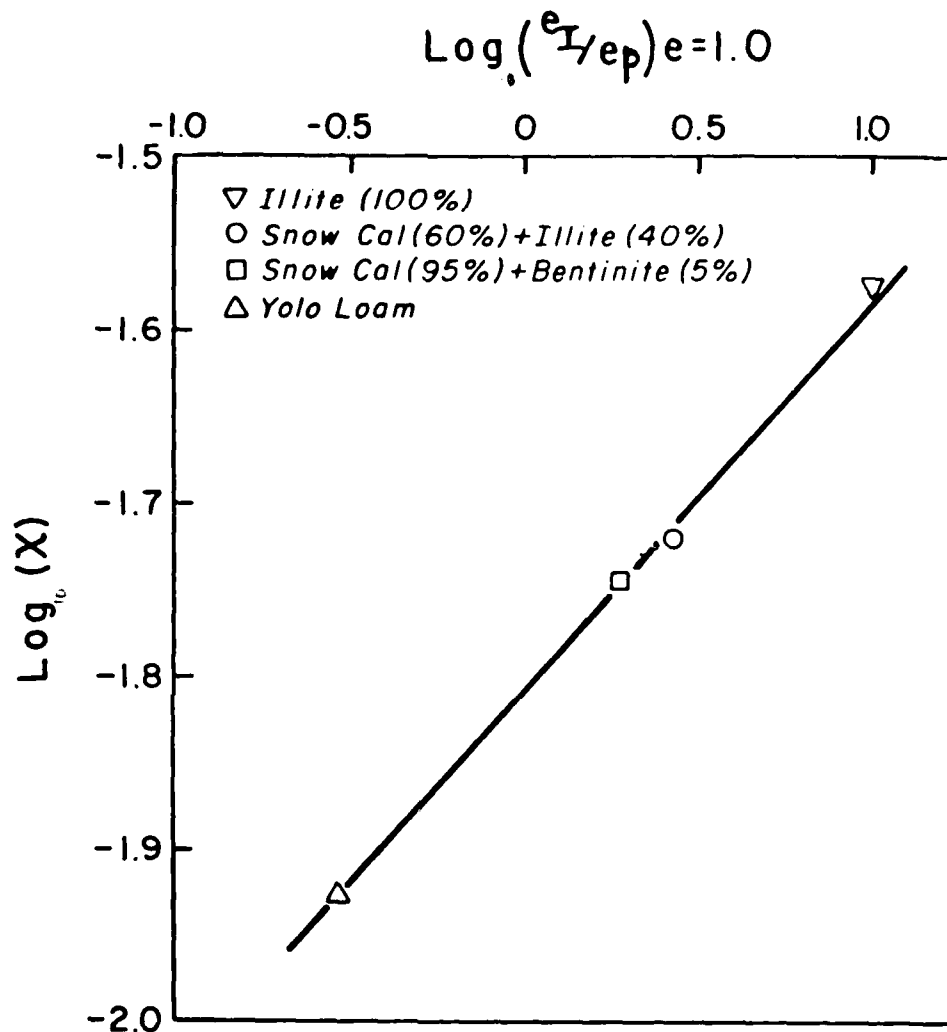
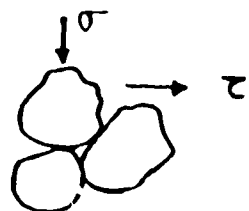
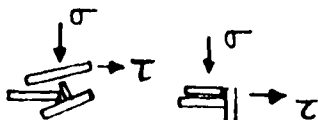


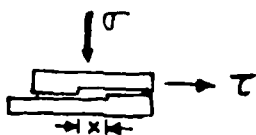
Fig. 37 The relationship between the slope of the isotropic swelling line,  $\kappa$ , and the ratios of intra and inter cluster void ratios at  $e=1.0$



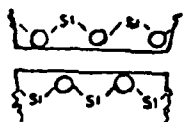
a. Interference in silt



b. Interference in clay



c. Friction between rough clay surfaces



d. Friction between smooth clay surfaces

#### FRICITION IN SOIL

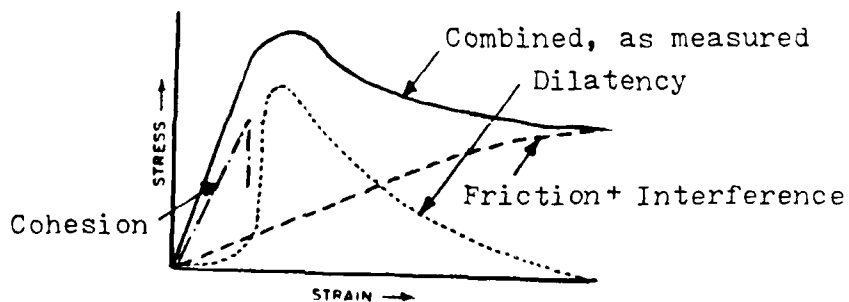


Fig. 38 COMPONENTS OF SHEAR RESISTANCE (LAMB, 1960)

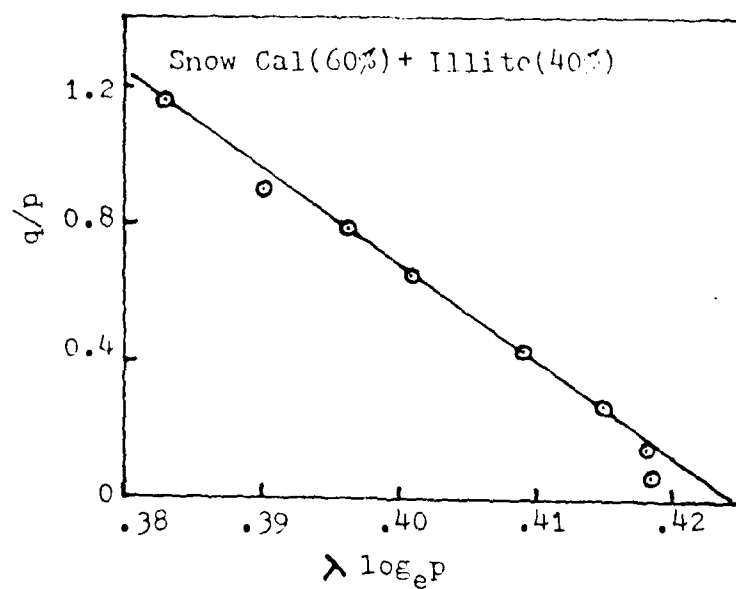


Fig. 39 The relationship between  $\lambda \log_e p$  and  $q/p$

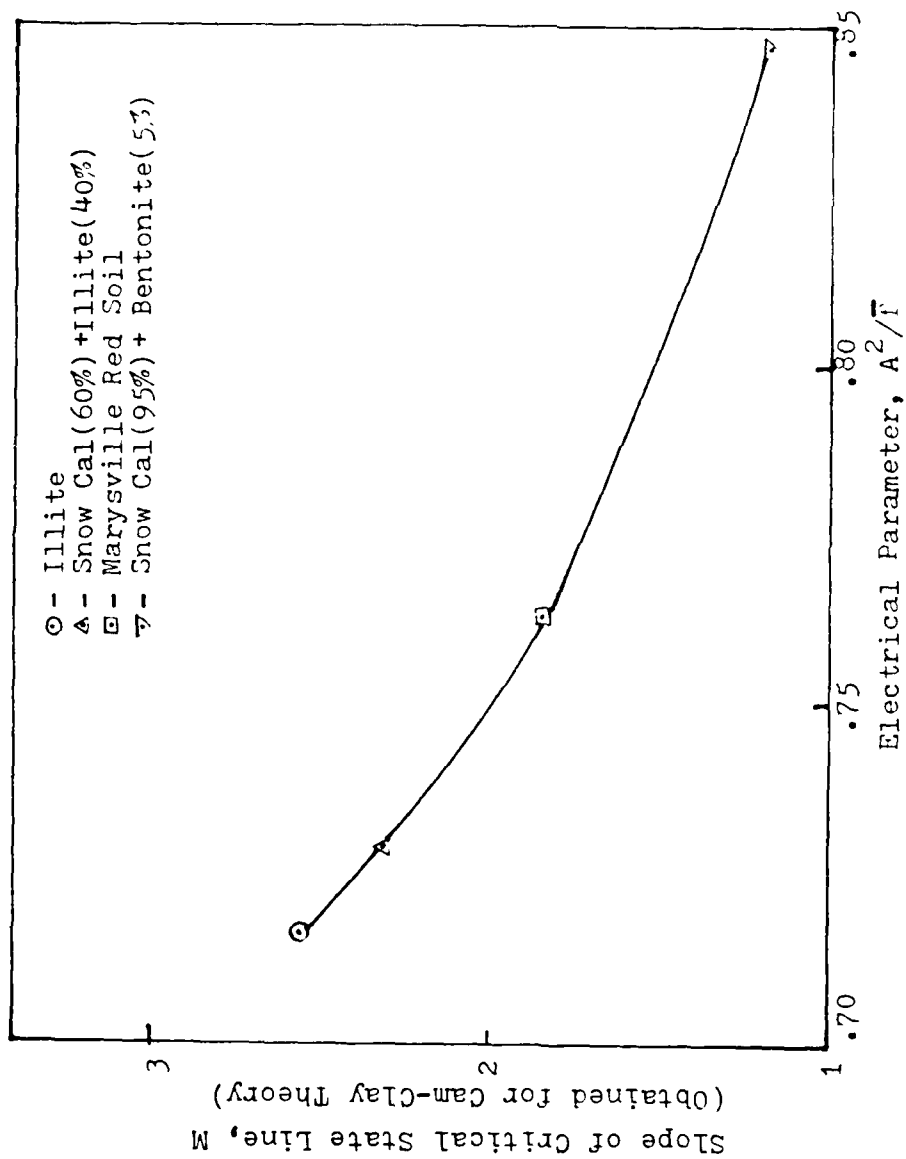


Fig. 40 The relationship between the slope of the critical state line,  $M$ , and the electrical index,  $A^2/\bar{\Gamma}$

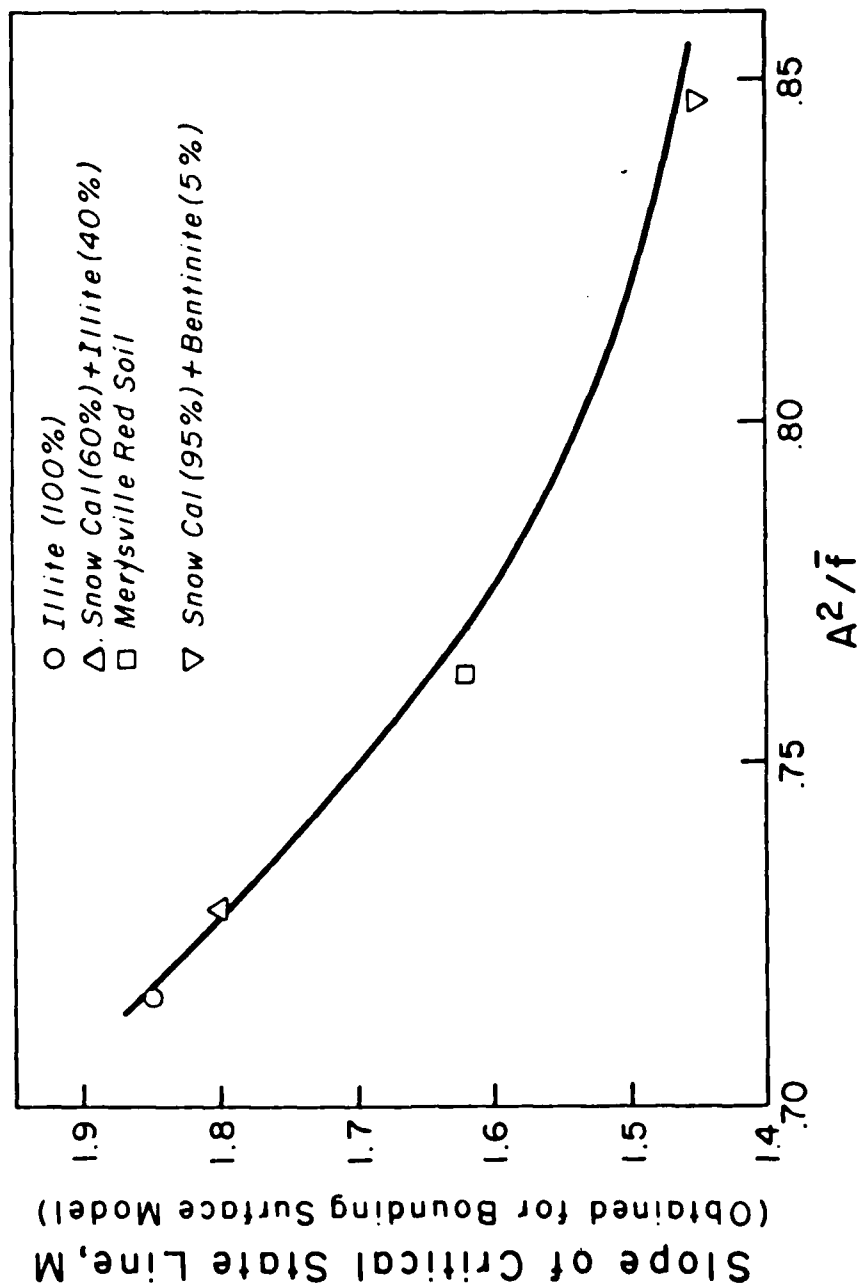


Fig. 41 The relationship between the slope of the critical state line,  $M$ , and the electrical index,  $A^2/\bar{f}$

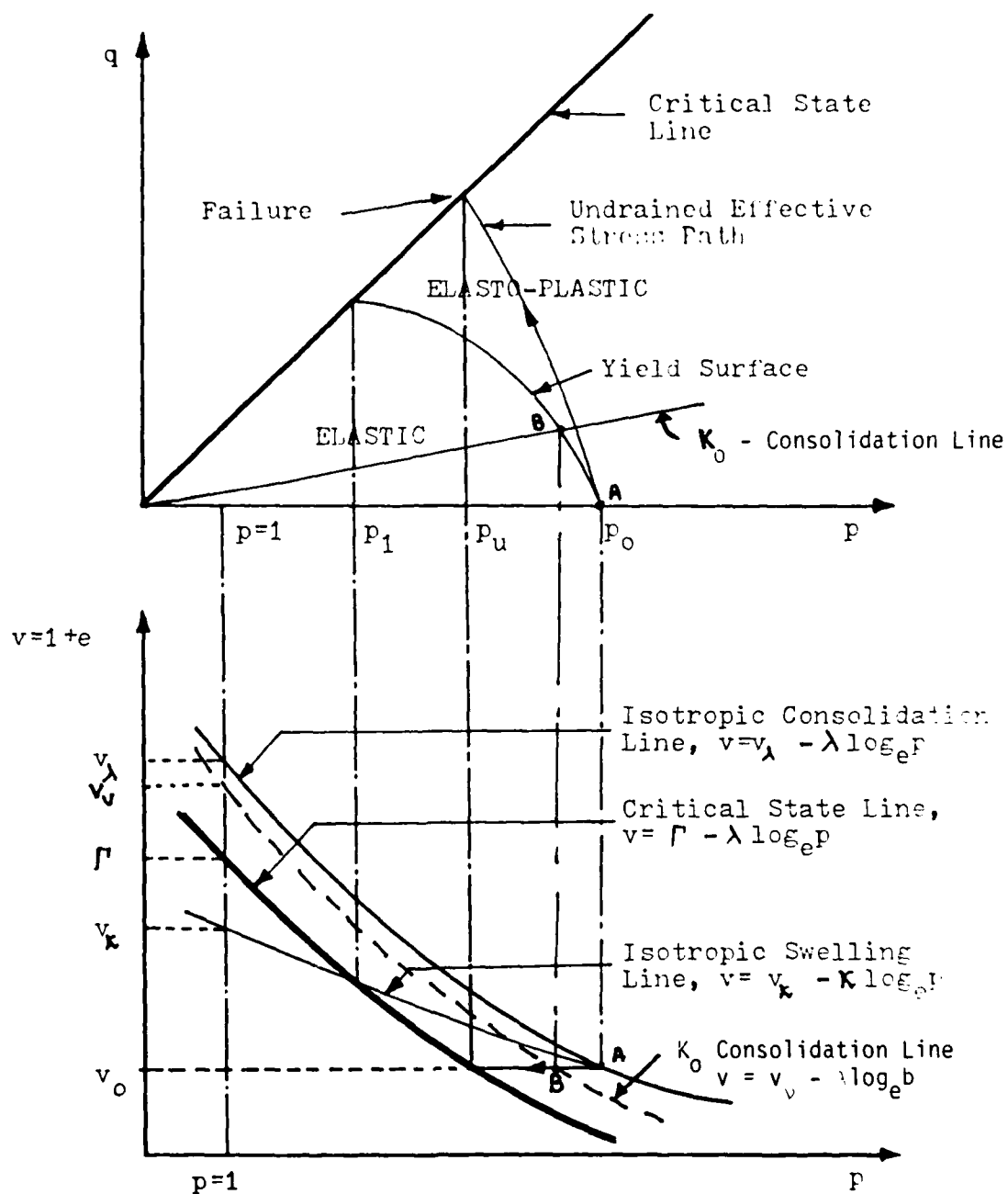


Fig. 42 The relationship between  $q$ ,  $p$  and  $v$  for undrained conditions.

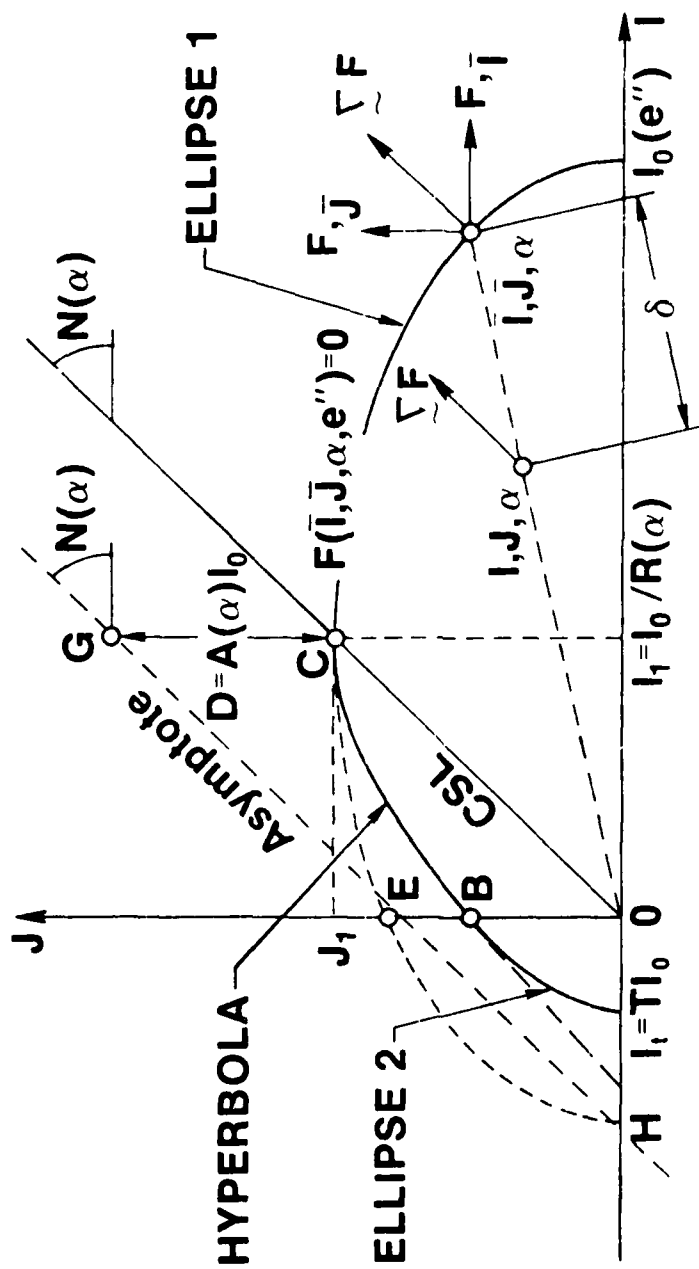


Fig. 43 Bounding Surface Model

SNOW CAL(60%) + ILLITE(40%) --  $p_0 = 69.3$  psi  
 ----- Predicted by bounding surface theory  
 ----- Predicted by Cam-Clay theory  
 ○ ○ Experimental results

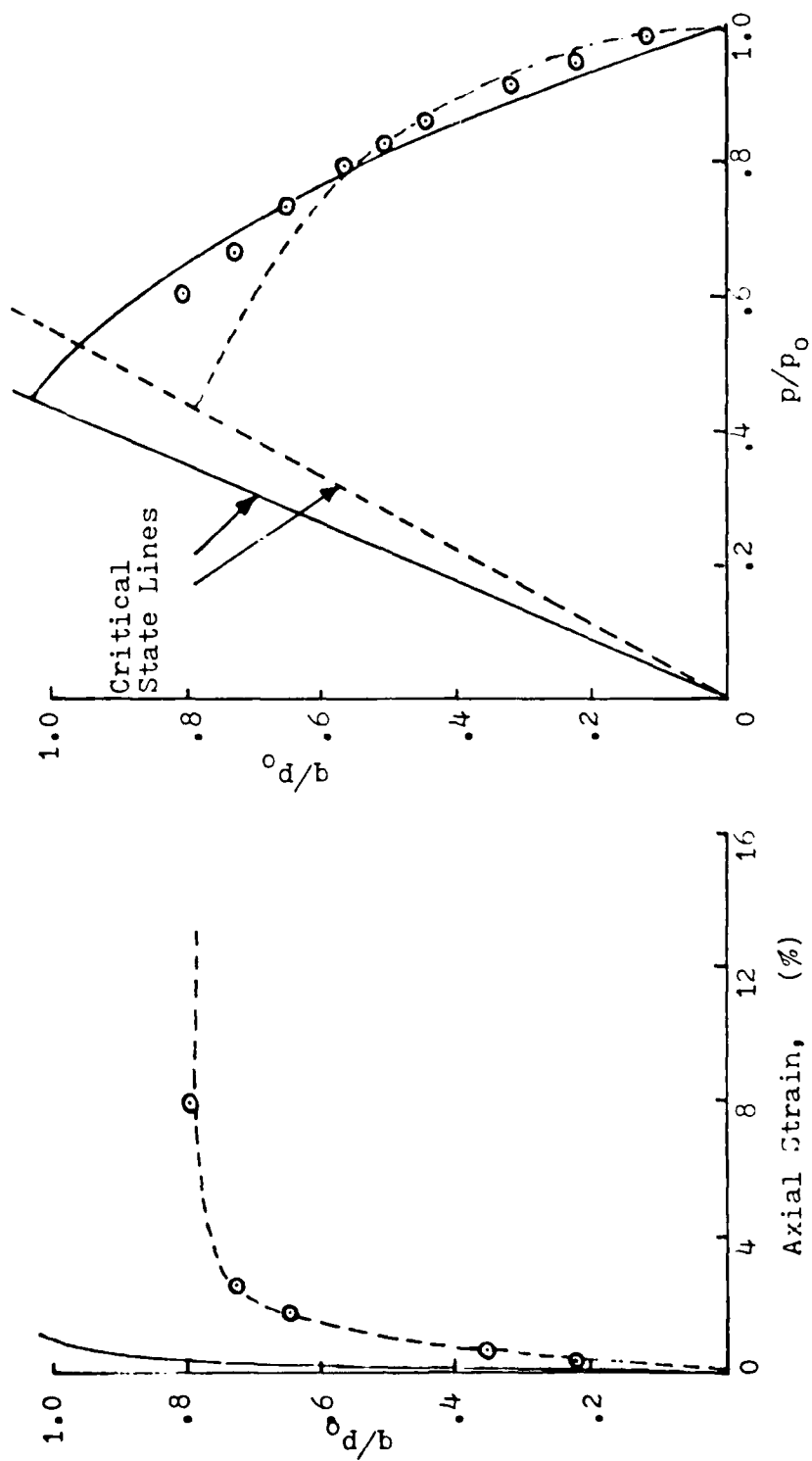


Fig. 44 Comparison of experimental and theoretical stress-strain relationships

Snow Cal (95%) + Bentinitite (5%),  $p_0 = 56.9 \text{ psi}$   
 ○—○ Experimental, ----- Theoretical

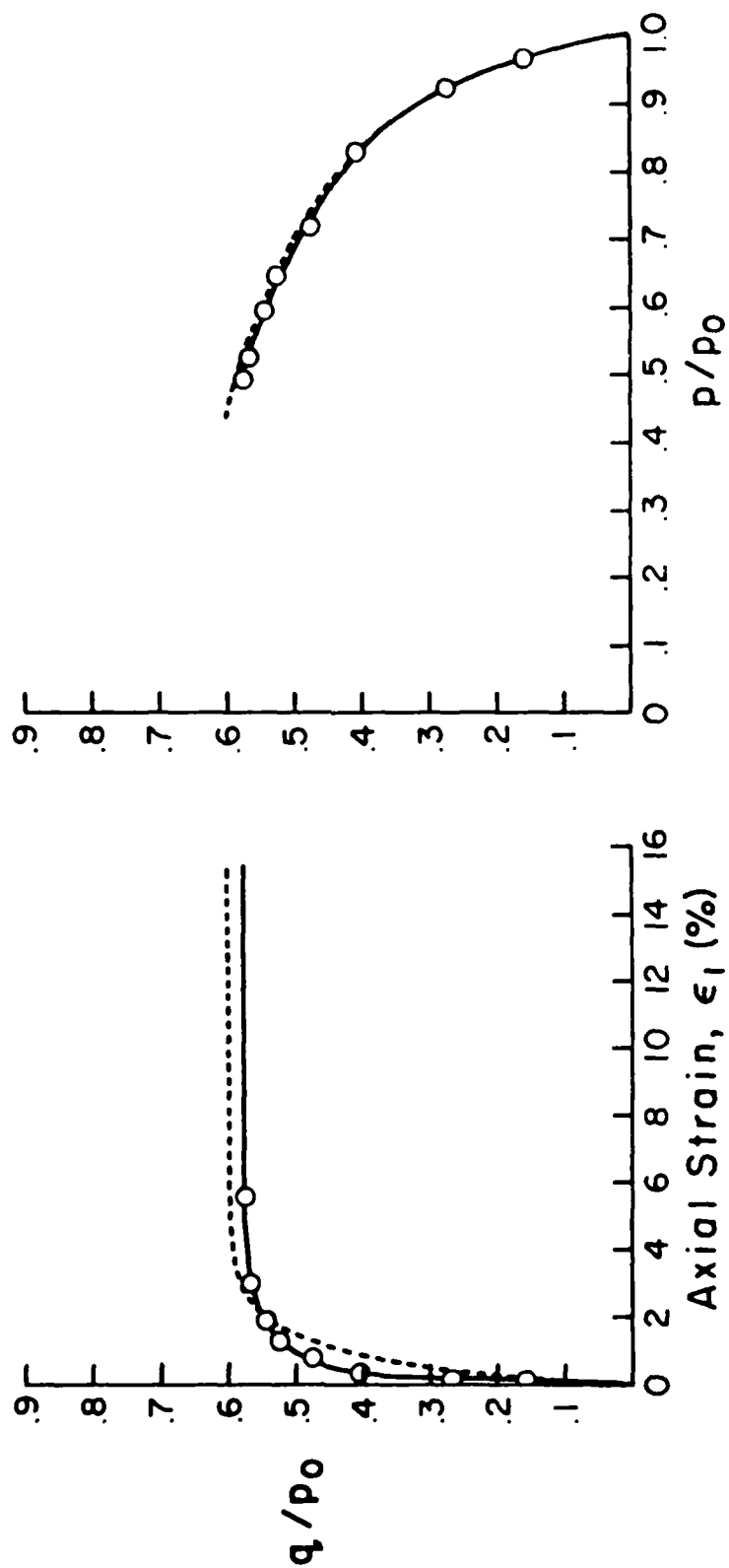


Fig. 45 Comparison of experimental and theoretical stress-strain relationships

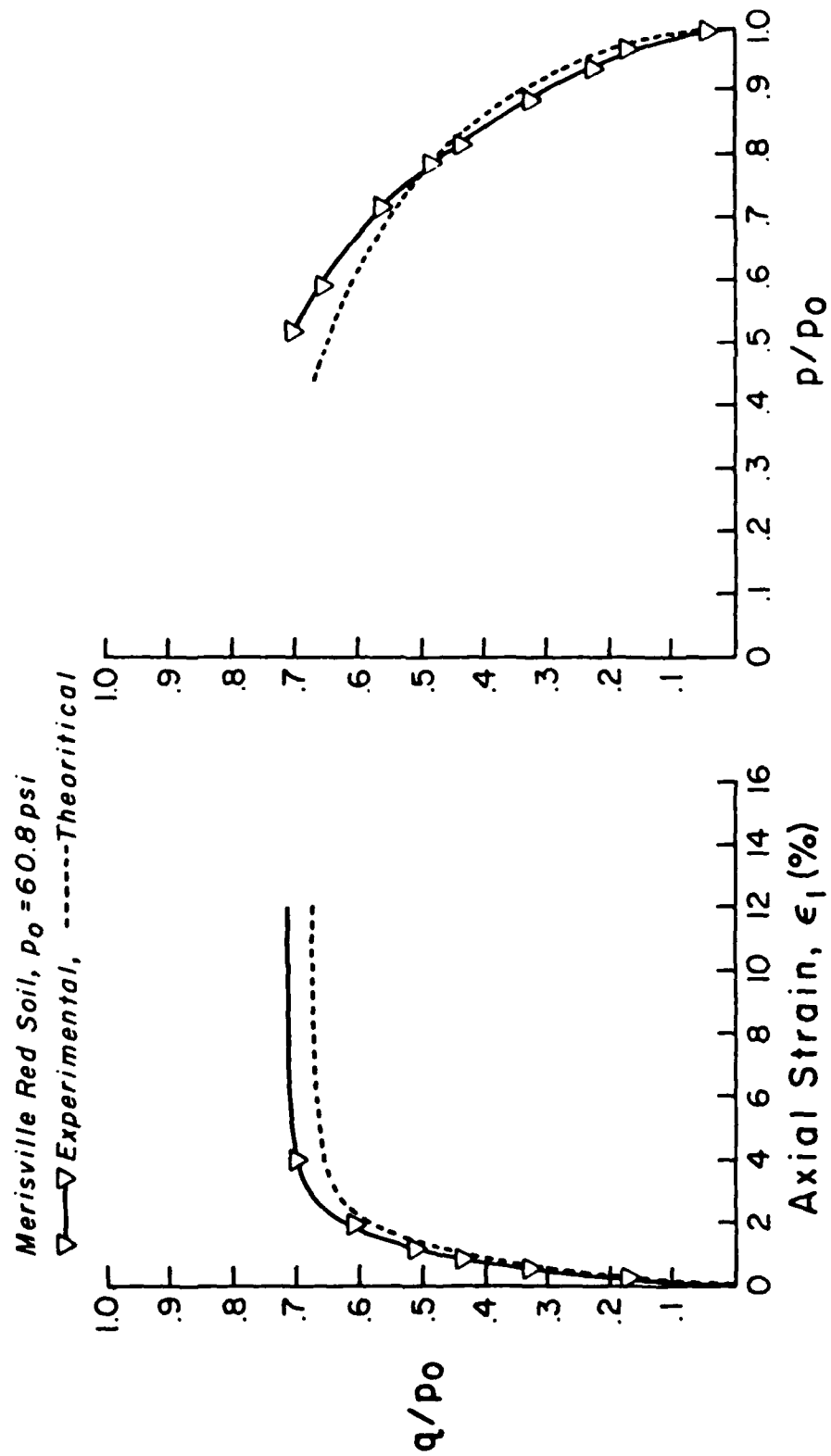


Fig. 46 Comparison of experimental and theoretical stress-strain relationships.

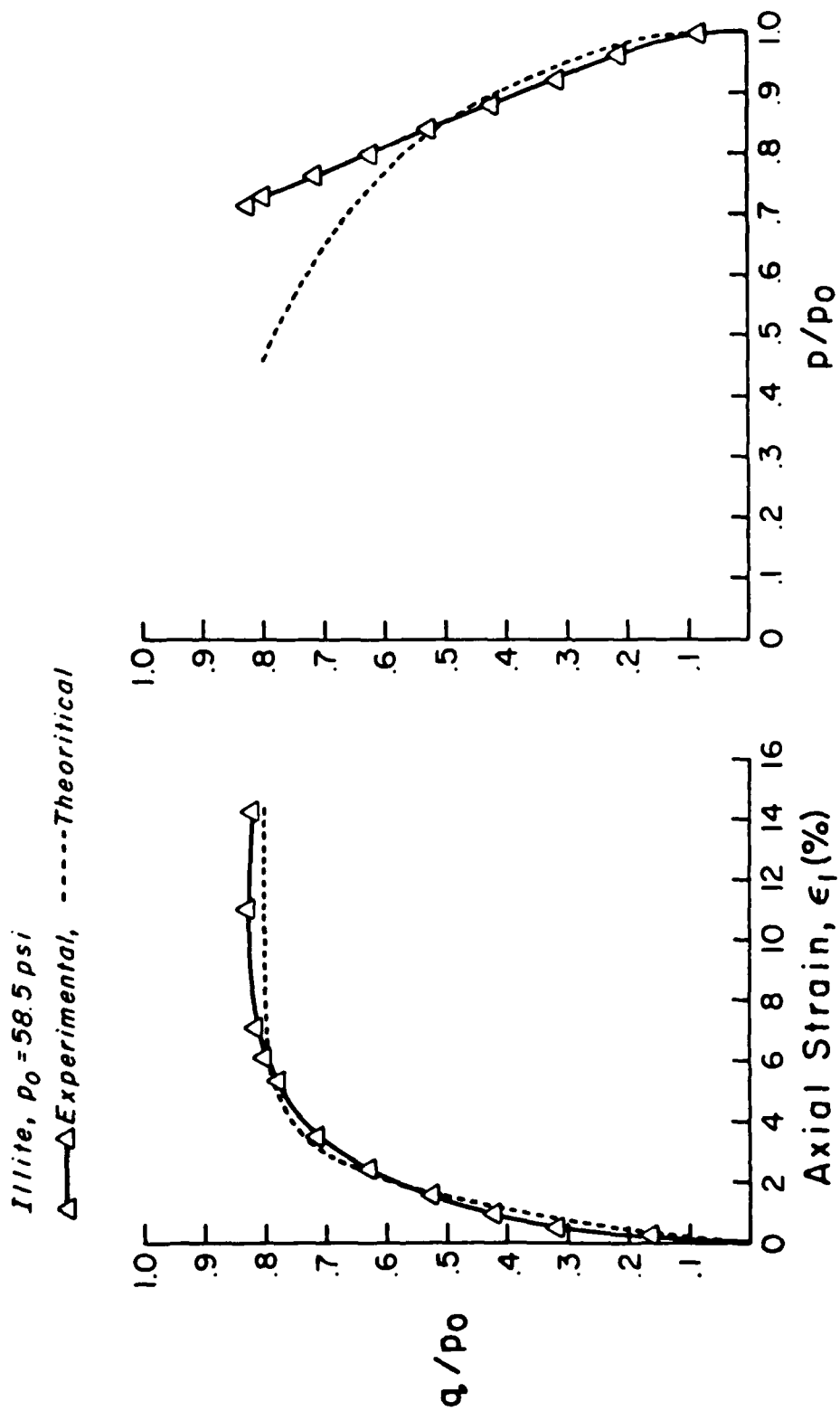


Fig. 47 Comparison of experimental and theoretical stress-strain relationships.

L MED  
- 8